(2) LEVEL II

AFML-TR-79-4060

AD A077270

CHARACTERIZATION OF CASTING DEFECTS IN TYPICAL CASTINGS OF A DIRECTIONALLY SOLIDIFIED SUPERALLOY

J.M. Marder and C.S. Kortovich
TRW Inc.
23555 Euclid Avenue
Cleveland, Ohio 44117

AUGUST 1979

TECHNICAL REPORT AFML-TR-79-4060

Approved for public release: distribution unlimited

AIR FORCE MATERIALS LABORATORY
AIR FORCE WRIGHT AERONAUTICAL LABORATORIES
Air Force Systems Command
Wright-Patterson Air Force Base, OH 45433

347250

79 11 07 015

NOTICE

When Government drawings, specifications, or other data are used for any purpose other than in connection with a definitely related Government procurement operation, the United States Government thereby incurs no responsibility nor any obligation whatsoever; and the fact that the government may have formulated, furnished, or in any way supplied the said drawings, specifications, or other data, is not to be regarded by implication or otherwise as in any manner licensing the holder or any other person or corporation, or conveying any rights or permission to manufacture, use, or sell any patented invention that may in any way be related thereto.

This report has been reviewed by the Information Office (OI) and is releasable to the National Technical Information service (NTIS). At NTIS, it will be available to the general public, including foreign nations.

This technical report has been reviewed and is approved for publication.

Dennis E. Wacha

DENNIS E. WACHA
Metals Behavior Branch
Metals and Ceramics Division

N G Tupper

NATHAN G. TUPPER, Chief
Metals Behavior Branch
Metals and Ceramics Division

"If your address has changed, if you wish to be removed from our mailing list, or if the addressee is no longer employed by your organization please notify AFML/LLN , W-PAFB, OH 45433 to help us maintain a current mailing list!"

Copies of this report should not be returned unless return is required by security considerations, contractual obligations, or notice on a specific document.

AIR FORCE/56780/18 October 1979 — 250

UNCLASSIFIED

SECURITY CLASSIFICATION OF THIS PAGE (When Data Entered)

REPORT DOCUMENTATION PAGE	READ INSTRUCTIONS BEFORE COMPLETING FORM
1. REPORT NUMBER: AFML-TR-79-4066	2. GOVT ACCESSION NO.
	3. RECIPIENT'S CATALOG NUMBER: Rept 1
4. TITLE (and Subtitle): CHARACTERIZATION OF CASTING DEFECTS IN TYPICAL CASTINGS OF A DIRECTIONALLY SOLIDIFIED SUPERALLOY	5. TYPE OF REPORT & PERIOD COVERED: FINAL OCT 1976 – DEC 1978
	6. PERFORMING ORG. REPORT NUMBER
7. AUTHOR(s): J. M. MARDER AND C. S. KORTOVICH	8. CONTRACT OR GRANT NUMBER(s): F33615-76-C-5373
9. PERFORMING ORGANIZATION NAME AND ADDRESS: TRW Inc. 23555 Euclid Avenue Cleveland, Ohio 44117	10. PROGRAM ELEMENT, PROJECT, TASK AREA & WORK UNIT NUMBERS: 7351-06-B8
11. CONTROLLING OFFICE NAME AND ADDRESS: Air Force Materials Laboratory (LLN) Air Force Wright Aeronautical Laboratories Wright-Patterson AFB, OH 45433	12. REPORT DATE: August 1979
	13. NUMBER OF PAGES: 124
14. MONITORING AGENCY NAME & ADDRESS (if different from Controlling Office)	15. SECURITY CLASS. (of this report): UNCLASSIFIED
	15a. DECLASSIFICATION/DOWNGRADING SCHEDULE

16. DISTRIBUTION STATEMENT (of this Report)

Approved for public release; distribution unlimited.

17. DISTRIBUTION STATEMENT (of the abstract entered in Block 20, if different from Report)

18. SUPPLEMENTARY NOTES

19. KEY WORDS (Continue on reverse side if necessary and identify by block number)

Directionally Solidified Superalloys, Casting Defects, Nickel Base Superalloys, Directionally Solidified Turbine Blades, Degradation of Mechanical Properties.

20. ABSTRACT (Continue on reverse side if necessary and identify by block number)

A program was conducted to assess the effects of casting defects in directionally solidified (DS) material. The technical approach involved two tasks, the first including the characterization of typical casting defects in F-100 1st and 2nd stage PWA-1422 production turbine blades and the second including the evaluation of thin sheet test specimens cast deliberately to contain defects. The defects included microshrinkage, inclusions and grain misorientation and represented a range of severity levels including conditions exceeding current production acceptance criteria. The analysis of production castings indicated that

DD FORM 1 JAN 73 1473 EDITION OF 1 NOV 65 IS OBSOLETE S/N 0102-014-6601

UNCLASSIFIED

SECURITY CLASSIFICATION OF THIS PAGE (When Data Entered)

Block 20 (continued)

substantial decreases in the rejection rate could be achieved with only minor relaxation of the acceptability criteria. In addition, dross inclusions were found to be the single most frequent cause for casting rejections. Mold breakage inclusions and misorientation defects also made substantial contributions to the overall rejection rate. Mechanical property evaluations included 1400°F (760°C) tensile and stress rupture as well as 1800°F (982°C) creep rupture and low cycle fatigue tests. The results were interpreted in terms of the defects actually associated with specimen fracture, because fracture was usually not associated with the intended defect or severity level. In general, failures were not associated with any of the grain misorientation defects. The 1400°F (760°C) tensile and stress rupture results indicated little sensitivity to the microshrinkage and inclusion defects at the current acceptability limits. This suggested that defects in excess of the 0.010" (.25 mm) limit could be tolerated as long as the linear groupings or clusters of defects were less than 0.30" (8 mm) in length or diameter. The 1800°F (982°C) creep rupture and low cycle fatigue properties, on the other hand, were extremely sensitive to the presence of microshrinkage and inclusions at all severity levels investigated thus indicating little potential for the relaxation of the rejection criteria.

FOREWORD

The work described in this final report was performed in the Materials Technology Laboratory of TRW Inc. under United States Air Force Contract F33615-76-C-5373, TRW Project No. 512-002824-88. The work was performed under the direction of Dr. C. S. Kortovich, the Program Manager, with J. M. Marder as the Principal Investigator. Technical assistance was provided by Mr. J. W. Sweeney and Mr. R. E. Ebert. D. E. Macha, AFML/LLN, was the Program Manager for the Air Force.

TABLE OF CONTENTS

Section			Page
I	INTRODUCTION		1
II	PROGRAM OUTLINE		3
III	TASK I - DEFECT CHARACTERIZATION		10
	A.	Experimental Procedures	10
		1. Nondestructive Inspection Procedures	10
		2. Destructive Evaluation Procedures	12
		3. Analysis of Quality Control Reject Records	12
		4. Analysis of Results	13
	B.	Results and Discussion	13
		1. Defect Characterization	13
		2. Relative Defect Importance	28
	C.	Summary	34
IV	TASK II - MECHANICAL PROPERTY TESTING		36
	A.	Experimental Procedures	36
		1. Defect Selection	36
		2. Specimen Preparation	37
	B.	Results and Discussion	47
		1. 1400°F (760°C) Tensile Results	49
		2. 1400°F (760°C) Stress Rupture Results	54
		3. 1800°F (982°C) Creep Rupture Results	59
		4. 1800°F (982°C) Low Cycle Fatigue Results	65
		5. Krypton Emission Technique (KET) Results	69
	C.	Summary	71
V	SUMMARY AND CONCLUSIONS		74
VI	RECOMMENDATIONS		76

TABLE OF CONTENTS (CONTINUED)

Section		Page
	APPENDICES	
A.	Production As-Blade Inspection Procedures	79
B.	Grain Etch Acceptability Criteria	82
C.	Fluorescent Penetrant Acceptability Criteria	83
D.	X-Ray Acceptability Criteria	85
E.	Examples of Casting Defects	86
F.	1400°F (760°C) Tensile Results	92
G.	Analysis of 1400°F (760°C) Tensile Results	96
H.	1400°F (760°C) Stress Rupture Results	100
I.	Analysis of 1400°F (760°C) Stress Rupture Results	104
J.	1800°F (982°C) Creep Rupture Results	106
K.	Analysis of 1800°F (982°C) Creep Rupture Results	110
L.	1800°F (982°C) Low Cycle Fatigue Data	113
M.	Analysis of 1800°F (982°C) Low Cycle Fatigue Data	117
N.	Examples of Fracture Surfaces Associated with Casting Defects	119
REFERENCES		123

LIST OF ILLUSTRATIONS

FIGURE		PAGE
1	Work Breakdown Structure of the Program	4
2	Mechanical Property Test Specimen Configuration Used for Tensile and Stress Rupture Tests. Specimens for Fatigue Testing Had a 2 Inch Fillet Radius Instead of 5/8 Inch Radius. All Dimensions in Inches.	7
3	Examples of Grain Misorientation Defects in D.S. Components.	15
4	Histogram Showing Number of Observed Diverging Axis Grains as a Function of Misorientation Angle.	16
5	Histogram Showing Number of Observed Diverging Adjacent Grains as a Function of Included Angle.	17
6	Histogram Showing Number of Observed Emergent Grains as a Function of Misorientation Angle.	19
7	Two Examples of Freckle Defects in D.S. Turbine Blades Occurring Near Airfoil-Root Fillet Radius. 50X Magnification	20
8	Histogram Showing Number of Observed Freckle Defects as a Function of Size in F-100 1st Stage Blades.	22
9	Histogram Showing Number of Observed Freckle Defects as a Function of Size in F-100 2nd Stage Turbine Blades.	23
10	Histogram Showing Number of Observed Fluorescent Penetrant Indications as a Function of Indication Size.	25
11	Positive of X-Ray and Photomicrograph of a Low X-ray Density Inclusion.	26
12	Positive of X-Ray and Photomicrograph of a Low X-Ray Density Inclusion.	27
13.	Histogram Showing Number of Observed Low X-Ray Density Inclusions as a Function of Indication Size.	29
14	Histogram Showing Number of Observed High X-Ray Density Inclusions as a Function of Indication Size.	30
15	Histogram Showing Number of Observed Cracks as a Function of Crack Length.	31

LIST OF ILLUSTRATIONS (CONTINUED)

FIGURE		PAGE
16	Photograph of a Mold of a Cluster of Mechanical Property Test Specimens.	47
17	Photograph Comparing Valid and Invalid Specimen Failure Locations.	48
18	Weibull Probability Plot for 1400°F (760°C) Ultimate Strength for Defect Free Specimens.	50
19	1400°F (760°C) Tensile Ductilities Versus Defect Type	51
20	1400°F (760°C) Tensile Ductilities Versus Defect Type	52
21	1400°F (760°C) Rupture Life Versus Defect Type. Arrows Indicate Suspended Test.	56
22	1400°F (760°C) Stress Rupture Ductility Versus Defect Type	57
23	1800°F (982°C) Creep Rupture Life Versus Defect Type	60
24	1800°F (982°C) Creep Rupture Ductility Property Versus Defect Type.	61
25	Photomacrograph of 1800°F (982°C) Stress Rupture Specimen Showing Location of a Crack Whose Path Deviated at a Diverging Adjacent Grain Condition.	64
26	1800°F (982°C) Low Cycle Fatigue Properties Versus Defect Type.	66
27	Transgranular Crack Propagation Rate Data for Defect Free and Defect Bearing PWA-1422.	70
28	Metallographic Examination of KET Indication	72

LIST OF TABLES

TABLE	TITLE	PAGE
1	Defects Included for Evaluation in Task I	5
2	Testing Requirements for the Task II Mechanical Property Evaluation	8
3	Chemistry of PWA-1422K D.S. Casting Alloy	11
4	Summary of Rejection Rate Data for F-100 1st and 2nd Stage Turbine Blades - January 1975 - December 1977	33
5	Defect Severity Classifications	38
6	Chemical Analysis of PWA-1422 (MAR-M200 + Hf) Master Heat JW-6048	39
7	Acceptance Test Data for PWA-1422K Master Heat JW-6048	40

SECTION I

INTRODUCTION

The development of advanced high temperature materials and processing systems has been primarily responsible for the improvements in the performance of advanced gas turbine engines. Recent emphasis upon reductions in life cycle costs through reduced fuel consumption and operating costs and increased engine reliability have imposed more stringent combined requirements for higher operating temperatures and longer turbine component lives (1). These new requirements will demand the use of more complex cooling schemes and the application of sophisticated heat resistant materials in critical turbine components. Cast nickel-base superalloys are currently the most useful and economically attractive materials in use for high temperature turbine blades and vanes. The reliability of these superalloys has been established as the result of thousands of hours service in a wide variety of engine applications both for military and commercial usage. The utility of these materials has been further improved through the use of a controlled cast structure produced by the directional solidification (D.S.) technique. This structure can add 30°F (17°C) to the operating temperature, or increase component stress rupture life by a factor of four to seven times as compared to conventionally cast, equiaxed airfoil parts (2).

The objective of applying D.S. to superalloy turbine airfoil fabrication is to eliminate grain boundaries transverse to the major stress axis. During high temperature engine operation, grain boundaries normal to the stress axis serve as crack initiation sites and paths for easy crack growth (3-10). Their elimination thus produces enhanced creep rupture and thermal fatigue properties over the conventional cast equiaxed material. An additional factor contributing to the enhanced thermal fatigue resistance of D.S. castings is that thermally induced stresses for a given temperature excursion are lower in the D.S. component because of the reduced Young's Modulus (11). This causes less accumulation of strain damage during the thermal cycling exposure.

Ideally, D.S. components should have all grain boundaries aligned along the axis direction of the airfoil (2). Although this does not always occur in actual production operations, exacting quality specifications have been imposed upon these parts to insure that deviation from the ideal condition be minimized. These stringent quality control requirements can result in low process yields and high part costs. To the present, there have been no systematic efforts to quantify the effects of non-ideal D.S. component structures upon mechanical properties. Nor have there been efforts to determine the effects of other common D.S. casting defects such as porosity, macrosegregation, and inclusions upon mechanical properties. The present acceptance criteria for all of these defects, therefore, may be excessively conservative, which results in increased component costs.

The present investigation was conducted to determine the effect of various defects found in D.S. superalloy castings upon mechanical properties and thus provide a more effective basis for establishing reject criteria in these components. The experimental approach involved two tasks. In Task I - Defect Characterization, casting defects in typical turbine blade castings were characterized in terms of size and location using

commercially available nondestructive inspection (NDI) techniques supplemented by destructive evaluation of the castings to verify NDI subsurface defect indications. In Task II - Mechanical Property Testing, tests were performed on specimens prepared specifically to contain certain casting defects at predetermined intensity levels in order to establish their effect upon mechanical properties. These evaluations included tensile, stress/creep rupture, and fatigue/fatigue crack propagation tests at temperatures representative of the operational environment of turbine blades. The results of the evaluations were analyzed in terms of present acceptance criteria for a number of defects and recommendations were made defining those reject criteria which may be refined without compromising component performance.

The results of this study are summarized in this final report. It includes a review of the program outline to characterize casting defects in typical castings of a directionally solidified superalloy, a review of the experimental procedures, a summary of the experimental results, and a discussion of these results.

SECTION II

PROGRAM OUTLINE

The basic goal of the program was to provide a rational basis for establishing a reject criteria for D.S. superalloy materials. To accomplish this, a basic knowledge of the effect of casting defects on mechanical properties had to be established. The study consisted of two major tasks and followed the outline presented in the Work Breakdown Structure of Figure 1. Task I of the investigation consisted of NDI and destructive examination of production D.S. superalloy turbine blade components to characterize defects such as grain misorientation, macrosegregation, porosity, and inclusions. Task II consisted of mechanical property tests including tensile, stress/creep rupture and fatigue/fatigue crack propagation tests performed upon cast specimens containing representative defects.

A. Task I - Defect Characterization

The objective of Task I was to characterize the defects in typical castings of an advanced superalloy in terms of type, size and location utilizing metallographic and commercially available NDI inspection techniques. This effort was conducted to determine the range of defects found in D.S. castings in order to insure that test results on specimens prepared to contain specific defects at predetermined intensity levels would be meaningful in terms of actual production quality control experience. F-100 engine 1st and 2nd stage turbine blades cast in PWA-1422 (D.S. MAR-M200 + hafnium) were selected for examination in Task I. PWA-1422 is an advanced nickel-base superalloy used for production of D.S. components for both military and commercial engines. The selection of F-100 turbine parts for evaluation in this study was based upon the high production volume of these parts.

The casting defects selected for analysis in the program are listed in Table 1. Grain misorientation defects consist of diverging axis grains, diverging adjacent grains and emergent grains. Diverging axis grains are those which have their growth axes at non-zero angles to the airfoil span. Diverging adjacent grains occur when two adjoining grains grow in acceptable directions with regard to the blade span, but have a large included angle between their growth directions. Emergent grains are diverging axis grains whose growth terminates at the leading or trailing edge of the airfoil. Shrinkage porosity results from improper casting design which allows isolated pools of molten material to solidify and contract without additional molten metal feeding in to compensate for the volume change. Freckles are macrosegregation defects consisting of equiaxed grains which appear on the surface of D.S. castings. Major alloying element segregation occurs during changes in solidification rate at casting section size changes. Inclusions are commonly of two types. Dross is the product of oxidation of an alloying element during the casting process and mold breakage inclusions arise when the mold material contaminates the molten metal. Surface cracks, or hot tears, occur while the casting is in the vacuum furnace and are usually associated with excessive amounts of primary gamma-prime in the intergranular regions (12). The defects in Table 1 are not listed in order of relative importance but rather represent a general listing of important types which has evolved from extensive experience in the inspection of D.S. PWA-1422 gas turbine engine blades and vanes. Also included in the table are the NDI techniques used to characterize these defects.

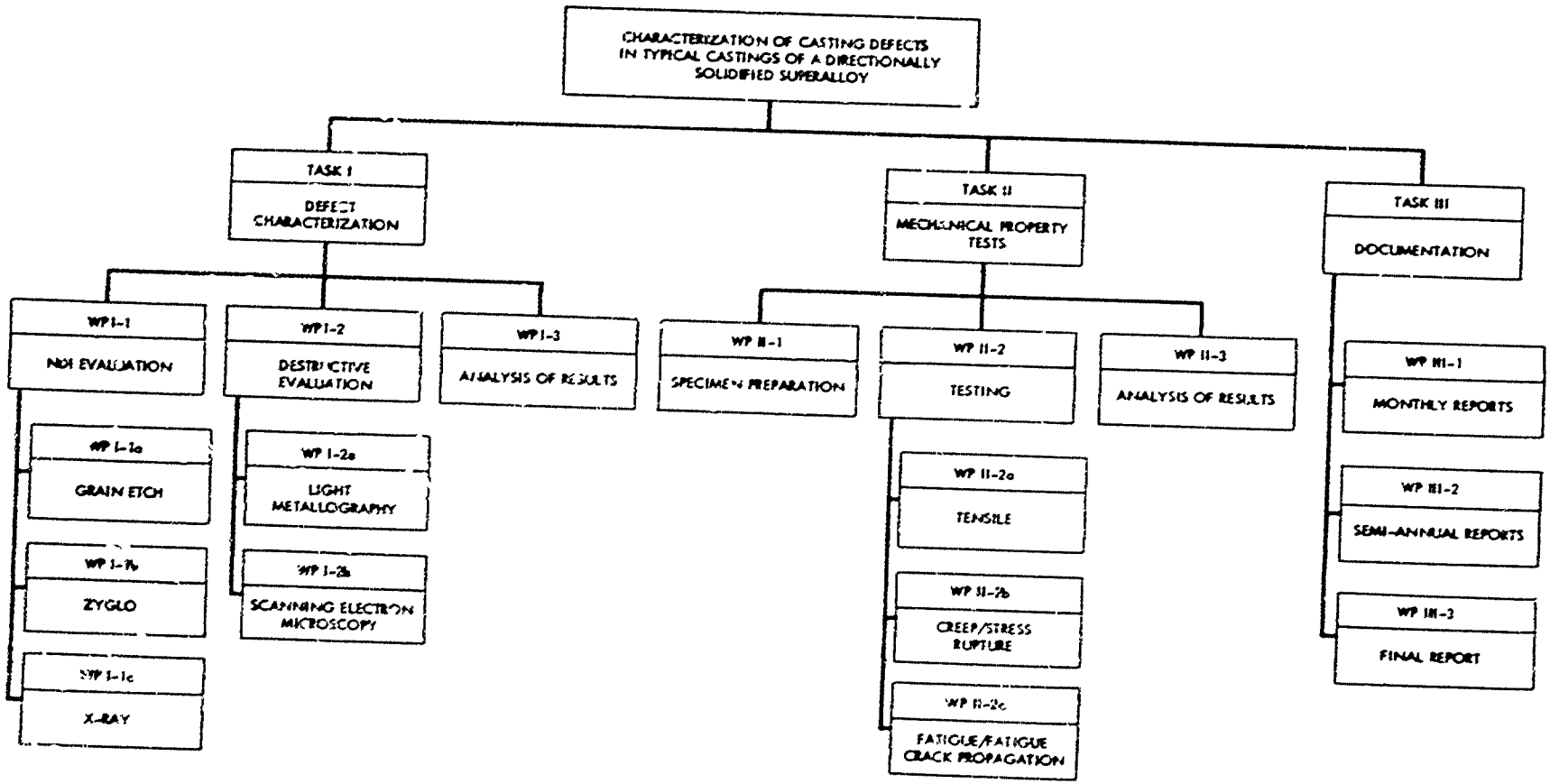

Figure 1. Work Breakdown Structure of the Program.

TABLE 1

DEFECTS INCLUDED FOR EVALUATION IN TASK I

Defect	Method of Characterization
Grain Misorientation	
Diverging Axis Grains	Grain Etch
Diverging Adjacent Grains	Grain Etch
Emerging Grains	Grain Etch
Porosity	
Shrinkage	Fluorescent Penetrant Inspection, X-ray
Macrosegregation	
Freckles	Grain Etch
Inclusions	
Dross	Fluorescent Penetrant Inspection, X-ray
Breakage	Fluorescent Penetrant Inspection, X-ray
Surface Cracks	Fluorescent Penetrant Inspection, X-ray

The defects found in the castings rejected at NDI were characterized in terms of the appropriate acceptance criteria. The severity of grain misorientation defects was characterized in terms of the misorientation angle. Porosity, shrinkage and inclusions were analyzed by cataloging the size and location of the FPI or X-ray indications. Freckle macrosegregation was defined by the number and size of these defects as determined during grain etch inspection. These results established the size range, distribution range and misorientation angle range typical of defects found in D.S. castings and required for the specimen preparation efforts of Task II.

In addition to the evaluation of specific NDI reject turbine blades, an analysis of the overall rejection rate data for the years 1975 and 1976 for D.S. component production at the Metals Plant of the TRW Turbine Components Division was included in the Task I characterization study. This study was conducted in order to define the major causes of blade NDI rejection as they effect the overall production acceptance rate of D.S. components. The results of this effort established the relative importance of the defects and served to highlight which required more careful study in the Task II mechanical property testing program.

B. Task II - Mechanical Property Testing

The objective of Task II was to establish the effect of the various D.S. casting defects upon mechanical properties. These evaluations included tensile, stress/creep rupture and fatigue/fatigue crack propagation testing at temperatures representative of the operational environment of turbine blades. Sheet type test specimens were cast to contain defects located within the specimen gage length. Shown schematically in Figure 2, this configuration was selected to simulate geometrical conditions in hollow turbine engine airfoil regions where defects most often occur, causing major quality control problems. Nonconventional casting procedures were employed to produce the required defects. Each defect type was ranked in one of three categories including mild, intermediate and severe. The specific ranges for the defects in these categories were established as a result of the defect characterization efforts in Task I. While each particular category was in itself fairly broad in terms of magnitude, each clearly represented a distinct degree of defect severity. As shown in the listing presented in Table 2 the mechanical property evaluations included 1400°F (760°C) tensile, 1400°F (760°C) stress rupture, 1800°F (982°C) creep rupture and 1800°F (982°C) fatigue/fatigue crack propagation tests conducted upon sets of specimens containing each type of severity of defect.

The NDI methods used to inspect the mechanical property test specimens included a novel inspection method, the Krypton Emission Technique (KET) in addition to the standard production grain etch, X-ray and FPI inspections (13). The KET method utilizes radioactive krypton in a manner analagous to liquid penetrant fluid. The radioactive nature of krypton allows it to expose photographic film thereby resulting in a permanent record of any surface connected defect. In Task II, KET was utilized with a limited number of test specimens to assist in evaluating this inspection method compared to the more standard NDI techniques. The KET effort was conducted under the sponsorship of the Naval Air Propulsion Test Center of Trenton, New Jersey. The KET results were compared to X-ray and FPI results, and to the actual defects revealed by metallographic examination.

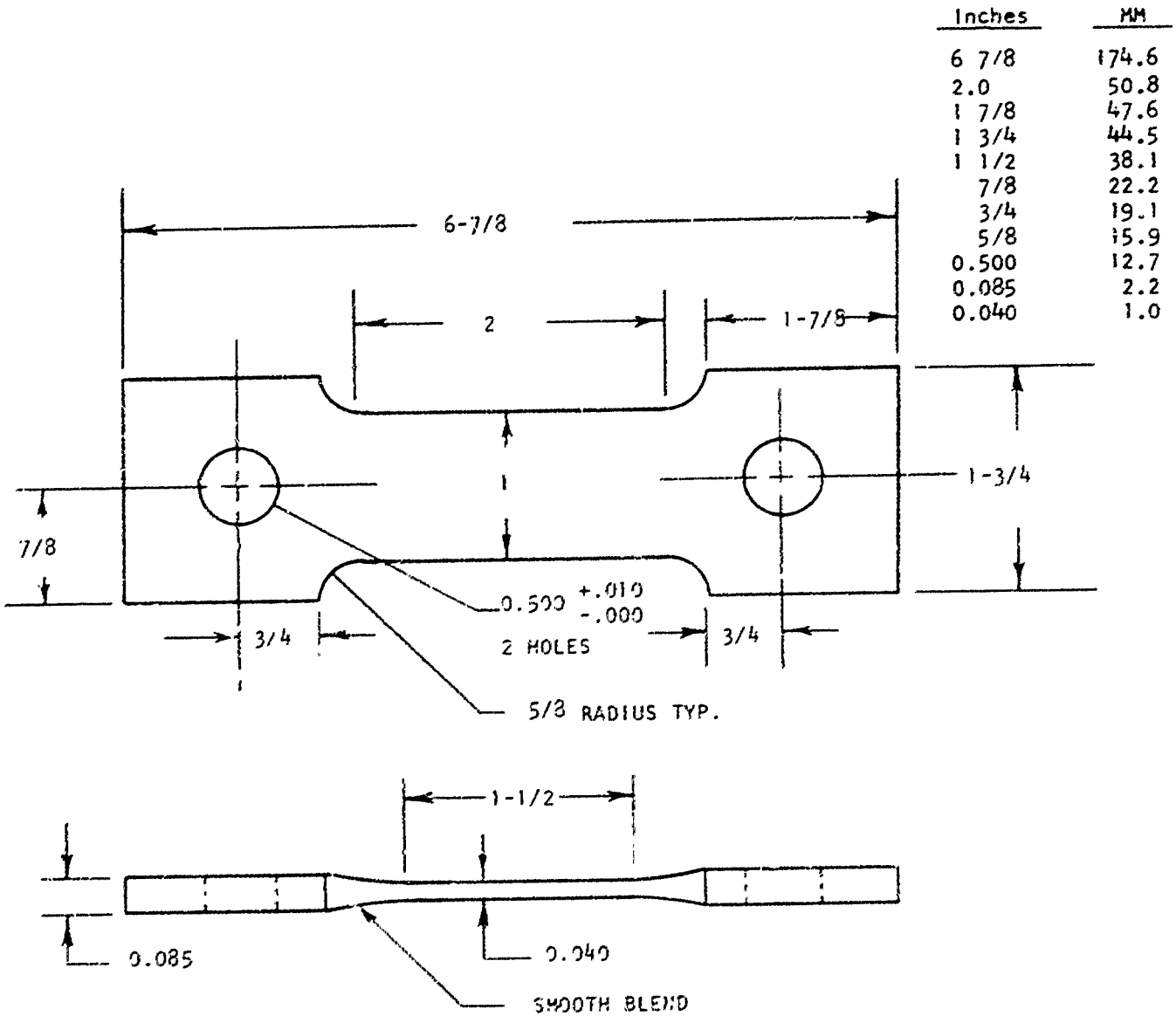

Figure 2. Mechanical Property Test Specimen Configuration Used for Tensile and Stress Rupture Tests. Specimens for Fatigue Testing Had a 2 Inch Fillet Radius Instead of 5/8 Inch Radius. All Dimensions in Inches.

TABLE 2

TESTING REQUIREMENTS FOR THE TASK II MECHANICAL PROPERTY EVALUATION*

Defect Type	Mechanical Property Evaluations
Divergent Axis Grains	1400°F (760°C) Tensile Tests
Divergent Adjacent Grains	1400°F (760°C) Stress Rupture Tests
Emerging Grains	1800°F (982°C) Creep Rupture Tests
Microshrinkage	1800°F (982°C) Fatigue/Fatigue Crack Propagation tests
Dross Inclusions	
Breakage Inclusions	
Defect Free Specimens	

* Tests were conducted on specimens prepared with "mild", "intermediate" and "slight" defect severity levels as discussed in the procedures for Task II - Mechanical Property Testing.

The mechanical property test results were analyzed to determine whether more objective criteria for D.S. PWA-1422 superalloy castings are feasible. This effort included the correlation of NDI measurements, destructive evaluation data and mechanical property response to determine the extent to which various casting defects can effect mechanical properties.

SECTION III

TASK I - DEFECT CHARACTERIZATION

A. Experimental Procedures

The following section contains a description of the destructive and nondestructive evaluation procedures employed in Task I - Defect Characterization. The nominal composition of the PWA-1422 F-100 1st and 2nd stage turbine blades examined in this study is listed in Table 3. These blades were produced at the TRW Turbine Components Metals Division and were rejected during production inspection operations. The defects characterized were therefore representative of those found in typical production castings. During the course of the investigation it was observed that a larger number of 2nd stage blades were rejected compared to the 1st stage blades. This simply reflected the fact that larger production requirements were needed at the time for the 2n stage blade and not that this particular configuration presented more troublesome quality control problems than the 1st stage blade. The overall sequence of the production inspection operations is discussed below in general terms and the specific details of the various procedures and equipment used are presented in Appendix A.

1. Nondestructive Inspection Procedures

a. Grain Etch Inspection

Grain etch inspection was used to detect and characterize grain misorientation and freckle macrosegregation defects. A total of 254 blades rejected at grain etch inspection were utilized in this portion of the study. 75 of these reject castings were 1st stage turbine blades, and 179 were 2nd stage turbine blades. Grain misorientation defects were categorized with respect to the misorientation angle. Freckle defects were categorized with respect to the size of the freckle indication. Grain etch inspection acceptance criteria are listed in Appendix B.

b. Fluorescent Penetration Inspection

Fluorescent penetrant inspection (FPI) was utilized to characterize surface connected defects. These included surface connected dross inclusions, mold breakage or deterioration inclusions, surface cracks and microshrinkage. A total of 366 blades, including 111 1st stage and 255 2nd stage reject castings were utilized in this study. The defects were characterized as to size, type and location. The acceptance criteria for FPI inspection are listed in Appendix C.

c. X-Radiographic Inspection

X-ray inspection was utilized to characterize defects such as dross and mold breakage inclusions, cracks, macroshrinkage and gas porosity which were not surface connected. A total of 120 X-ray rejectable blades were examined, including six 1st stage blades and 114 2nd stage blades. The defects were characterized in terms of

TABLE 3

CHEMISTRY OF PWA-1422K D.S. CASTING ALLOY

Element	Chemistry Range in w/o
C	.12-.16
Mn	.20 maximum
P	.015 maximum
S	.015 maximum
Si	.20 maximum
Cr	8.0-10.0
Co	9.0-11.0
W	11.5-12.5
Cb	0.75-1.25
Ti	1.75-2.25
Al	4.75-5.25
Hf	1.50-2.50
B	.010-.020
Zr	.20 maximum
Fe	.35 maximum
Cu	.10 maximum
Bi	.5 ppm maximum
Pb	5 ppm maximum
Se	3 ppm maximum
Th	To be reported
Te	To be reported

either high or low X-ray density, as well as with regard to size and locations. High X-ray density inclusions are characterized by particles lighter in density than the material being analyzed and therefore appear darker on the X-ray image. Low X-ray density inclusions are just the opposite and represent particles more dense than the material being analyzed. The acceptance criteria for X-ray inspection are presented in Appendix D.

2. Destructive Evaluation Procedures

In this portion of the study destructive evaluation including optical metallographic and electron microprobe analyses were utilized to identify the high and low density X-ray indications. These techniques were also used to establish relationships between the size of the X-ray indications and the defects which caused them. Both 1st and 2nd stage turbine blades rejected during X-ray inspection were selected for these examinations.

a. Optical Metallographic Analysis

Specimens for this analysis were selected on the basis of production X-ray films. The blades were sectioned to reveal the location of the X-ray defects and metallographic specimens were prepared. The preparation procedure included grinding on 180 to 600 grit silicon carbide papers using a water lubricant. This was followed by polishing on billiard cloth with Linde A abrasive (Al_2O_3 - 3 microns). Polishing was continued using a Syntron Automatic polisher, using gamel cloth with Linde B abrasive (Al_2O_3 - .05 micron). Fry's etch (150 ml H_2O, 50 ml HCl, 25 ml HNO_3 and 1g $CuCl_2$) was used as required to delineate microstructural features. Optical photomicrographs of the defect and surrounding areas were taken with a Bausch and Lomb Research II metallograph to document the analysis.

b. Electron Microprobe Analysis

Subsequent to the location and identification of the defects by optical metallography, specimens were subjected to electron microprobe analysis in order to determine the chemical compositions and the probable origin of the defects. A Phillips AMR/3 electron microprobe analyzer was employed for this study. This instrument has a beam resolution of less than 1 micron, and utilized three detectors for the identifications of microconstituents. It is capable of detecting the presence of elements with atomic numbers as low as Boron[3].

3. Analysis of Quality Control Reject Records

An analysis of quality control reject records was conducted in order to determine the relative importance of the defects included in the characterization study and to highlight those which would warrant more extensive evaluation in the mechanical property testing effort. This was accomplished by a compilation of the rejection records for the F-100 1st and 2nd stage turbine blades for the years 1975 and 1976. The study was comprehensive in that all causes for rejection were included in the analysis. For example, reject causes such as improper dimensions, core break and misruns (pour errors) were included in addition to the typical casting defects for which ranges of

acceptance criteria exist. In this way, a completely relative ranking in importance was achieved. The reject causes were characterized in a semi-quantitative manner as being either of major, intermediate or minor importance depending upon the number of production castings rejected for each particular reason.

4. Analysis of Results

In this portion of the program, the grain etch, FPI and X-ray data obtained for NDI reject castings and the production quality control data were classified. Histograms for each type of defect were prepared which included the various acceptance criteria. In the case of grain misorientation defects, the number of occurrences were plotted as a function of misorientation angle. In the case of dross inclusions, mold breakage inclusions and freckles, the number of occurrences were plotted as a function of the size of the indications. These histograms were used to establish the range and distribution of defect severity as encountered in typical production castings. For the production quality control data, a listing was made of all reject causes including an evaluation of their relative importance in terms of representing quality control problems. The histograms were employed in conjunction with the listing of reject causes to determine those important defects and their ranges for inclusion in the Task II mechanical property determinations.

B. Results and Discussion

In the present investigation defects were analyzed and classified in typical production castings in terms of type, size and location utilizing metallographic and nondestructive inspection techniques. This was done in order to insure that the types of defects and intensity levels incorporated specifically into mechanical property test specimens were typical of those observed in normal production operations. These defects included grain misorientation, porosity, macrosegregation, inclusions and surface cracking. The relative importance of these defects in terms of representing serious quality control problems was also established by analysis of NDI production records. The results of these characterizations are presented in the following sections.

1. Defect Characterization

a. Grain Misorientation

Grain misorientation includes diverging, or off-axis, grains which have their growth direction at an angle to the axis of the blade. This condition is generally caused by a random undesired nucleation event as solidification initiates at the chill plate. Improper positioning of the mold upon the chill or too low a pour temperature can also result in misoriented, or diverging grains. This type of defect is detectable during grain etch inspection and may be divided into three major categories: (1) diverging axis grains, (2) diverging adjacent grains and (3) emergent grains. Examples of all three types were found in the Task I study.

i. Diverging Axis Grains

This defect is primarily a misorientation of the grain in relation to the axis of the blade. Blade grain etch inspection standards permit one grain at an angle of up to 15° to the blade span. The most severe case of a diverging axis grain is found when a nucleation event occurs at the leading or trailing edge, resulting in a 90° misorientation. An example of a typical diverging axis grain is shown in Figure 3a.

Of the 254 grain etch reject castings studied in Task I, 84 blades containing diverging axis grains were observed. Of this total, 33 were 1st stage and 51 were 2nd stage blades. The defect distribution results for both blades were similar and are shown in the combined histogram of Figure 4. Here the frequency of the diverging axis grains are plotted as a function of misorientation angle. A total number of 174 diverging axis grains were recorded for the 84 blades in this study indicating that each blade contained one or more defects. A maximum occurred in the distribution at 45°. For this particular defect, an increase of 5° of divergence in the acceptance criteria would eliminate approximately 12% (20 out of 174) of the observed defects. This figure could represent a substantial improvement in yield accomplished by a small increase in the specifications. In the specific population studied in this program for example, if the 20 particular defects occured as single observations on specific blades, approximately 24% (20 out of 84) of the blades would not be rejected. This figure, of course, would be modified depending on the occurrences of other defects in the blades.

ii. Diverging Adjacent Grains

Failure criteria for diverging adjacent grains are defined by the condition wherein the included angle between two adjacent grains or their primary dendrites exceeds 20°. An example of this type of defect is shown in Figure 3b. Competitive growth of these grains during solidification will sometimes cause the more favorably oriented grain to grow over the less favorably oriented grain.

Thirteen castings containing rejectable divergent adjacent grains were observed among the 254 blades rejected at grain etch in Task I. Each defect appeared as a single occurrence and ten cases were found in the 1st stage blade and three cases in the 2nd stage blade. Combining these results and plotting the frequency of occurrence as a function of the included angle indicated a continuous decrease in frequency with increasing angle, Figure 5. The small sample size does not permit this result to be generalized to larger populations, but does indicate that this problem occurs in a substantially smaller number of blades than does the case of simple divergence. For the distribution shown in Figure 5 a 30% (4 out of 13) improvement in yield could be expected for an increase of 5° in the acceptance specifications.

iii. Emergent Grains

The emergent grain is a special case of a divergent axis grain. The distinguishing characteristic of an emergent grain is that it terminates at the leading or trailing edge of the airfoil, rather than at the blade tip or root. This condition is cause for rejection if the grain boundary intersects the edge of the airfoil at an angle of 10° or more. An example of an emergent grain is shown in Figure 3c.

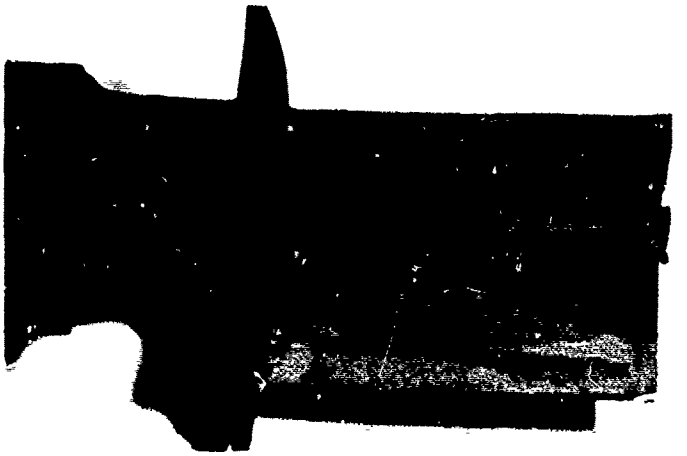

a. Diverging Axis Grain

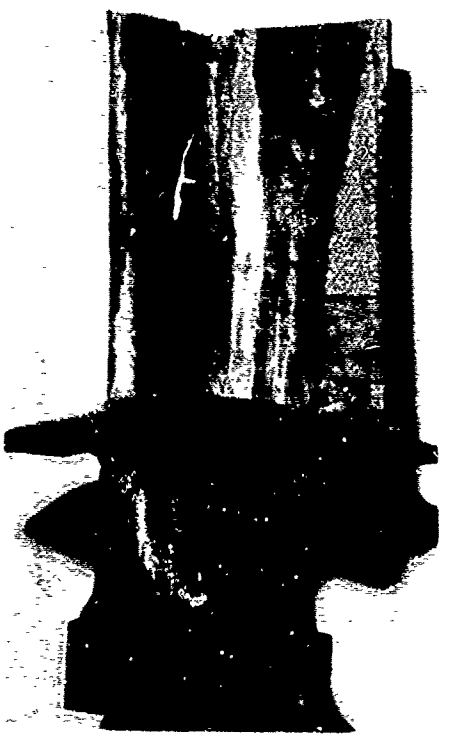

b. Diverging Adjacent Grain

c. Emergent Grain

Figure 3. Examples of Grain Misorientation Defects in D.S. Components.

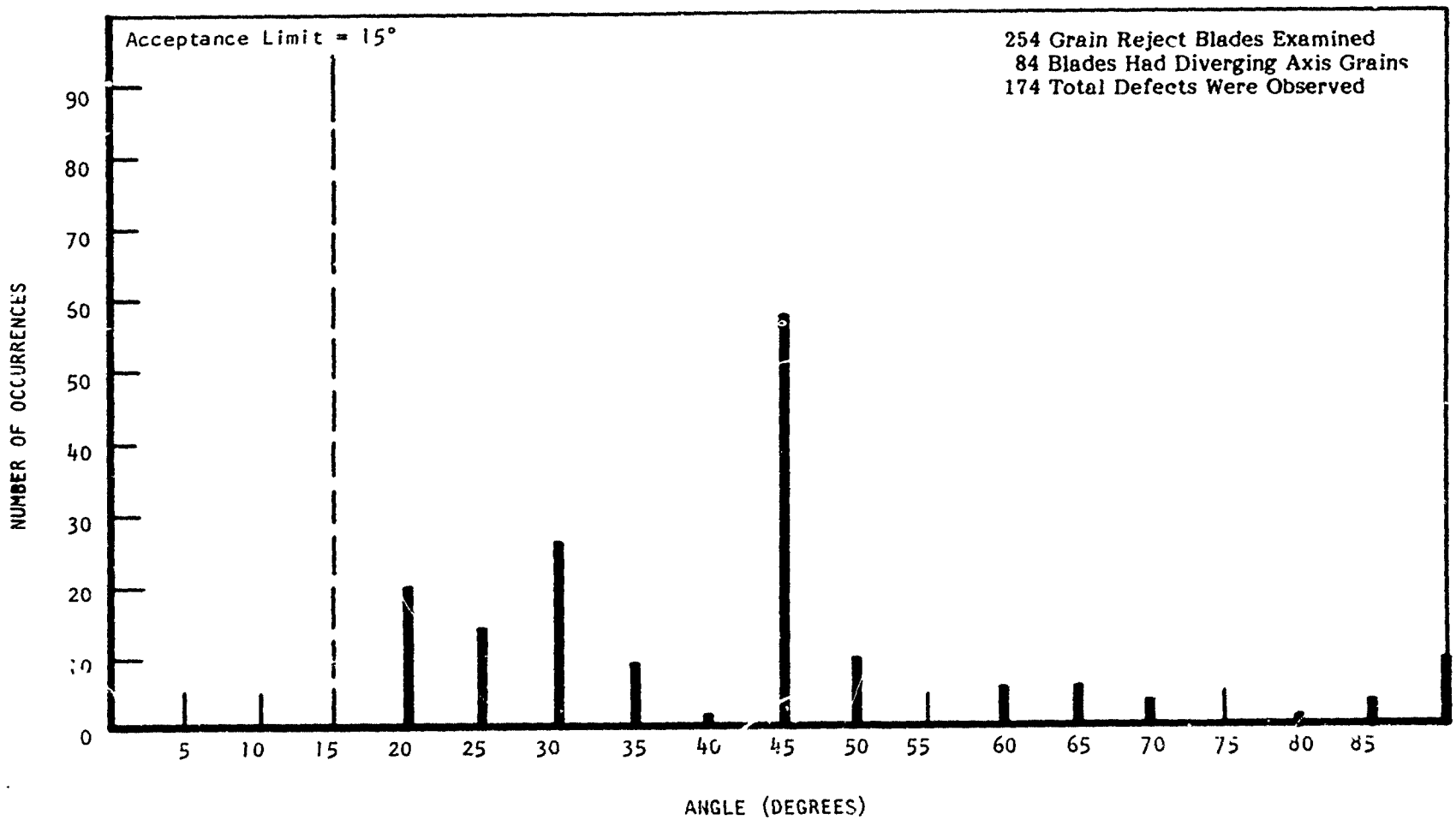

Figure 4. Histogram Showing Number of Observed Diverging Axis Grains as a Function of Misorientation Angle.

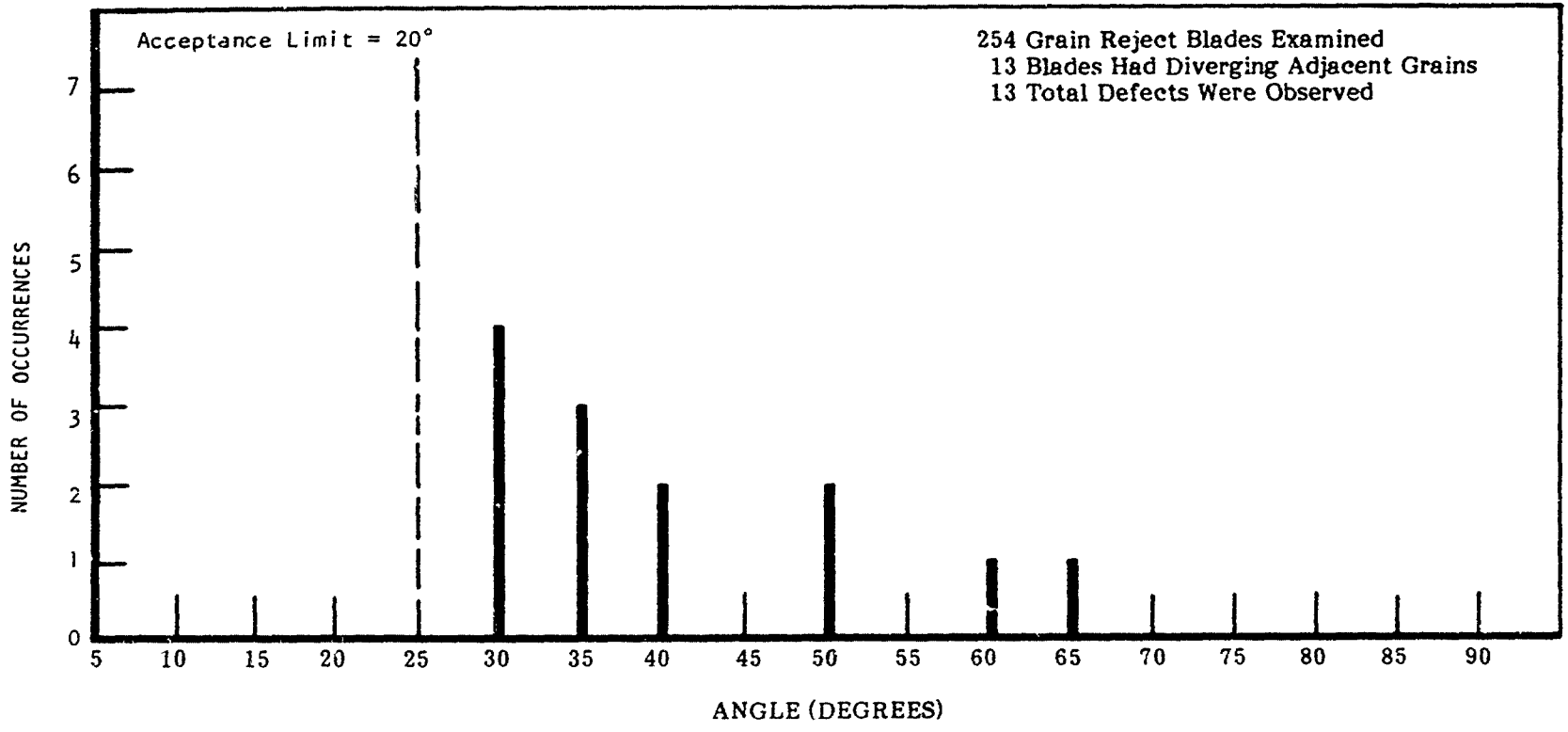

Figure 5. Histogram Showing Number of Observed Diverging Adjacent Grains as a Function of Included Angle.

A total of 126 castings containing rejectable emergent grains were observed during the Task I study. All of these defects occurred as single observations in specific blades. Of these, 45 occurred in the 1st stage blade and 81 occurred in the 2nd stage blade configuration. In a number of cases it was noted that a reject blade had both divergent and emergent types of grain misorientation defects. The distribution results for both blades were similar and are shown in the combined histogram of Figure 6. Peaks in the frequency distribution were observed at 15^0, 30^0, and 45^0. For this distribution a 5^0 increase in the acceptance criteria would result in a 15% (38 out of 126) improvement in yield.

b. Porosity

Gas porosity and microshrinkage were included in this program because these defects have occurred with regularity during D.S. production operations. Their presence is particularly troublesome during process development efforts associated with modified casting configurations or entirely new components. As such, both FPI and X-ray reject criteria are quite specific about the acceptance levels for these defects (see Appendices III and IV). However, during the conduct of the Task I - Defect Characterization portion of the program porosity and microshrinkage were not noted as causes for rejection of F-100 production turbine blades. As such it was not possible to obtain a distribution or size range for these defects in terms of production castings.

c. Macrosegregation

Macrosegregation defects in D.S. castings can be grouped into two different types: freckles and major alloying element segregation. These defects were analyzed separately in Task I.

i. Freckles

Freckles, or surface recrystallization, consist of equiaxed surface grains which appear on D.S. castings. Their presence is not only a cosmetic problem but since they are of different chemical composition than the bulk alloy, mechanical property effects may be expected. These defects result when low density interdendritic liquid is trapped by an overlying layer of high density liquid of the bulk alloy composition. This is a density inversion, which is eventually relieved by molten metal flow which exchanges high density for low density liquid. This flow perturbs the liquid-solid interface compositional equilibrium, resulting in the freckle segregation defect. Two examples of freckle defects are shown in Figure 7.

Freckles are detected at grain etch inspection where defects up to 1/32" (0.8 mm) are permitted. During the course of the Task I defect study none of the production F-100 blades were rejected for this cause. However, castings rejected because of grain misorientation were checked for freckles. Of the 254 castings rejected for grain etch defects, 29 1st stage blades contained freckles and 25 2nd stage blades contained the defects. Large numbers of these defects were observed on the castings but in all instances they were small enough to fall below the required acceptance level. The separate distributions for these freckle defects are shown in the histograms of

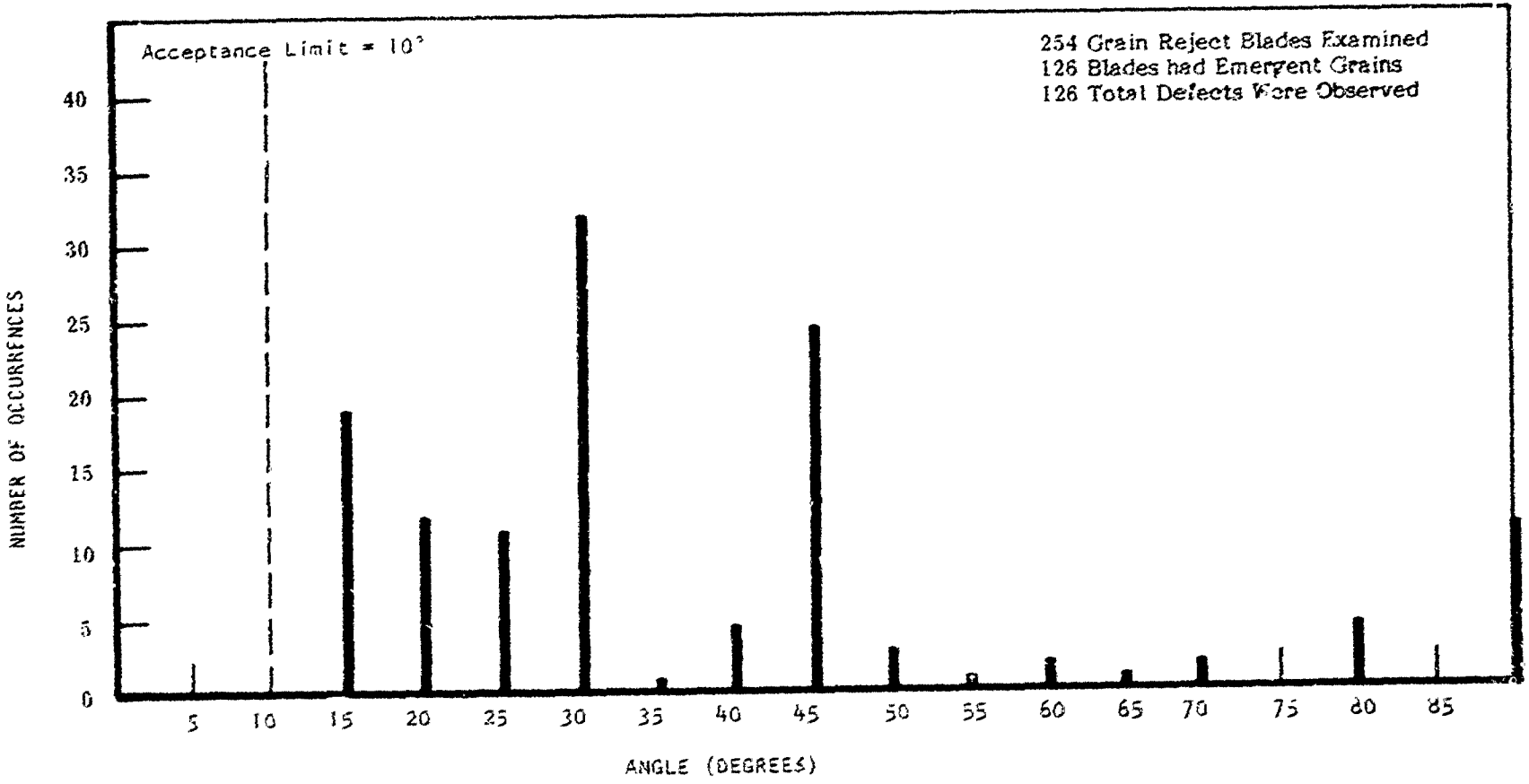

Figure 6. Histogram Showing Number of Observed Emergent Grains as a Function of Misorientation Angle.

Figure 7. Two Examples of Freckle Defects in D.S. Turbine Blades Occurring Near Airfoil-Root Fillet Radius. 50X Magnification

Figures 8 and 9 where frequency of occurrence are plotted as a function of freckle size for the 1st (Figure 8) and 2nd (Figure 9) stage F-100 blades. While the distributions are similar for both blades the larger number of freckles in the 1st stage blade, Figure 8, would suggest that their occurrences are strongly dependent upon the geometry and the casting process used for the components.

ii. Major Alloying Element Segregation

Major alloying element segregation is a complex function of casting geometry, alloy composition and manufacturing process. Areas can exist in castings in which the local composition is far different than that of the base alloy; this implies that the properties in these locations will also differ from those expected of the nominal alloy. In D.S. superalloys this type of segregation usually involves chromium and hafnium. It occurs when changes in section size result in momentary changes in the solidification rate. This disturbance of the solidification rate can cause deviations in the compositional equilibriums of the liquid-solid interface. These localized deviations from the equilibrium chemistry result in macrosegregation.

This type of segregation is usually avoided by using qualified master alloys which have alloying element levels balanced to insure that the level of any element will remain within the PWA-1422 specification in spite of macrosegregation. Efforts in the present investigation included analysis of the results of X-ray fluorescence tests conducted on three different locations in each of three different blades per part configuration per master heat of PWA-1422. There were no instances of major element macrosegregation encountered in the Task I study.

d. Inclusions

Inclusions are nonmetallic particles which become embedded on the surface or within the casting during the solidification process. Inclusions may be characterized as dross or mold breakage, distinguishable by composition, morphology and location within the casting. Examples of both types were encountered during the Task I study.

i. Dross Inclusions

Dross is a reaction product between reactive elements in the molten alloy and a source of oxygen. Aluminum, titanium and hafnium within the melt can react with oxygen in the furnace atmosphere or evolved from the core, mold or crucible to form dross. All hafnium-bearing cast nickel-base superalloys are particularly susceptible to hafnium-oxide type dross inclusions. Because the density of hafnium oxide is very similar to that of the molten alloy the dross particles tend to remain within the part as inclusions rather than floating or sinking to innocuous locations in the casting. D.S. casting operations are particularly susceptible to dross formation because the extended process times allow ample opportunity for reaction to take place between hafnium and oxygen.

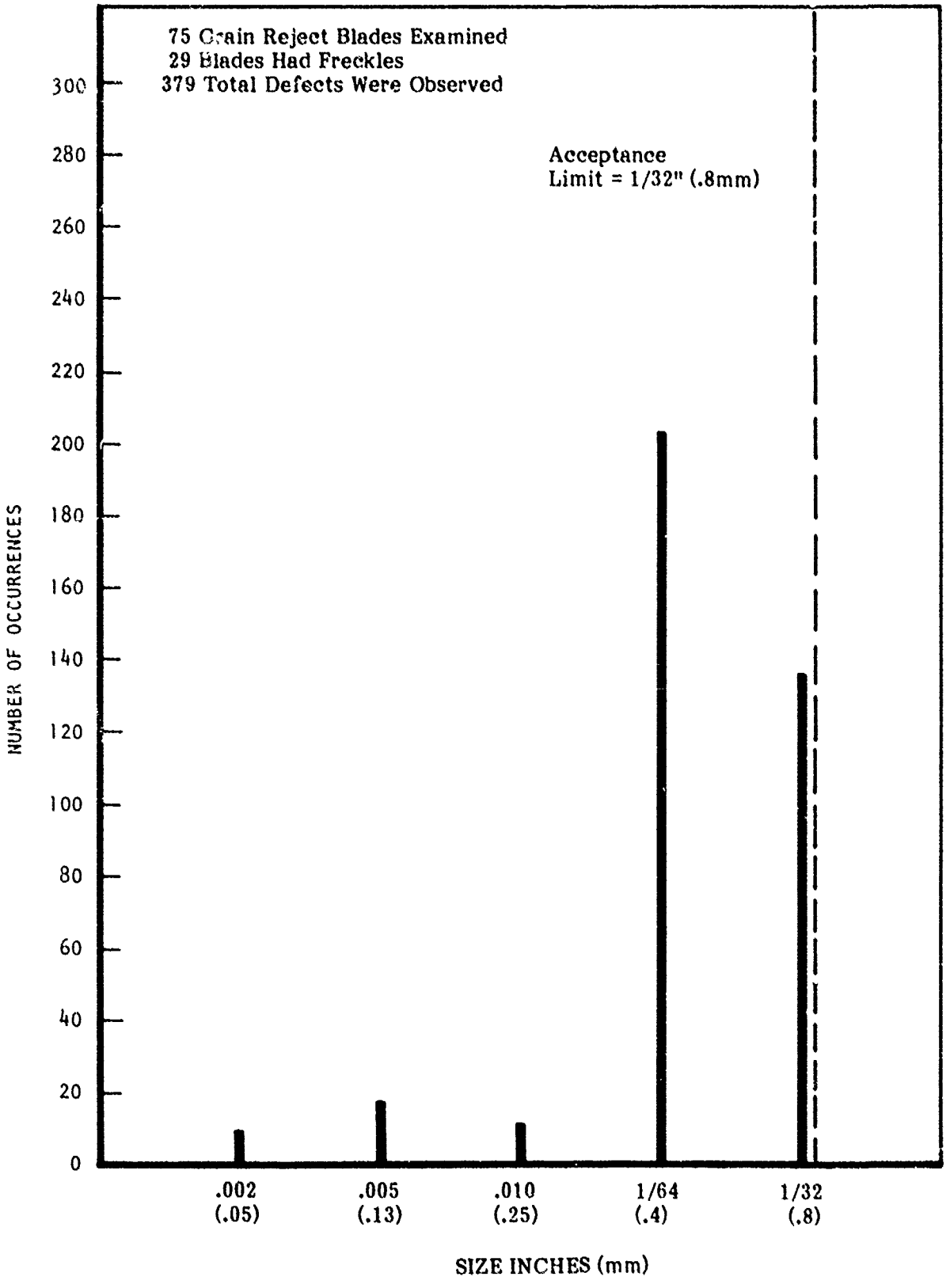

Figure 8. Histogram Showing Number of Observed Freckle Defects as a Function of Size in F-100 1st Stage Blades.

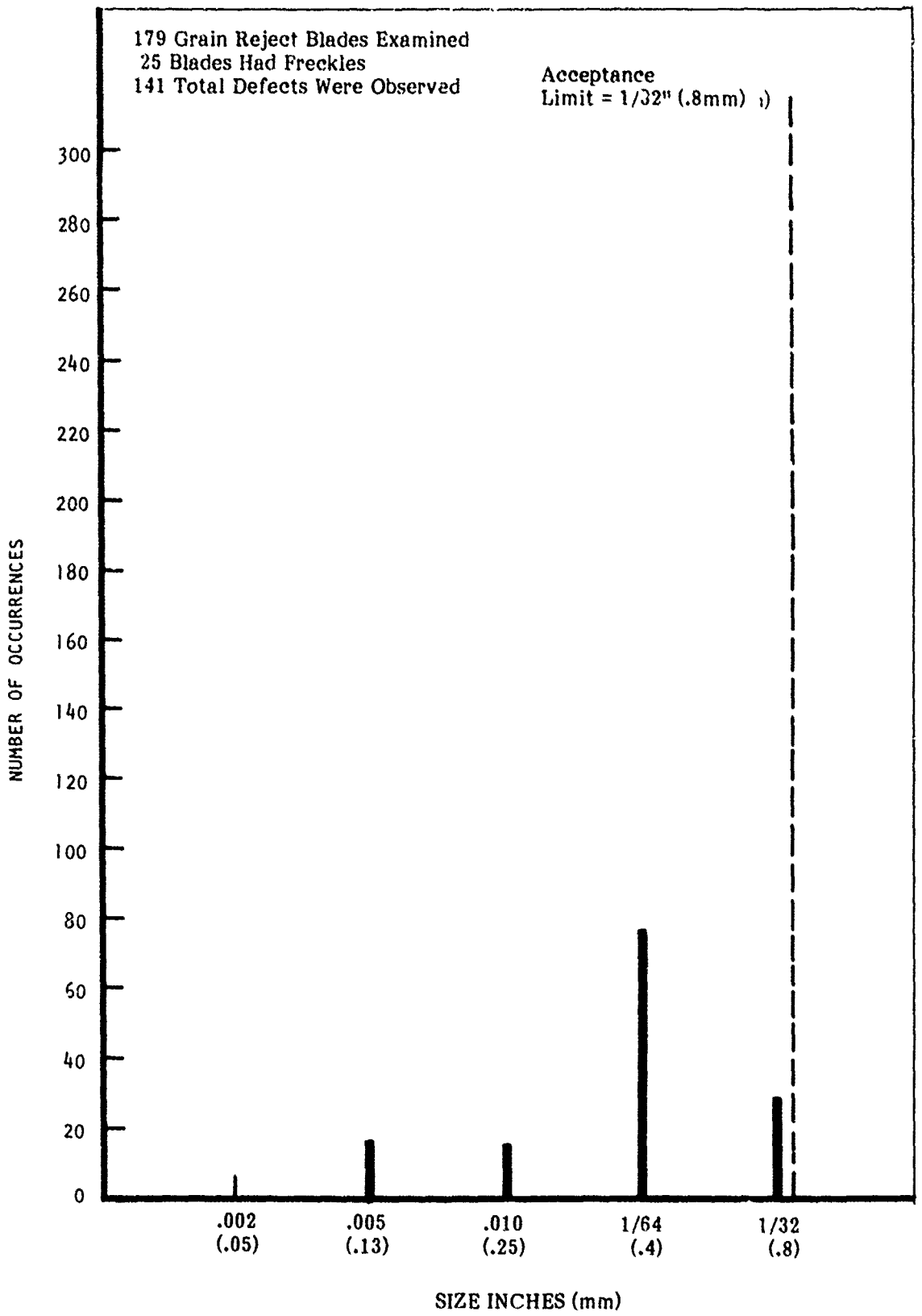

Figure 9. Histogram Showing Number of Observed Freckle Defects as a Function of Size in F-100 2nd Stage Turbine Blades.

Dross is usually surface connected and is therefore detectable by fluorescent penetrant inspection. It has a filamentary or linear shape which can generally distinguish it from porosity or other defects which present a point indication during FPI. It has been observed that more than 90% of all FPI indications are dross inclusions. Because these are surface indications efforts are usually made to repair parts which are initially rejected. Reinspection operations including dimensional checks are then conducted on the repaired components.

A total of 366 FPI reject blades were examined in Task I prior to any repair operations. Of these 111 were 1st stage blades and 255 were 2nd stage blades. A combined plot of frequency versus defect size for the FPI indications is shown in the histogram of Figure 10. Over 2000 indications were observed, the majority of which were below 0.010" (.25 mm) in size. Indications smaller than this are regarded as non-interpretable and are included in Figure 10 only to indicate the size range observed in production castings. As shown in the complicated FPI reject criteria in Appendix III castings are rejected primarily on the basis of the proximity of small indications to one another in critical areas of the blade and not on the absolute size of the defects. These areas include the leading and trailing edges of the airfoil and the platform-airfoil fillet. Partial relaxation of these criteria would require that clusters of small dross inclusions near the gage edges of the test specimen shown in Figure 2 have little detrimental effect on mechanical properties.

ii. Mold Breakage Inclusions

Mold breakage inclusions result from the flaking or spalling of granules of the mold into the melt. This can occur through errors in mold formulation, poor wax assembly, loss of control of mold making operations or as the result of inadequate raw materials in the mold. Breakage inclusions are not generally surface connected and are detectable by X-ray inspection where they reveal themselves primarily as low X-ray density indications. These defects are identified by their blocky, non-linear appearance, in contrast to the linear or filamentary appearance of dross inclusions and by their distinctive chemistry as revealed by electron microprobe analysis.

Characteristically, mold breakage inclusions are aluminum oxide or Al-Si-Zr rich particles, which are similar in composition to the mold material. A typical X-ray photo and accompanying light photomicrograph of a mold breakage inclusion is presented in Figure 11. Note that the X-ray photo is a positive print of the original X-ray negative. Electron microprobe analysis identified this low density inclusion to be an aluminum rich particle, typical in composition to production D.S. mold material. It is estimated that in excess of 90% of all production X-ray defects are due to similar mold breakage inclusions. However, in a small number of instances high X-ray density inclusions are also cause for rejection. These inclusions are typically hafnium oxide dross particles which have become embedded within the casting. An example of this type of high X-ray density hafnium oxide inclusion is shown in Figure 12.

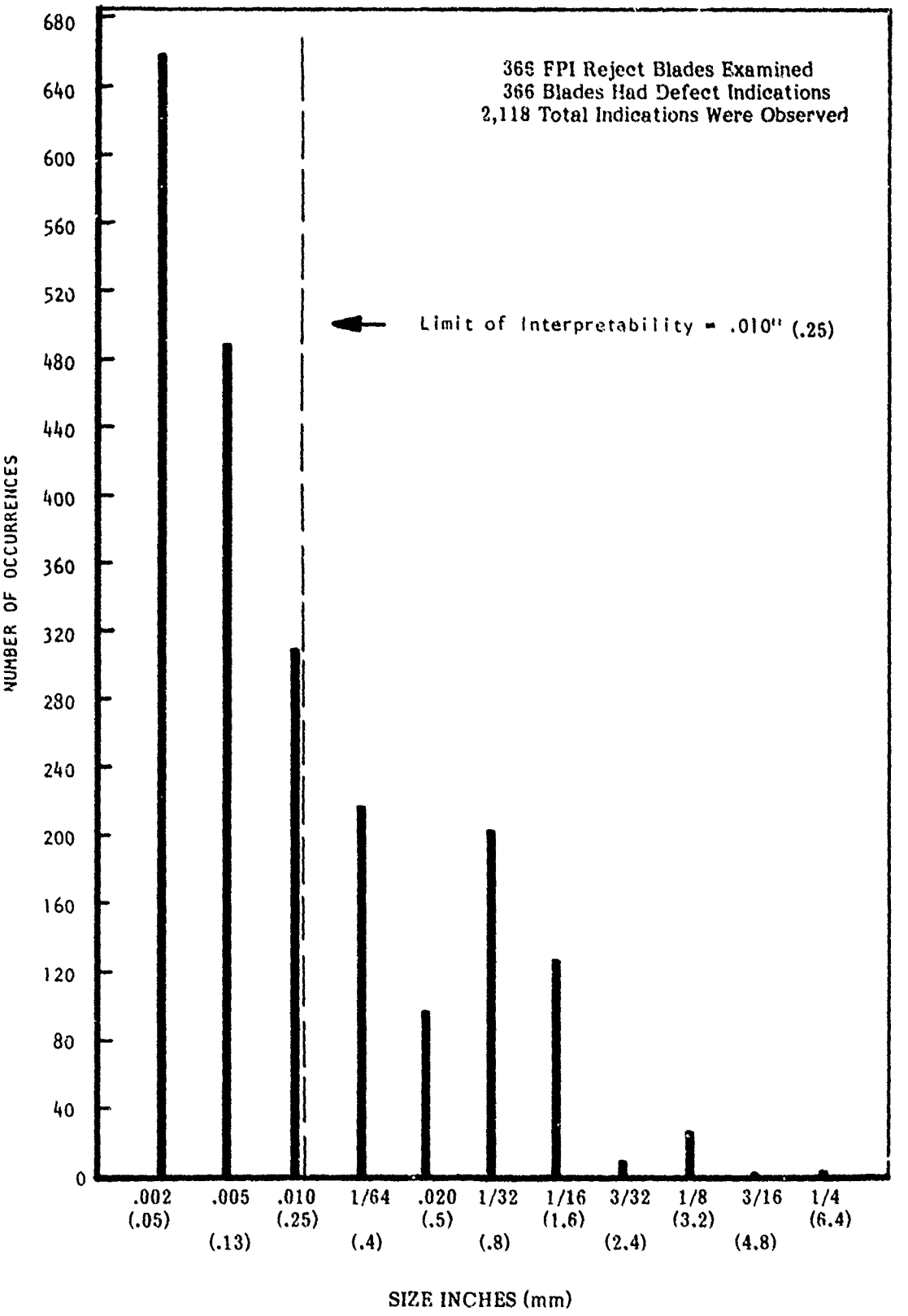

Figure 10. Histogram Showing Number of Observed Fluorescent Penetrant Indications as a Function of Indication Size.

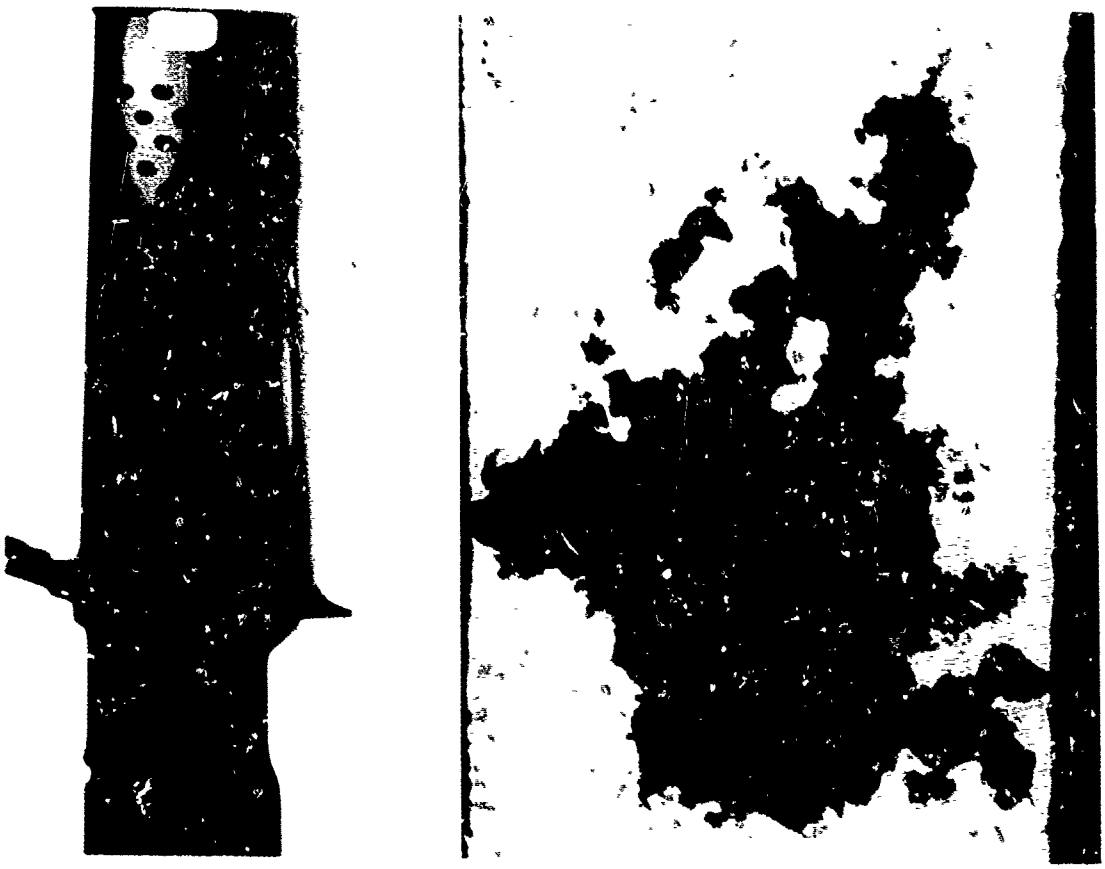

Figure 11. Positive of X-Ray and Photomicrograph of a Low X-Ray Density inclusion.

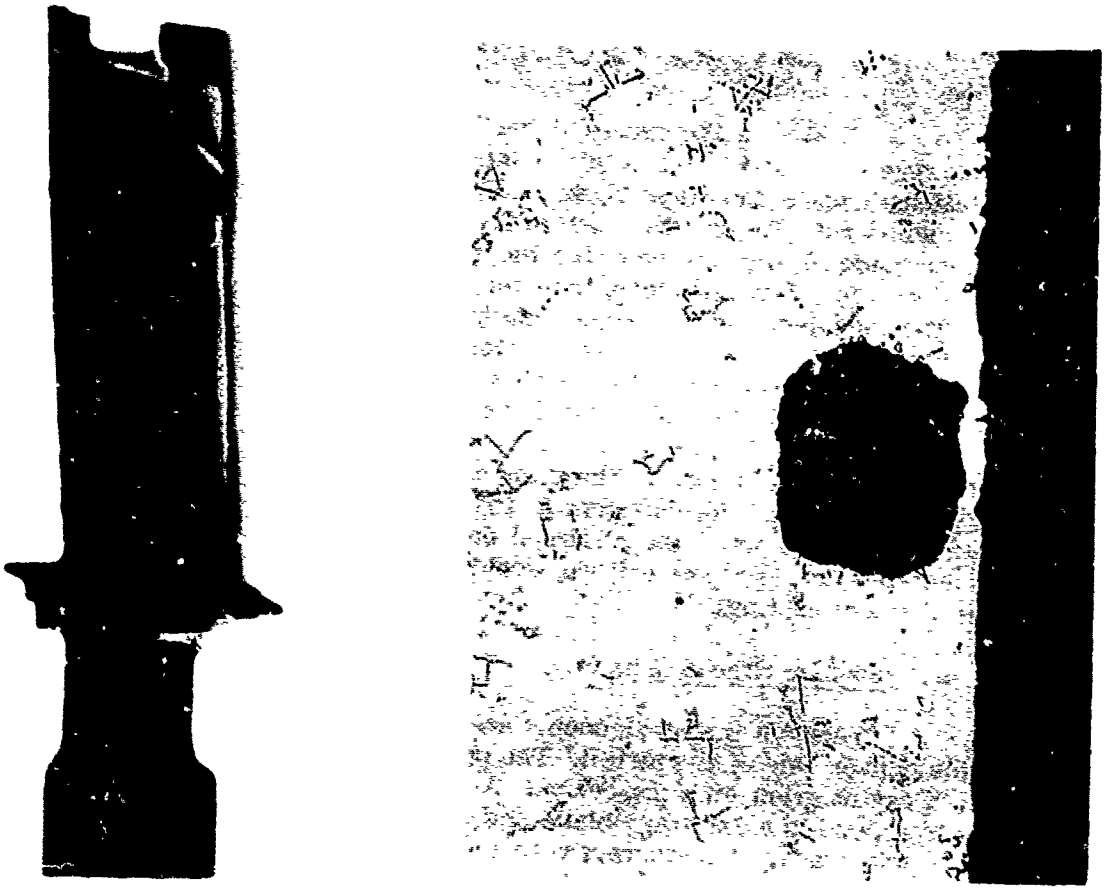

Figure 12. Positive of X-Ray and Photomicrograph of a Low X-Ray Density Inclusion.

During the course of the Task I investigation a total of 110 X-ray reject blades were examined. This total included five 1st stage blades (exhibiting low density inclusions) and 66 2nd stage blades (35 exhibiting low density and 31 exhibiting high density inclusions). The blades rejected for high density inclusions each contained one defect per blade as was the case for the majority of the blades rejected for low density inclusions. In a few instances, however, more than one inclusion was observed per blade. The remainder of the reject blades exhibited defects such as cracks or excess metal within core passages, the latter of which appeared as high density indications. The distribution histograms of frequency of occurrence versus defect size for both blades combined are presented in Figures 13 (low X-ray density inclusions) and 14 (high X-ray density inclusions). For comparative purposes the reject criteria have also been included on these figures. These indicate that acceptance limits depend upon part location and are much more strigent at the leading and trailing edges and the fillet radii. The size distribution of the observed defect indications does suggest however that slight modification in reject criteria could result in the acceptance of substantial percentages of reject castings.

e. Surface Cracks

Cracks in D.S. components are generally intergranular and observed at the tip of the convex side of the airfoil. The presence of these cracks can be detected during FPI, X-ray or grain etch inspection. A total of 34 cracks were observed during the Task I effort, one in a 1st stage blade and 33 in the 2nd stage blades. Each blade contained a single crack. A histogram with the number of occurrences plotted against the observed crack length is shown in Figure 15. Since cracks are not allowed to be repaired, the presence of any crack is sufficient cause for rejection. The occurrence of cracking is most commonly attributed to loss of furnace control (e.g., withdrawal rate, high furnace leak rate) during casting. Cracking in blades is generally eliminated when proper process control is restored. Engine manufacturers generally regard any part with an identifiable crack as rejectable. The situation exists, therefore, that design modifications such as the use of a damage tolerant concept would probably be required to relax the current requirement so that certain cracked castings would be acceptable.

2. Relative Defect Importance

Directionally solidified superalloy castings are inspected by a number of different methods and at various stages during their production Production experience has indicated that air cooled D S. casting rejections can be attributed to a variety of causes including:

- o Cracks
- o Dross Inclusions
- o Mold Breakage Inclusions
- o Grain Etch Defects

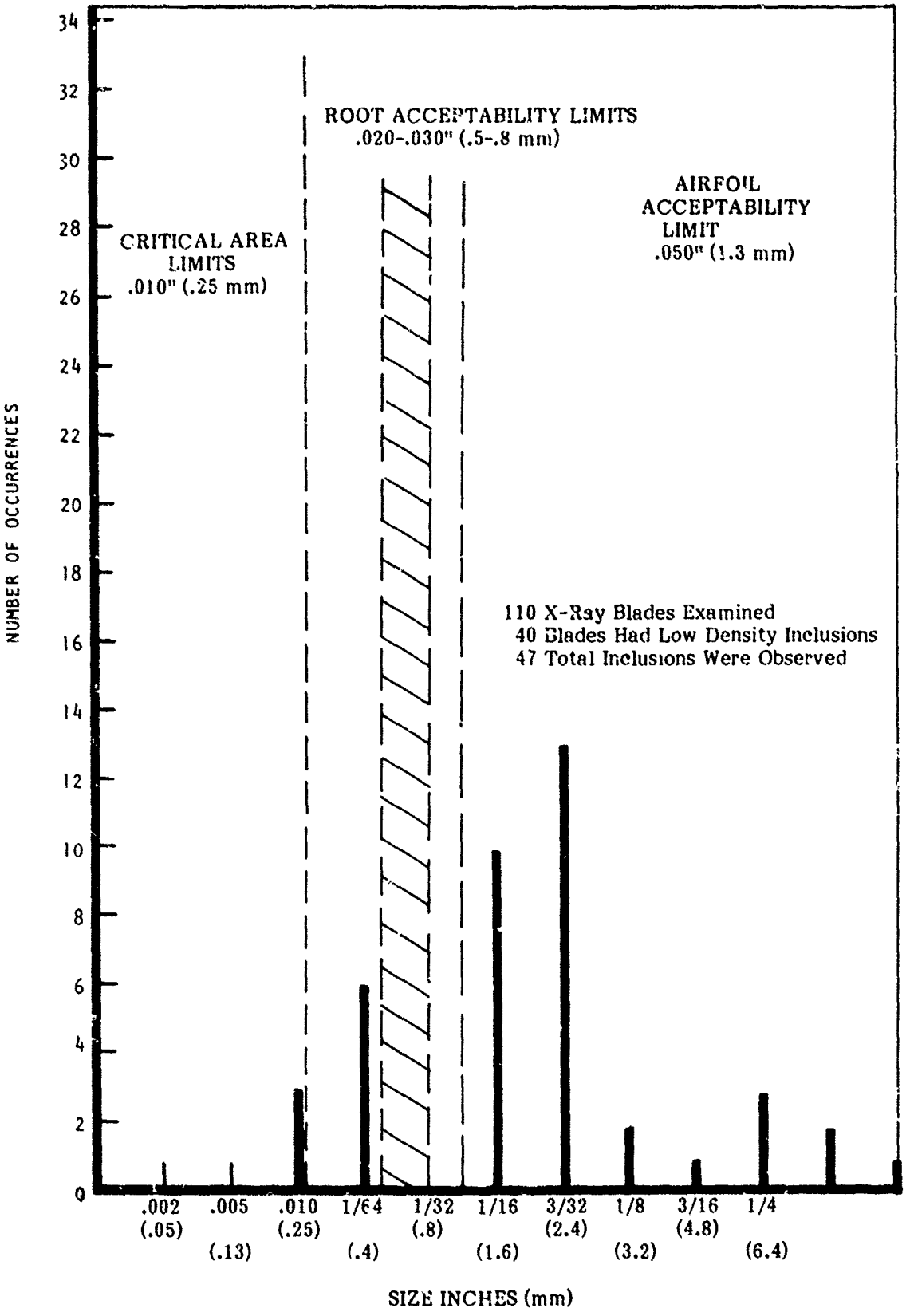

Figure 13. Histogram Showing Number of Observed Low X-Ray Density Inclusions as a Function of Indication Size.

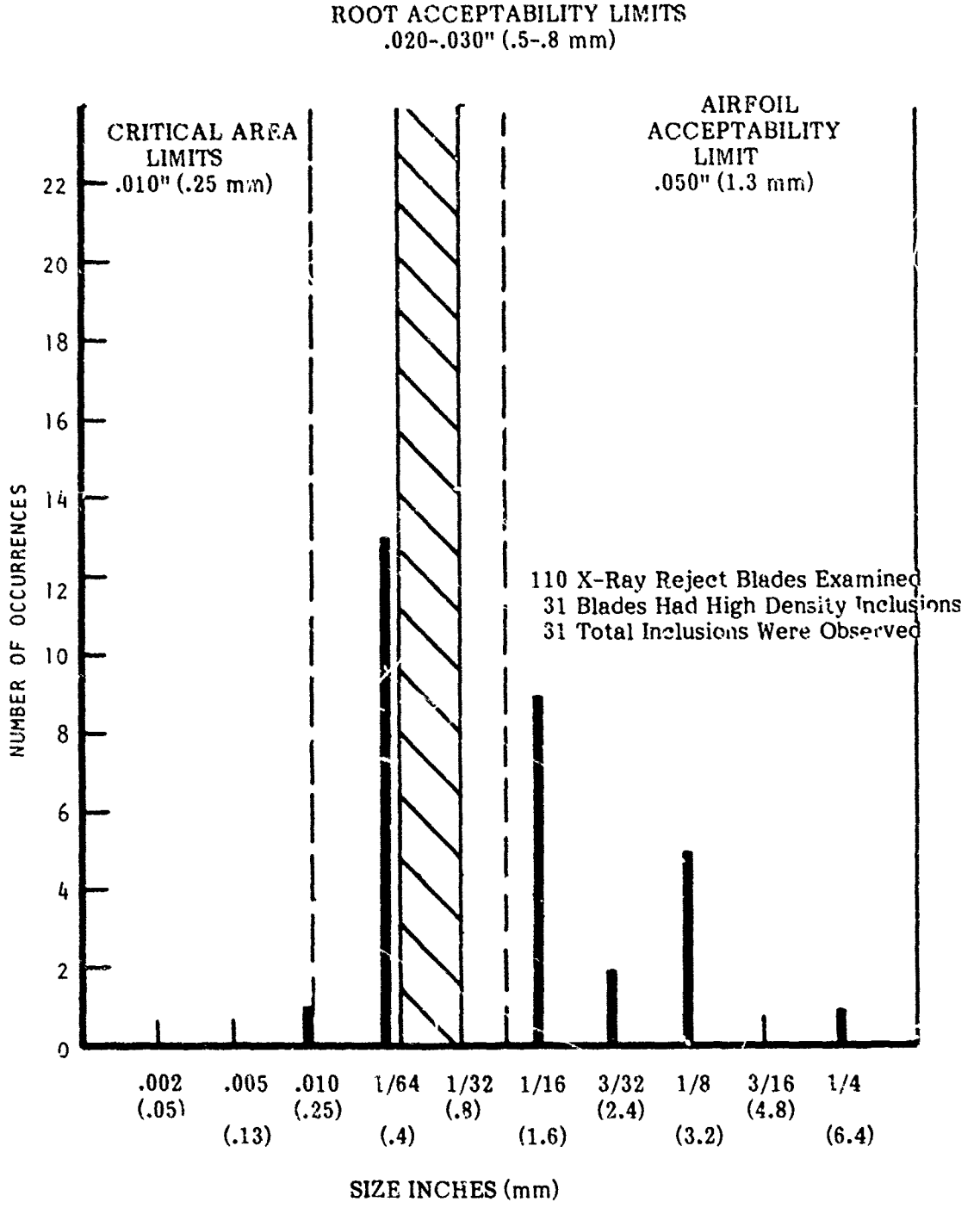

Figure 14. Histogram Showing Number of Observed High X-Ray Density Inclusions as a Function of Indication Size.

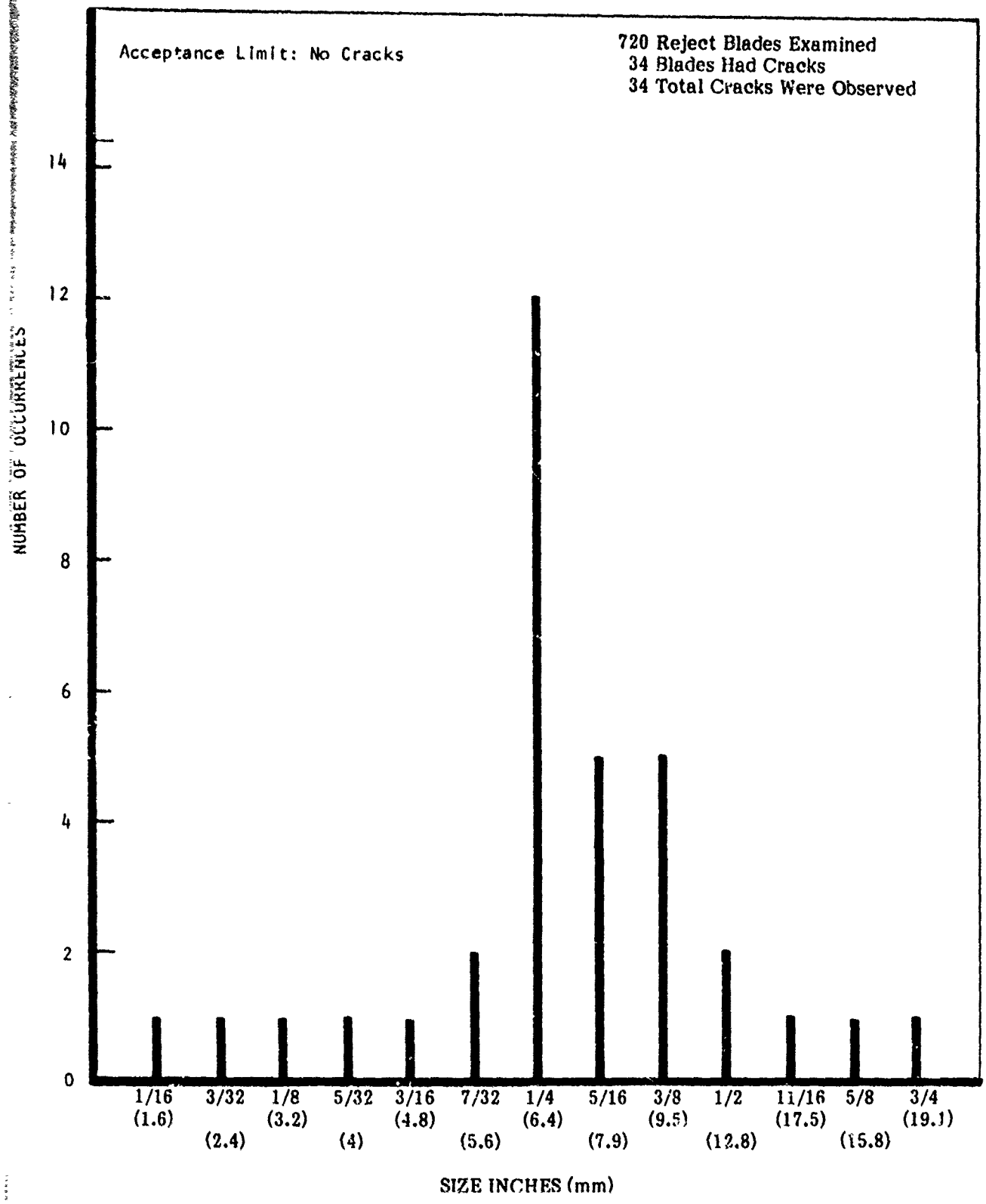

Figure 15. Histogram Showing Number of Observed Cracks as a Function of Crack Length.

- o Handling Damage
- o Imperfect Pattern
- o Improper Dimensions
- o Misruns (Pour Errors)
- o Missing Cooling Passage Post
- o Shrinkage
- o Excess Metal
- o Wall Thickness Variation
- o Core Break

These defects are not listed in order of importance. The grain etch defect category includes grain axis divergence, adjacent grain divergence, grain emergence and freckles.

In a number of the above instances it is recognized that relaxation of the acceptance criteria is not possible. This group includes handling damage, imperfect patterns, improper dimensions, misruns, missing cooling passage posts, excess metal, wall thickness variation and core break. These items reflect on the basic integrity and design of the component and in fact act to define a specific part. As such, alterations could not be made in the acceptance criteria for these defects.

The relative importance of the defects included in the Task I characterization study was established in comparison to the overall listing of rejection causes. This was accomplished by an analysis of the rejection records for the F-100 1st and 2nd stage turbine blades for the years 1975 and 1976 available at the Metals Plant of the TRW Turbine Components Division. The results of this analysis are shown in Table 4. The defect types were characterized as either of major, intermediate or minor importance. For both blade configurations dross inclusions represented the single major cause of reject castings. As indicated in the Task I study, surface connected dross inclusions are detectable by FPI inspection. The reject criteria are complicated and are based primarily on the proximity of small indications to one another in critical areas on the blade. The economic advantages associated with the establishment of a rational basis for FPI reject criteria can readily be appreciated.

After dross inclusions, mold breakage inclusions and grain etch defects represented the next most serious causes for casting rejections. Both the mold breakage and grain etch defects represented problems of a comparable magnitude. In terms of grain etch, diverging axis grains and emergent grains were significantly more of a problem than diverging adjacent grains or freckles. In fact, over the two year period included in the results in Table 4 freckles rarely resulted in casting rejections. Although mold breakage inclusions and grain etch defects were not as numerous as those resulting from dross, appreciable numbers of reject castings could be recovered if more tolerant rejection criteria were in effect.

TABLE 4

SUMMARY OF REJECTION RATE DATA FOR F-100 1st AND 2nd STAGE TURBINE BLADES
JANUARY 1975 - DECEMBER 1977

Cause for Rejection	1st Stage Blade	2nd Stage Blade
Cracks		
Dross Inclusions	X	X
Mold Breakage Inclusions	O	O
Grain Etch Defects	O	O
Handling Damage		
Imperfect Pattern		
Improper Dimensions	O	O
Misruns		
Missing Post		
Shrinkage		
Excess Metal		
Wall Thickness		O
Core Break		

Symbol	Importance
None	Minor
O	Intermediate
X	Major

The remainder of the important reject causes included inaccurate dimensions and wall thickness problems. These items were not within the scope of the present investigation. The other causes for casting rejection listed in Table 4 were all of relatively minor importance.

C. Summary

The Task I - Defect Characterization study was conducted to characterize and classify defects in typical production castings (F-100 1st and 2nd stage turbine blades) of D.S. PWA-1422 superalloy in terms of type, size and location. These defects included grain misorientation, porosity, macrosegregation, inclusions and surface cracking. The relative importance of these defects was established by analysis of NDI production records.

The grain misorientation type defect included diverging axis grains, diverging adjacent grains and emergent grains. While all three types were observed the diverging axis and emergent grain defects were more numerous. The misorientation angle distributions for the three defects indicated that as small an increase as 5^{o} in the acceptance criteria could result in substantial reductions in the numbers of castings rejected for misorientation defects (up to 30% depending upon the defect). These reductions would result in appreciable cost savings for the D.S. process.

During the conduct of the defect characterization, porosity and microshrinkage were not noted as causes for rejection of F-100 production turbine blades. As such it was not possible to obtain a distribution or size range for these defects. Macrosegregation defects in D.S. castings occur as either freckles or major alloying element segregation. While numerous freckles were observed during grain etch inspection, none of these were large enough to cause rejection. This indicated that freckles do not represent a production control problem at the present time. Since major alloying element segregation is controlled through the proper qualification of master metal, it was not observed during the Task I defect characterization of production castings.

Inclusions occur as dross or mold breakage and numerous examples of each were encountered. Dross inclusions are usually detectable by FPI. Complicated rejection criteria now exist for these defects based primarily on their proximity to one another in critical areas. The establishment of a rational basis for FPI rejection criteria could result in: (1) increased castings yields and (2) decreased inspection costs through more simplified procedures. Both of these would contribute to process economy. Mold breakage inclusions are usually detectable by X-ray inspection where they reveal themselves primarily as low density indications. Acceptance limits depend upon part location and are much more stringent at the leading and trailing edges and fillet radii. The size distribution of the observed defects does suggest that slight modifications in reject criteria could result in the acceptance of substantial percentages of reject castings.

Surface cracks were observed at intergranular regions at the tips of the convex sides of airfoils Weld repair operations are not allowed for cracks and their presence is sufficient cause for rejection. Since engine manufacturers generally regard cracked parts as having failed it would not be possible to relax the current acceptance requirements unless damage tolerant design concepts were applied to the F-100 engine.

The relative importance of these defects was established by an analysis of the rejection records for the F-100 1st and 2nd stage blades for the years 1975 and 1976. Dross inclusions represented the single major cause of rejection. Mold breakage inclusions and grain etch defects including diverging axis and emergent grains represented the next most serious problems. In comparison to these, the remainder of the casting defects studied in Task I were of minor significance. These results thus identified which specific defects would be most responsive to more tolerant criteria in terms of increased casting yield.

SECTION IV

TASK II - MECHANICAL PROPERTY TESTING

A. Experimental Procedures

Test specimen design and preparation efforts were directed towards achieving a simulation of the conditions which exist in production D.S. components. For example, the F-100 1st and 2nd stage blades are thin walled, air cooled components. The test specimen configuration was therefore selected to approximate the wall thickness of such a blade. The following sections contain detailed descriptions of the techniques used for the preparation and evaluation of the mechanical property test specimens.

1. Defect Selection

The defects selected for evaluation in Task II were chosen on the basis of their importance as reject causes in production D.S. components. The Task I evaluation of production quality control records indicated that dross inclusions, followed by mold breakage inclusions, grain etch defects, improper dimensions and wall thickness variations were the most frequent causes for rejection of D.S. parts. For those cases in which parts were out of dimensions, or which had wall thickness deviations, reject criteria reflect conditions of unsound aerodynamics and restricted air cooling and as such the acceptance criteria cannot be relaxed. These particular reject causes were not included in the test program. A defect type included in the Task II evaluation, although not appearing as important in terms of production quality control problems, was microshrinkage. This defect can often occur in new casting designs and extensive casting development effort, both in time and expense, is often required to eliminate the problem. This high development cost is translated into higher costs for sound production castings. Both freckles and surface cracks were included in the Task I characterization studies conducted on production D.S. castings but were not included in the Task II test program. Freckle indications were observed on a number of production castings but in all instances were within the current acceptability limits. Because the freckle defects do not represent a major quality control problem they were not included in the test program. Surface cracks were observed on rejected production blades and at present are considered as immediate causes for rejection. Surface repair operations are not allowed for these defects. It was felt that relaxation of the cracking requirement could only be accomplished within the framework of a damage tolerant design concept and this was beyond the scope of the present investigation. In summary, the defects selected for mechanical property evaluation included dross inclusions, mold breakage inclusions, microshrinkage and grain misorientation defects (diverging axis, diverging adjacent and emergent grains).

For each defect included in the test program, three severity levels were chosen for evaluation. These were defined as a mild, intermediate or severe condition, and were generally selected on the basis of the ranges of severities noted in the Task I effort as well as upon nondestructive evaluation standards for production castings. The slight condition, for example, was chosen to represent a situation near or a little worse than the usual limit for part rejection. It was recognized that although each particular

category was in itself fairly broad in terms of magnitude, each clearly represented a particular degree of defect severity. Problems were experienced with specimens containing diverging axis and diverging adjacent grain defects in that misorientation angles appreciably above current rejection limits resulted in grain intersections along test specimen edges, thus representing an emergent grain condition. To avoid the occurrence of emergent grains in these specimens, the limiting criteria for the severe category included the most severe condition which could be achieved without encountering grain emergence. The intermediate and mild conditions were then established on the basis of this limiting condition. All of the various severity criteria established for all the defects are presented in Table 5 and typical examples of each defect at each severity level are illustrated in Appendix E.

2. Specimen Preparation

In addition to incorporating the desired casting defects within test specimen gage sections, the second major objective of specimen preparation efforts included producing gage sections processed in a manner similar to that of production castings. To accomplish this, the mold shake out and handling procedures used for specimen preparation followed current blade production practice. This insured that surface quality would be similar to that of cast turbine blade components.

a. Material

A production qualified heat, JW-6048, of PWA-1422K (MAR-M200 + hafnium) was procured for use in Task II of this program. The heat conformed to all PWA-1422K specification requirements. The certified chemical analysis is presented and compared to the specified composition ranges in Table 6. This heat was qualified for use in blades and vanes and the required mechanical property evaluations consisted of creep rupture tests performed upon specimens machined from the airfoils of these components. The castings used for mechanical property qualification tests were cast as solid parts, rather than as production, thin wall, hollow components in order to facilitate machining of the test specimens. The qualification test results are presented in Table 7 which includes the PWA-1422K specification requirements.

b. Specimen Configuration

The specimen configuration used for mechanical property evaluation was designed to simulate the wall thickness and length of a typical production D.S. turbine blade. The original specimen design incorporated a uniform specimen thickness of .040" (0.10 cm). This specimen was found to be suitable for 1400°F (760°C) stress rupture tests, but grip failures occurred during the course of 1400°F (760°C) tensile tests. The test specimen was therefore revised to incorporate thicker grips while retaining the desired gage section thickness and width. The final configuration is shown in Figure 2. Stress analysis of this specimen showed significant reduction in the concentrated stress in the grip pin holes as compared to the original specimen, which encouraged specimen fracture in the gage section. This configuration was found to be suitable for the tensile and stress rupture evaluation, with failure occurring in the specimen gage section. Low cycle fatigue testing, however, revealed that the 5/8" (15.9

TABLE 5

DEFECT SEVERITY CLASSIFICATIONS(1)

Defect Type	Mild	Intermediate	Severe	Standard Acceptance Limit
Dross Inclusion	.010"-.30"	.30"-50"	> .50"	.010"
Mold Breakage Inclusion	.010"-.30"	.30"-50"	> .50"	.010"
Microshrinkage	.010"-.30"	.30"-.50"	> .50"	.010"
Diverging Axis Grain	0^{o}-5^{o}	5^{o}-20^{o}	> 20^{o}	15^{o}
Diverging Adjacent Grain	0^{o}-5^{o}	5^{o}-20^{o}	> 20^{o}	20^{o}
Emergent Grains	10^{o}-30^{o}	30^{o}-60^{o}	60^{o}-90^{o}	10^{o}

(1) For the dross inclusions, mold breakage inclusion and microshrinkage defects, the severity classifications represent linear groupings or clusters of defects the lengths of areas of which are indicated by the size ranges.

TABLE 6

CHEMICAL ANALYSIS OF PWA-1422 (MAR-M200 + Hf)
MASTER HEAT JW-6048

Element	JW-6048	PWA-1422K
C	.13	.12-.16
S	.010	.015 maximum
Si	.10	.20 maximum
Mn	.02	.20 maximum
Cr	8.39	8.0-10.0
Fe	.17	.35 maximum
Ti	1.89	1.75-2.25
Al	4.95	4.75-5.25
Co	9.66	9.0-11.0
W	11.6	11.5-12.5
Cu	.02	.10 maximum
Zr	.082	.20 maximum
Cb	.97	.75-1.25
Hf	2.2	1.5-2.5

TABLE 7

ACCEPTANCE TEST DATA FOR PWA-1422K
MASTER HEAT JW-6048

1. Machined From Blade Specimens
Solid FR-8572 Turbine Blades

A. 1400°F (760°C/100 ksi (689 MPa) Creep/Rupture

	Rupture Life (Hours)	Elongation at 48 Hours (%)
JW-6048	48+*	1.2
PWA-1422K	48	<4

B. 1800°F (982°C)/32 ksi (221 MPa) Creep/Rupture

	Rupture Life (Hours)	Elongation at 20 Hours (%)	Rupture Elongation (%)
JW-4048	49	1.3	21
PWA-1422K	32	< 2	10

* Test Discontinued

mm) fillet radius was a common site for crack initiation independent of whatever defect was located in the specimen gage section. Failure analysis indicated that this was caused by microshrinkage, preferentially forming within this area during the casting process. For the fatigue test specimens, therefore, the fillet was ground and blended to a 2" (51 mm) radius to remove the microshrinkage and to reduce the local stress concentration factor. This change was successful in producing failure within the specimen gage section.

c. Casting Process Development

Standard production operations for D.S. components have been developed to minimize casting defects and as such modified procedures were employed in order to produce the test specimens for this program. These procedures are described in detail in the following sections.

i. Defect-Free Specimens

Defect free specimens were produced in 19 piece clusters. A seven-dip mold was used and the following casting parameters were employed:

Pour Temperature -2850°F (1566°C)

Mold Preheat Temperature - 2700°F (1482°C)

Withdrawal Rate - 15 inches/hour (38 cm/hour)

A photograph of the mold is shown in Figure 16. These basic parameters were also used for the production of all of the defect-bearing specimens with the modifications discussed below.

ii. Emergent Grain Defects

In order to produce emergent grain defects, mold clusters were prepared containing test specimens tilted at various angles. The solidification direction was thus at an angle to the longitudinal axis of the finished test specimen. Although this technique was capable of producing emergent grains, diverging axis grains could not be produced because the length of the test specimen resulted in grains intersecting the specimen edges for any appreciable tilt angle. Alternative methods were therefore required to produce diverging axis and diverging adjacent grain defects.

iii. Diverging Axis and Diverging Adjacent Grains

In order to produce diverging axis and diverging adjacent grains, a "cold start" process was used. This technique employed a chill plate which was colder than the mold at the beginning of the casting process. The large initial undercooling of the molten metal just ahead of the chill plate resulted in a high nucleation rate of randomly oriented grains. The continued growth of these grains during withdrawal resulted in directionally solidified components with a large number of off-axis grains.

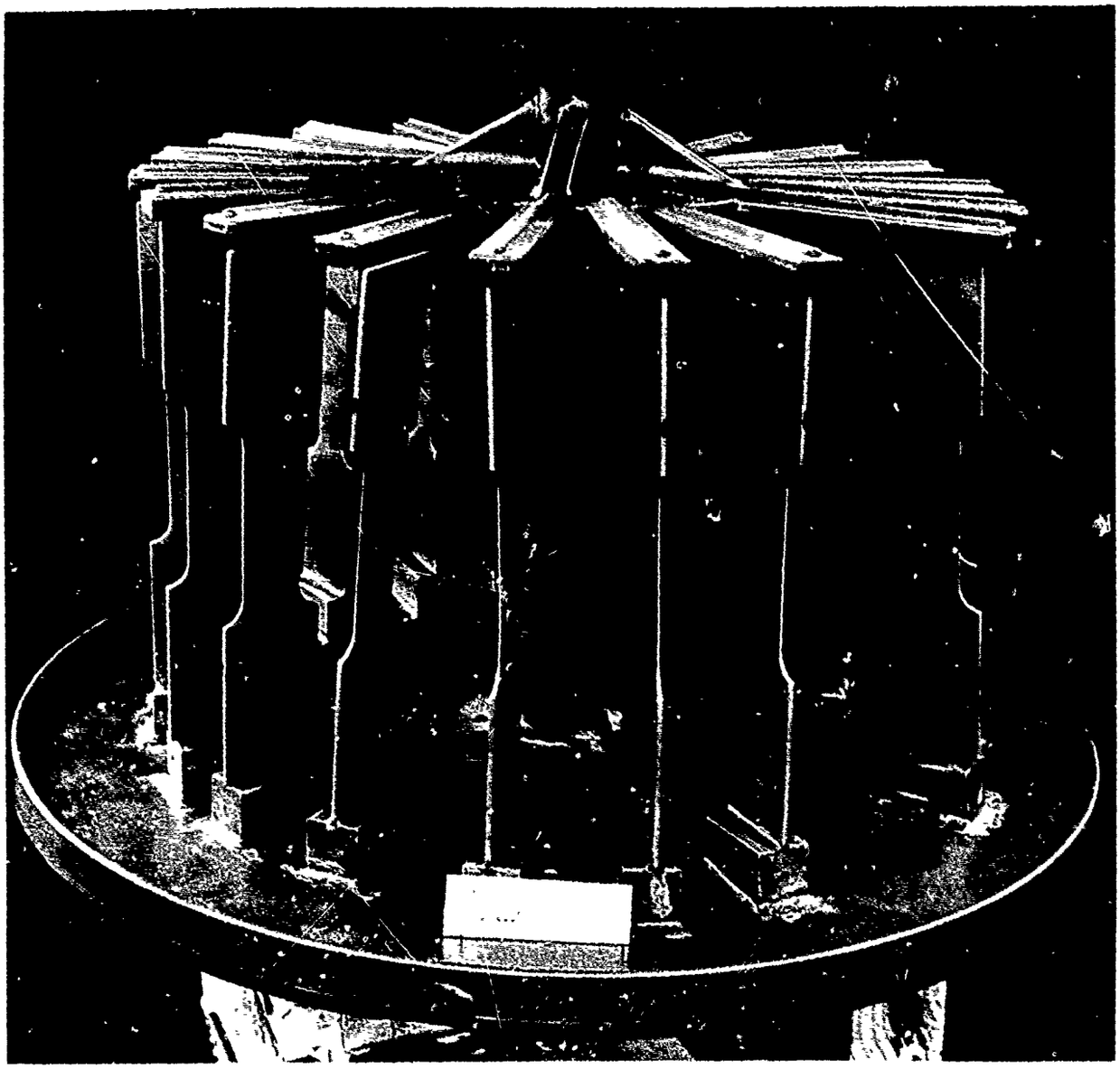

Figure 16. Photograph of a Mold of a Cluster of Mechanical Property Test Specimens.

iv. Microshrinkage

Microshrinkage was produced by decreasing the thermal gradient to increase the distance that feed metal must travel down the narrow channels between growing dendrites. The channels, therefore, no longer were filled by molten metal. This was accomplished by using the power-down or gradient mold process, which was characterized by low thermal gradients in the grip area farthest from the chill. Microshrinkage thus resulted in the gage section of the test specimens.

v. Mold Breakage Inclusions

Mold breakage inclusions were produced by introducing loose granules of mold material into the mold cavity prior to pouring the metal. These granules were trapped in the thin gage section of the test specimen, resulting in mold breakage inclusions.

vi. Dross Inclusions

Dross inclusions were incorporated into the test specimens by permitting the casting furnace vacuum to degrade by adjusting the leak up rate so that oxidation reactions readily occurred during the casting process. A wide range of dross inclusions were thus achieved in the test specimens.

d. Heat Treatment

Subsequent to casting, specimens were heat treated in accordance with the PWA-1422K specification, which included:

2200°F (1204°C)/2 hours in argon

+ 1975°F (1080°C)/4 hours in air

+ 1600°F (871°C)/32 hours in air

e. Specimen Machining

Limited machining operations were carried out on the heat treated castings. These operations were conducted to produce the grip pin holes and to expand the fillet radius of the low cycle fatigue test specimens. The specimen surface was intentionally undisturbed, thus simulating the surface condition of production castings.

f. Nondestructive Investigation (NDI)

After casting and heat treatment, the specimens were subjected to the same series of NDI procedures as production blades and vanes. In addition to the standard production blade inspection steps, however, a novel inspection method, the krypton emission technique (KET), was used to inspect specimen which had FPI and X-ray defects. The details of these inspection procedures are described in the following sections.

i. Grain Etch

Specimens were anodically etched in a solution of approximately 67% H_3PO_4, and 33% water, to which was added 1% of 56% HCl. Parts were etched at 47 amp per piece for 4-1/2 minutes to reveal the macrostructure. Grain misorientation, freckles and cracks were revealed during this inspection step.

iii. X-ray Inspection

X-ray inspection of test specimens was performed using process parameters identical to those of production blades. These included the following:

Film - Gaevert Fine Grain industrial X-ray Film

Focal Spot - 4 mm

Amperage - 10 ma

X-ray Tube to Film Plate Distance - 48" (122 cm)

For production castings these particular parameters result in a sensitivity level of approximately 1-1/2%. Because production blades are double walled, however, it was estimated that the use of these parameters for the single walled test specimens in this investigation actually resulted in much greater sensitivity than achieved in actual cast components.

iii. Fluroescent Penetrant Inspection

The specimens were cleaned ultrasonically using a detergent solution and dried at 250°F (121°C) for 10 minutes. They were then dipped in ZL-54 penetrant for at least 18 minutes, washed in 80°F (27°C) agitated water for 2 minutes and hot air dried at 190°F (80°C) for 1 minute and 45 seconds. They were dusted with ZP-4 powder and allowed to develop for 10 minutes prior to being read.

iv. Krypton Emission Technique (KET) Inspection

This inspection was carried out in order to detect surface connected defects with greater sensitivity than that afforded by FPI. The evaluation was conducted under the sponsorship of the Naval Air Propulsion Test Center and the detailed results were summarized in a separate publication (14). The KET exposure operations were conducted at the Qual-X Company of Hilliard, Ohio. The inspection sequence consisted of the following steps:

a) Place parts in a controlled atmosphere chamber and evacuate.

b) Back fill with one atmosphere of radioactive Kr_{85}. Expose specimens to krypton for 1 hour.

c) Remove specimen and expose radiation sensitive film to the work-piece for approximately 4 hours.

d) Develop film.

The radioactive krypton gas which adheres to the internal surfaces of surface connected discontinuities exposes the X-ray film resulting in a permanent record of the defect.

g. Mechanical Property Tests

i. Determination of Test Conditions

The test conditions utilized in this program were determined empirically. Defect free specimens were used to determine the stresses required in the 1400°F (760°C) and 1800°F (982°C) stress-creep/rupture tests to produce failure in approximately 100 hours. It was reasoned that this failure time would represent a condition of increased sensitivity of rupture properties to the presence of defects. Similarly, low cycle fatigue testing at 1800°F (982°C) was conducted to determine the stress necessary to produce failure in 1000 to 10,000 cycles. Determination of test parameters in this manner was necessary because of the strong influence that section size exerted upon mechanical properties. Published data generally refers to .252" (0.6 cm) diameter bar castings, rather than to the .040" (.1 cm) gage thickness castings employed in this study. For example, the specification minimum stress rupture life requirement for .252" (0.6 cm) D.S. MAR-M200 + Hf castings at 1400°F (760°C) 100 ksi (689 MPa) is 48 hours. The life of .040" (.1 cm) thick flat specimens tested initially in the present program under these conditions ranged from 1.7 to 10.3 hours. Similarly, the ultimate and 0.2% yield strengths of 0.252" (0.6 cm) diameter D.S. MAR-M200 castings at 1400°F (760°C) were 152 ksi (1080 MPa) and 134 ksi (925 MPa), respectively, compared to 136.5 ksi (941 MPa) and 124 ksi (857 MPa) for the thin walled castings. It was necessary, therefore, to develop defect-free baseline data for the present study. Utilizing this procedure the following test conditions were selected :

Test Type	Desired Life	Stress Levels
a) 1400°F (760°C) Tensile	-	-
b) 1400°F (760°C) Stress Rupture	100 hours	90 ksi (621 MPa)
c) 1800°F (982°C) Creep Rupture	100 hours	30 ksi (207 MPa)
d) 1800°F (982°C) LCF	1000-10,000 Cycles	0-50 ksi (0-345 MPa)

ii. Tensile Tests

Tensile tests were performed at 1400°F (760°C) in laboratory air on an Instron Universal testing machine at a strain rate of 0.005 per minute. Ultimate and 0.2% offset yield strength, percent elongation and reduction of area were recorded for each specimen. This temperature was selected because 1400°F (760°C) is representative of the regime in which superalloys experience a ductility minimum and thus is usually of concern to materials and design engineers.

iii. 1400°F (760°C), 1800°F (982°C) Stress/Creep Rupture Tests

The stress/creep rupture tests were performed in laboratory air under constant load on Satec stress rupture testing machines with all specimens run to failure. For all specimens, rupture life, percent elongation and percent reduction of area were reported. In addition, the data for the 1800°F (982°C) creep rupture test included measurements of percent elongation after 20 hours. This was accomplished by unloading the specimens and measuring the elongation at room temperature. The specimens were then reloaded to the original load level.

iv. Low Cycle Fatigue Tests

Low cycle fatigue tests were performed at 1800°F (982°C) in laboratory air utilizing the smooth sheet specimens under load control on an Instron Universal testing machine at a frequency of 0.1 Hz. This test frequency was selected to minimize creep interaction damage in the specimens. Testing was conducted under a zero-to maximum stress cycle utilizing a maximum applied load to produce failure in defect-free specimens in less than 10^5 cycles and to produce measurable cyclic plastic strain. These conditions are considered to be within the low cycle fatigue test regime. Several trial specimens of defect-free material were used in order to develop the proper applied stress. Data for these low cycle fatigue tests were reported in terms of:

a) Cycles to crack initiation (measured by visual inspection by periodically interrupting the fatigue test).

b) Initiation site.

c) Cycles to failure (N).

Fatigue crack propagation tests were conducted utilizing the same equipment and specimen configuration as the low cycle fatigue tests. To aid in the visual observation of the propagating crack, however, a single edge notch was placed in the test specimens such that the crack would grow through an area known to contain the specific defects of interest. The notch was produced with an abrasive grinding wheel and was approximately 0.20" (.5 mm) deep with a radius of 1/32" (.8 mm). Crack growth measurements were obtained optically through a view port arrangement in the test fixture furnace.

B. Results and Discussion

The results of the mechanical property test program and the subsequent metallographic, fractographic, and statistical analyses are presented and discussed in the following sections. The raw data for the 1400°F (760°C) tensile, 1400°F (760°C) stress rupture, 1800°F (982°C) creep rupture and 1800°F (982°C) low cycle fatigue tests are presented in Appendices F, H, J, L, respectively. In addition to the usual data reported for mechanical property tests, these appendices contain the results of subsequent fractographic studies conducted on the failed test specimens to determine those defects actually associated with the fracture surfaces. The efforts to obtain these data were conducted for several reasons. First, with the exception of one specimen, none of the misorientation defect specimens exhibited fractures associated with any of the defects. Second, in a number of instances test specimens contained more than one NDI detected defect in the fracture surface. Third, other specimens exhibited failures associated with defects not found during NDI inspection. Fourth, other specimen fracture surfaces were observed to contain defects at more severe levels than identified during NDI inspection. In one case, for example, a 1400°F (760°C) stress rupture specimen was found to fail through a severe microshrinkage defect while NDI inspection rated the indication as a mild defect. The appendices include all of these observations and thus represent a comprehensive listing of data including the intended defect for each specimen as well as the defects actually associated with the fracture surfaces. In order to illustrate the defect severity criteria used in the interpretation of the fractures, examples of the surfaces associated with each defect type and severity level are shown in Appendix N. This includes fractographs of typical microshrinkage, mold breakage and dross inclusion defects located within fracture surfaces.

Several final comments concerning the raw data involve the definition of two terms appearing in the appendices. The first concerns defect free specimens/defect free fracture surfaces. Defect free specimens were identified on the basis of the fact that no identifiable defects were found during NDI inspection located within the gage length. Defect free surfaces, on the other hand, were those found free of any defects on the fracture face. Those instances in which failure occurred through a defect free area of specimens known to contain defects in other areas are discussed individually in the following sections. The second definition concerns the valid/invalid terms appearing in the appendices. It was observed that a number of the specimens did not fracture within the gage section. These specimens generally failed in the fillet radius in the transition between the gage section and the specimen grips and were considered invalid. An illustration of a valid and an invalid test specimen is shown in Figure 17. The subsequent analysis of the mechanical property data included only those specimens considered valid and was conducted on the basis of defects actually associated with the fracture surfaces. When more than one defect was identified on a fracture surface, both were included in the defect populations for those particular defects.

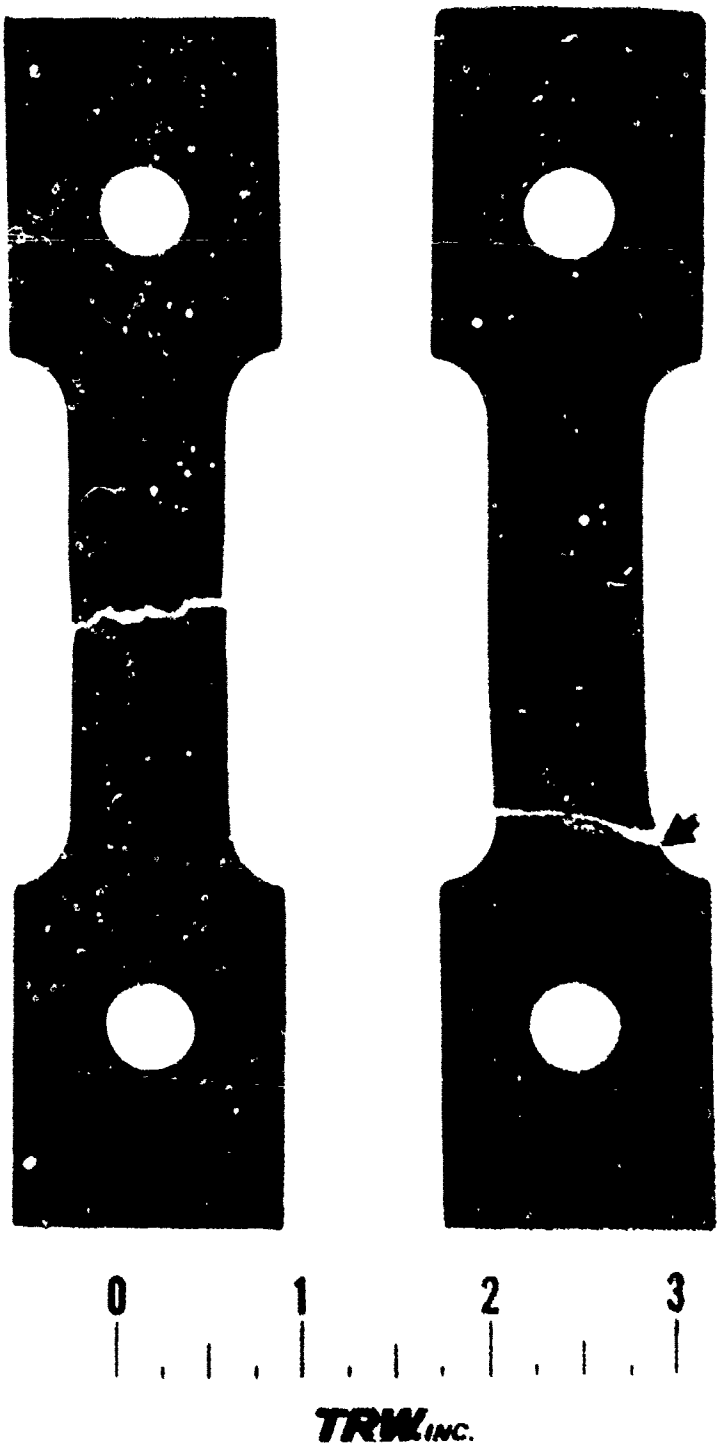

Figure 17. Photograph Comparing Valid and Invalid Specimen Failure Locations.

Left: Valid Failure
Right: Invalid Failure

The Weibull method of statistical analysis was used to determine the significant statistical parameters of the various test specimen populations (15). Each individual population represented all the observed instances in which a particular defect was associated with the fracture surface. An example of this analysis is presented in Figure 18 for the ultimate tensile strength at 1400°F (760°C) for specimens exhibiting defect free fracture surfaces. The straight line plot indicated that the data points comprised a single failure population with -2σ limit of 87.5 ksi (603.4 MPa). The -2σ limit indicates that for the large population represented by the sampling observed in the present investigation 97.5% of the ultimate tensile strength values would be above this particular number. The difference between the average value of all the data points and the -2σ limit is an indication of the relative spread in the data. The Weibull analyses of all the mechanical property data are listed in Appendices G, I, K, and M for the 1400°F (760°C) tensile, 1400°F (760°C) stress rupture, 1800°F (982°C) creep rupture and 1800°F (982°C) low cycle fatigue tests, respectively. Included in these appendices are the number of data points for each population, the high and low values, the average value and the -2σ value.

1. 1400°F (760°C) Tensile Results

The raw data from the 1400°F (760°C) tensile tests are presented in Appendix F and the results of the statistical analysis of the data are presented in Appendix G. The Weibull analysis indicated that all the various defect populations comprised single failure populations. This indicated, for example, that in the group of specimens containing a severe condition of microshrinkage on the fracture surface, no other defect or defect level had a statistically significant effect upon the mechanical properties. Approximately 78% of the tensile tests conducted during this program were valid, indicating that the majority of failures occurred within the gage sections. Of the invalid tests, the fracture surfaces were located at the fillet radii and usually contained evidence of microshrinkage. Of the valid tests, however, only 35% of the specimens failed through the intended defect area. In a number of instances undetected defects were associated with the fracture surfaces. In other cases several different types of defects were located on the same fracture surface. For these reasons the tensile test results were analyzed not in terms of the intended defects, but rather in terms of those defects actually appearing on the fracture surfaces. It was observed that microshrinkage and dross inclusions were most often associated with fracture surfaces. Microshrinkage was found in approximately one half the fractures while dross inclusions appeared on about 1/3 of the fractures. One other important fact was the observation that none of the grain misorientation type defects were located near any of the fracture origins. In the case of the emergent grain defects, for example, none of the fractures occurred at those locations where the emergent grain intersected the specimen surfaces.

The tensile properties and the results of the statistical analyses of the tensile properties are plotted in Figures 19 (strength properties) and 20 (ductility properties) as a function of the defects and their severity levels as observed on the actual fracture surfaces. Included in the figures are the maximum values, minimum

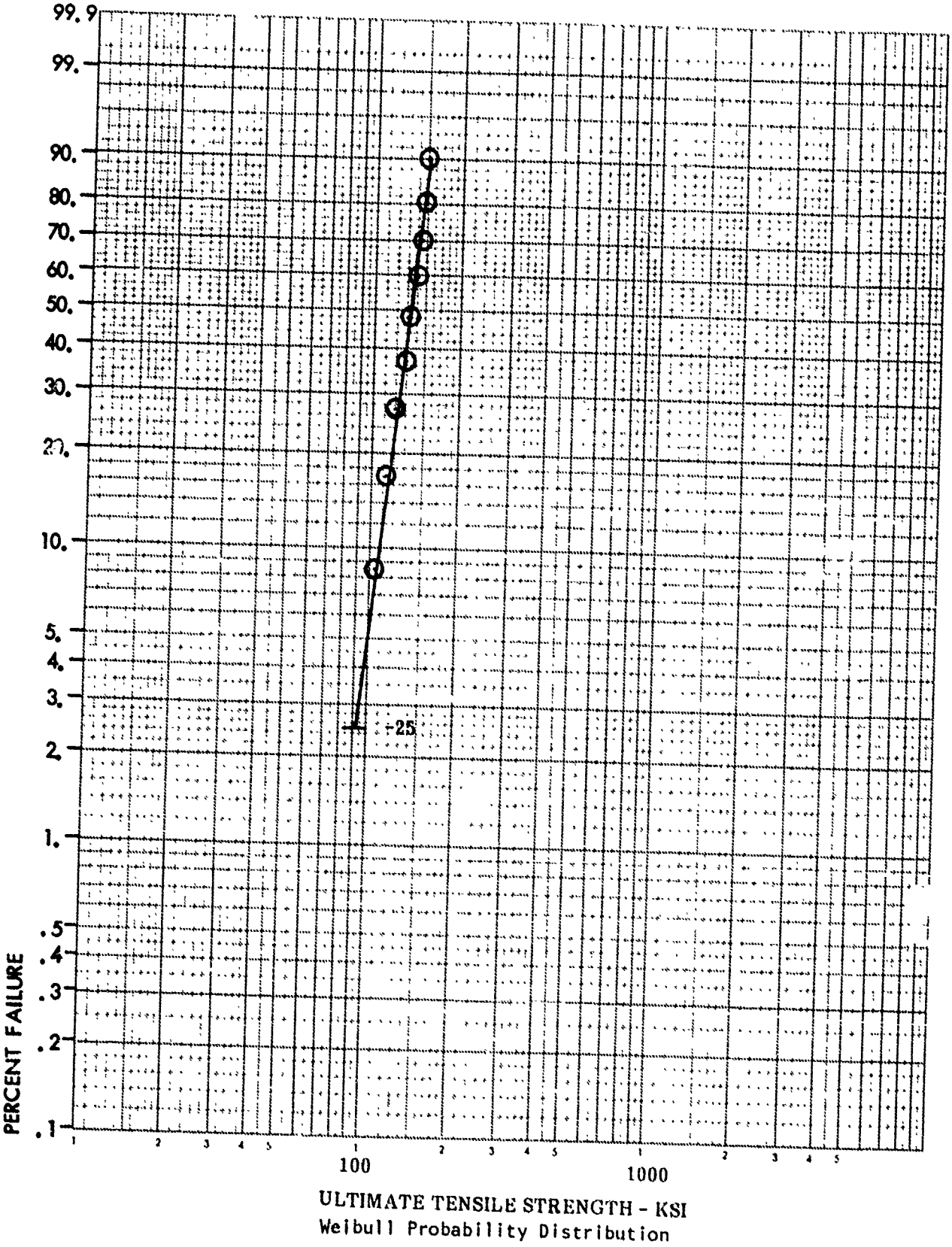

Figure 18. Weibull Probability Plot for 1400°F (760°C) Ultimate Strength for Defect Free Specimens.

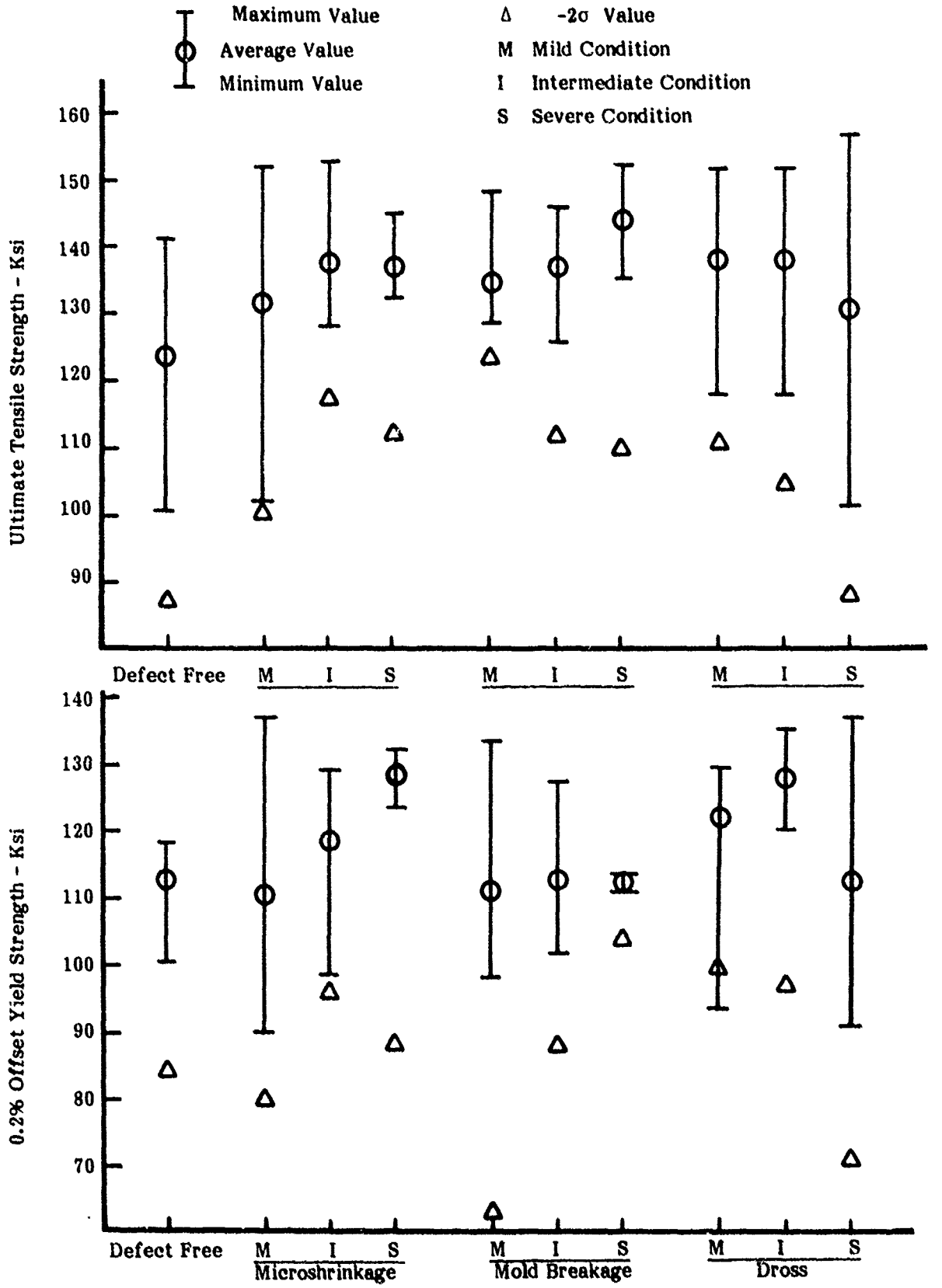

Figure 19. 1400°F (760°C) Tensile Strength Properties Versus Defect Type

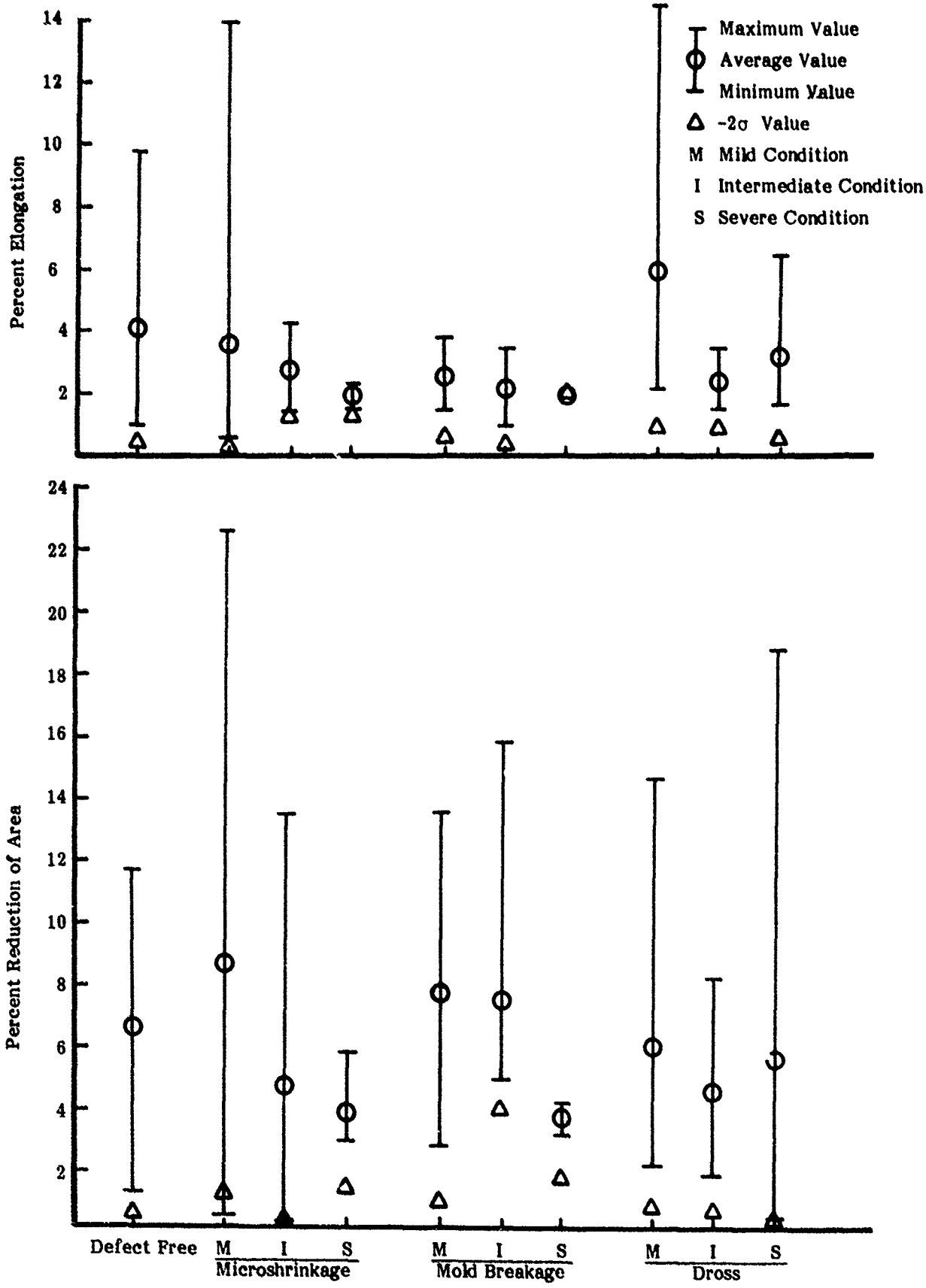

Figure 20. 1400°F (760°C) Tensile Ductilities Versus Defect Type.

values, averages and -2σ values for the ultimate tensile strength, 0.2% offset yield strength, percent elongation and percent reduction of area plotted for defect free, microshrinkage, dross inclusion and mold breakage inclusion specimens. These three defect categories represented the only defects associated with the tensile fracture surfaces.

Analysis of the microshrinkage results indicated that while this defect was present on numerous fracture surfaces at all three severity levels, there was no significant decrease in either ultimate tensile or yield strengths. In fact, average values for these properties were higher for those specimens containing the microshrinkage defects compared to the defect free specimens. Because it was difficult to rationalize this behavior in terms of microshrinkage acting as a strengthening or crack blunting mechanism, the statistical interpretation of the results suggested only an absence of any strength degradation even at the most severe defect level. This condition would consist of a linear grouping or cluster of shrinkage indications in a region approximately 0.50" (12.8 mm) or larger in length or diameter. Present acceptability criteria limit such indications to 0.010" (.25 mm) or less. The tensile ductility results, however, indicated a systematic reduction in both precent elongation and reduction of area with an increase in severity level. It was significant, however, that this degradation did not begin at the mild condition, but rather at the intermediate condition. This consisted of groupings or clusters of indications in an area approximately 0.30"-0.50" (8-12.8 mm) in length or diameter. At the most severe defect condition ductility properties were approximately 50% of those of the defect free material. A single instance was observed in which a microshrinkage containing specimen failed through a defect free area. The specimen was, however, rated at the mild severity level. Because microshrinkage defects at this level had no degrading effects upon strength or ductility, it was concluded that this was a random occurrence with equal probability that fracture could have occurred through the defect or through the defect free area.

After microshrinkage defects, dross inclusions were the next most common defects observed on the fracture surfaces of tensile test specimens. Similar to the microshrinkage results for the strength properties, dross inclusions did not have a significantly degrading effect on ultimate and yield strength values when compared to defect free material. It was observed, however, that comparisons between the various dross containing specimens indicated a decrease of approximately 5-8% in the average values of ultimate and yield strengths between the mild and severe conditions. At the severe level, however, the average values were still comparable to those of defect free material. The ductility results for the dross inclusions were also similar to the trends for the microshrinkage defects. No degradation in percent elongation or reduction in area was observed until an intermediate defect condition was evaluated. The magnitude and distribution of the defects for this intermediate condition for both microshrinkage and dross was similar. At the mild dross condition ductility properties were comparable to those of defect free material. The tensile data suggested that indications in excess of the current 0.010" (.25 mm) limit would not significantly degrade the properties as long as the linear groupings or clusters of defects were less than 0.30" (8 mm) in length or diameter. A single instance was observed in which a dross containing specimen failed through a defect free area. Similar to the situation for the microshrinkage specimen, however, the defect was classified as mild and failure could thus have occurred just as easily in the defect free area as through the defect. Dross defects at this severity level had no degrading effects on the tensile properties.

Mold breakage inclusions represented the final group of defects located on the fracture surfaces of tensile test specimens. The magnitudes and distributions of the mold breakage severity levels were similar to those of the microshrinkage and dross inclusion defects. In general, the mold breakage type of defects did not significantly degrade the tensile strength properties. Average values of ultimate tensile and yield strength for the defect containing material were comparable to those of the defect free material. Similar to the results for the microshrinkage defects and dross inclusions, the presence of mold breakage particles resulted in a significant decrease in ductility, particularly at the most severe level where reductions in ductility values of approximately 50% compared to the defect free material were observed. Unlike the microshrinkage and dross inclusions, however, mold breakage inclusions appeared to have a detrimental effect even at the mild severity level. A reduction of approximately 40% in percent elongation was observed for specimens exhibiting the mild mold breakage condition. These results suggested that while the presence of defects in excess of the allowable acceptability limits would not cause significant degradation in strength properties, they would result in appreciable reductions in ductility even at levels slightly above the current acceptability limits.

In summary, the 1400°F (760°C) tensile test results indicated that microshrinkage, dross inclusions and mold breakage inclusions were usually associated with test specimen fracture surfaces. In general, however, the specimens did not fail through the intended defects but rather were associated with other defects located throughout the specimen gage section. Microshrinkage appeared in approximately one half the fracture surfaces while dross inclusions were observed in approximately 1/3 the fractures. Grain misorientation defects including emergent, diverging axis and diverging adjacent grains had little effect on the tensile properties. None of the fractures were associated with any of these defects. The general trends for the microshrinkage, dross and mold breakage defects were quite similar in that no significant degradation in either ultimate tensile or yield strength was observed as the result of the presence of these defects even at the most severe levels. An embrittling effect was observed, however, in the form of ductility reductions in the presence of these defects. This reduction was most pronounced at the most severe defect level and usually included a loss of approximately 50% of the ductility of the defect free material. Microshrinkage and dross inclusion defects were not observed to be harmful to ductility at the mild severity level, but mold breakage inclusions were harmful at all three severity levels.

2. 1400°F (760°C)/90 ksi (620.7 MPa) Stress Rupture Results

The raw data from the 1400°F (760°C) stress rupture tests are presented in Appendix H and the results of the statistical analysis of the data are presented in Appendix I. The Weibull analyses indicated that all the defect populations comprised single failure populations. Approximately 75% of the stress rupture tests conducted during this portion of the program were valid, indicating that the majority of the fractures occurred within the gage section. Similar to the results for the 1400°F (760°C) tensile tests, the fracture surfaces for the invalid tests were located at the fillet radii and usually contained evidence of microshrinkage. Of the valid tests,

however, a number had to be suspended in view of the extraordinarily long lives accumulated during testing. The suspended tests were fractured by overloading the specimens by 25% in order to obtain a fracture surface for examination. Suspended life values were included in the average life computation because, as a minimum, the various specimens did exhibit these lives. These lives were treated as suspended data for the Weibull analysis. The elongation and reduction of area data for overloaded specimens were not used in computing average values nor were they included in the Weibull analysis. Approximately 22% of the valid tests required suspension of testing. For the valid tests, approximately 43% failed through the intended defect at the intended severity level, indicating that in the majority of cases other defects/severity levels were responsible for failure. None of the observed failures were associated with any of the emergent, diverging axis or diverging adjacent grain misorientation defects. Similar to the results for the 1400°F (760°C) tensile tests, microshrinkage and dross inclusions were commonly associated with the fracture surfaces and at approximately the same number of occurrences. Microshrinkage was present on approximately one half the fractures and dross inclusions were present on slightly more than 1/3 the fractures.

The stress rupture properties and the results of the statistical analysis of these properties are plotted in Figures 21 (rupture lives) and 22 (ductility properties) as a function of the defects and their severity levels as observed on the actual fracture surfaces. Included in the figures are the maximum values, minimum values, averages and -2 values for the rupture lives, percent elongation and percent reduction of area plotted for the various defects. As shown in Figure 21, the rupture lives exhibited considerable scatter. In the defect free specimens, for example, failure lives ranged from 52 to over 800 hours. This scatter was obtained in spite of the fact that the stress levels were selected on the basis of actual defect free specimens failing at approximately 100 hours. This type of scatter in 1400°F (760°C) rupture life has been observed in production quality control D.S. test specimens machined from solid blade components (16) and in cast cylindrical test specimens used to evaluate grain misorientation effects in D.S. MAR-M247 superalloy (17). Scatter of this nature has been observed previously in equiaxed cast material and has been attributed to interdendritic segregation (3) and in other instances to porosity or microshrinkage, trace or tramp elements, and cracks present in the carbides within the microstructure (18). These factors may all be operative in one form or another in the present investigation of D.S. material.

Microshrinkage indications were the most common defects observed on the fracture surfaces of 1400°F (760°C) stress rupture specimens. In spite of the considerable scatter in rupture lives of these specimens, a trend of decreasing rupture life with increasing defect severity level was observed for the average values of rupture life. The decrease was not apparent, however, until defect sizes appreciably larger than current acceptance limits were evaluated. At the larger defect sizes, though, the decrease was quite significant. At the intermediate level average rupture life decreased by approximately 50% compared to defect free material while at the severe level a decrease of approximately 70% was observed. Ductility was also significantly affected by microshrinkage defects, but, similar to the rupture lives, the decreases

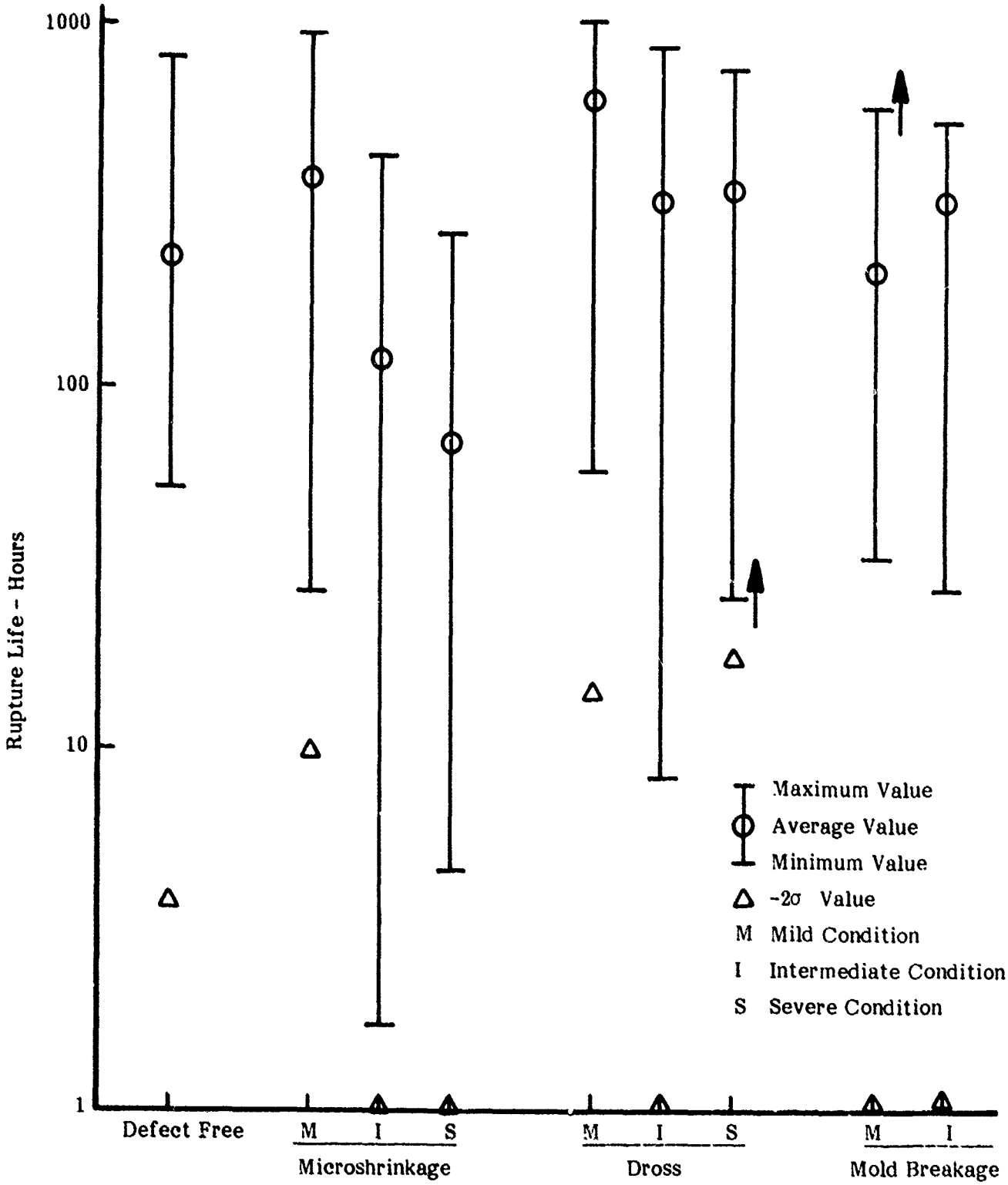

Figure 21. 1400°F (760°C) Rupture Life Versus Defect Type. Arrows Indicate Suspended Test.

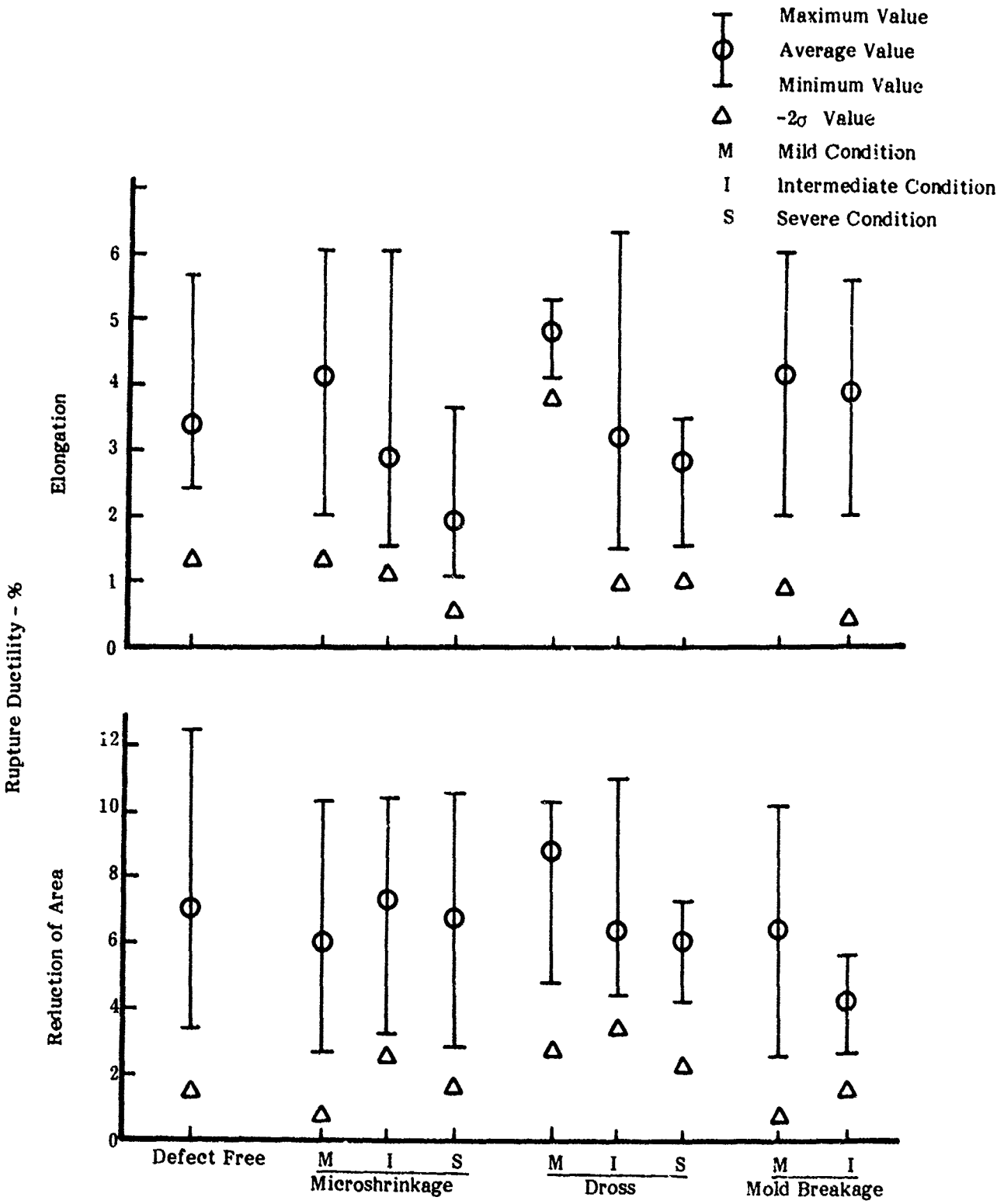

Figure 22. 1400°F (760°C) Stress Rupture Ductility Versus Defect Type

were not observed until the more severe defect categories. Reductions in percent elongation of approximately 25 and 50% were recorded for the intermediate and severe defect levels, respectively. One of the test specimens exhibited anomalous behavior in that failure occurred through a defect free area in spite of the fact that severe microshrinkage indications were observed during NDI examination. The ductility exhibited by this specimen was comparable to that of defect free specimens, but the rupture life of 41.3 hours was appreciably shorter than the 229 hour average for defect free material. No explanation was apparent for this isolated instance of anomalous behavior with the microshrinkage defects.

Dross inclusions were the next most common defects observed on the fracture surfaces of failed stress rupture test specimens. Because of the large degree of scatter in the dross specimens, no conclusions were drawn concerning the effect of these defects upon rupture life. For example, average rupture life was quite low for dross inclusions at the intermediate level but was relatively high for those specimens at the severe level. It was concluded that either the sampling size was too small to determine the effects of dross on rupture life or that other subtle interactions were having a more powerful effect than the dross inclusions. The ductility results indicated a degradation in both percent elongation and reduction of area with the presence of the dross defects but only at the more severe defect levels. Comparison within the dross specimens themselves indicates an appreciable reduction in ductility with the presence of the defects, but the decreases were much smaller when compared to the defect free material. At the intermediate and severe levels, for example, decreases in ductility of approximately 15-20% were observed when compared with the defect free material. These ductility results suggested that dross indications in excess of the current 0.010" (.25 mm) limit would not significantly degrade the properties as long as the linear groupings or clusters of defects were less than 0.30" (8 mm) in length or diameter.

After microshrinkage and dross inclusions, mold breakage inclusions represented the next most common defects observed on the fracture surfaces of stress rupture test specimens. Since no instances of severe mold breakage inclusions were observed with valid test specimens, all of the following discussion concerns defects 0.50" (12.8 mm) or smaller in size. The results indicated no appreciable degradation in stress rupture life as a result of the presence of mold breakage inclusions. Average rupture lives for specimens in the mild and intermediate defect categories were comparable to the average rupture life of defect free material. Ductility, however, was significantly affected by mold breakage inclusions but only at the intermediate, 0.30-0.50" (8-12.8 mm), level where a degradation of approximately 33% was observed in percent reduction of area. These stress rupture ductility results differed from the 1400°F (760°C) tensile ductility results in that significant degradation was observed even at the mild severity level for the tensile specimens. The stress rupture results thus indicated that the presence of microshrinkage defects in excess of the allowable acceptability limits (0.010" (.25 mm)) would not cause significant degradation in rupture life and result in appreciable ductility reductions only when the defect indications were larger than 0.30" (8 mm) in size.

In summary, the 1400°F (760°C) stress rupture results indicated that microshrinkage, dross inclusions and mold breakage inclusions were usually associated with test specimen fracture surfaces. In general, the specimens did not fail through the intended defects but rather were associated with other defect/defect severity levels located throughout the specimen gage location. Microshrinkage was observed in approximately one half the fracture surfaces while dross inclusions were present in approximately 1/3 the fractures. Grain misorientation defects had no degrading effects upon the stress rupture properties and in no instance was a fracture surface associated with any misoriented or emergent grain. While considerable scatter was obtained in the life data, general trends for the microshrinkage defects included reductions of approximately 50-75% in average rupture life at the intermediate and severe defect conditions. Because of the scatter, no conclusions could be made concerning the effect of dross inclusions on rupture life. Data for mold breakage inclusions were available only for defects 0.50" (12.8 mm) or less in size but indicated little degrading effects. Ductility results indicated that microshrinkage, dross and mold breakage inclusions all produced significant reductions, but only at the intermediate and severe defect levels. Thus, indications in excess of the current 0.010" (.25 mm) limit would not significantly degrade ductility as long as the linear groupings or clusters of defects were less than 0.30" (8 mm) in length or diameter.

3. 1800°F (982°C)/30 ksi (207 MPa) Creep Rupture Results

The raw data from the 1800°F (982°C) creep rupture tests are presented in Appendix J and the results of the statistical analysis of the data are presented in Appendix K. With the exception of the percent elongation for defect free material and percent reduction of area for the mild dross specimens the Weibull analyses indicated that all the defect populations comprised single failure populations. The two exceptions are discussed in the following paragraphs. Approximately 80% of the creep rupture tests conducted in this portion of the program were valid indicating a majority of gage section failures. Similar to the 1400°F (760°C) tensile and stress rupture tests, the fracture locations for invalid tests were generally located at the fillet radii and usually contained microshrinkage. Of the valid tests, approximately half failed through the intended defect at the intended severity level, indicating a greater percentage of failures through intended defects than was obtained with the 1400°F (760°C) tests. Grain misorientation specimens represented the majority of those which did not fail through the intended defect locations. With the exception of one diverging adjacent grain specimen, none of the observed failures were associated with any of the emergent or diverging grains. Similar to the results for the 1400°F (760°C) tests, microshrinkage and dross inclusions were commonly associated with the fracture surfaces and at approximately the same number of occurrences. Microshrinkage was present on more than half the fractures and dross inclusions were present on slightly less than 1/3 the fractures.

The creep rupture properties and the results of the statistical analysis of these properties are plotted in Figures 23 (rupture lives) and 24 (ductility properties) as a function of the defects and their severity levels as observed on the actual fracture surfaces. Included in the figures are the maximum values, minimum values, averages and -2σ values for the rupture lives, percent elongation and percent reduction of area

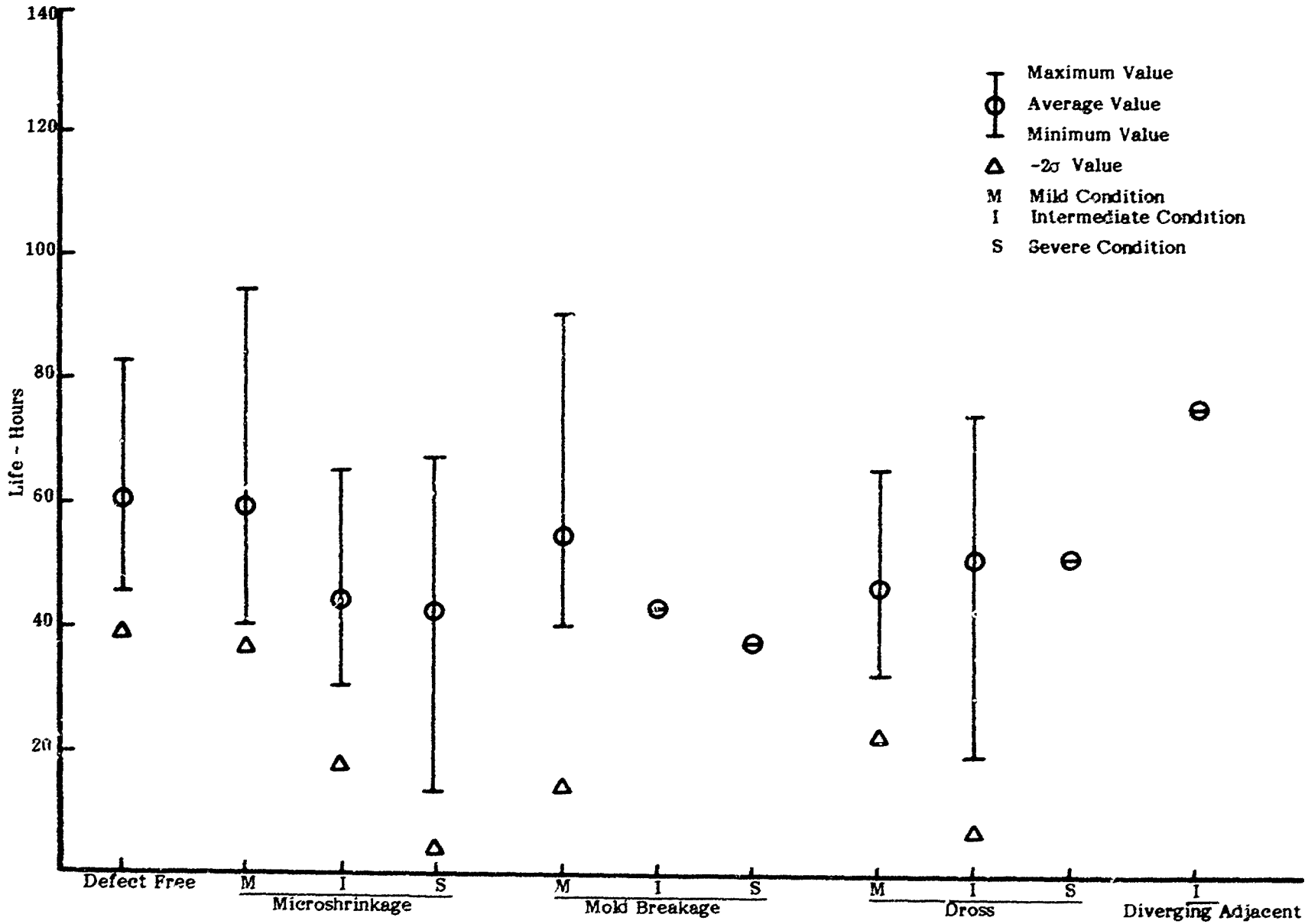

Figure 23. 1800°F (982°C) Creep Rupture Life Versus Defect Type

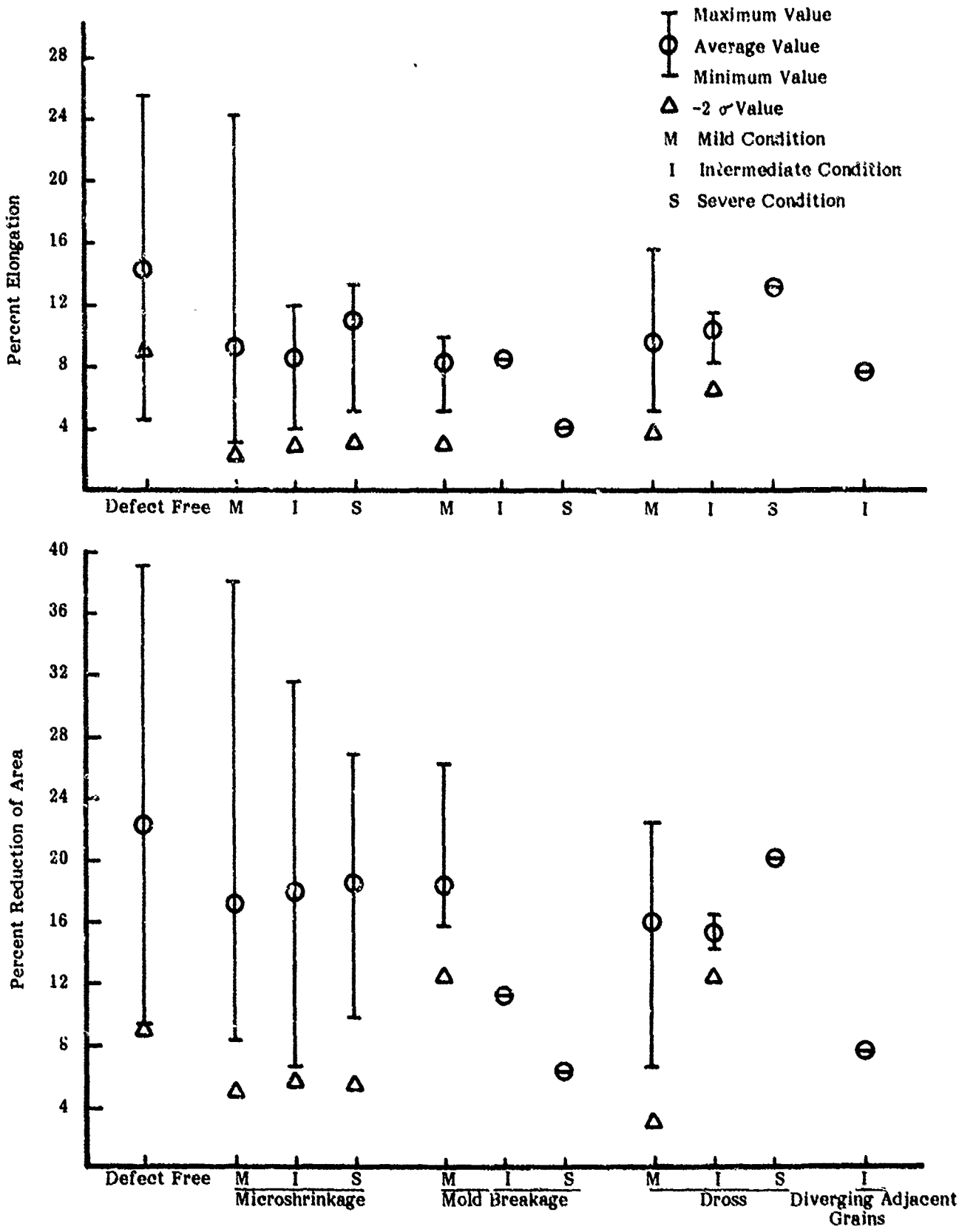

Figure 24. 1800°F (982°C) Creep Rupture Ductility Property Versus Defect Type.

plotted for the various defects. The 20 hour percent elongation measured at room temperature was not plotted in Figure 24 because all of the values varied within the narrow band of 0.5 to 2.0% without the appearance of any identifiable trends in the data. Casting defects thus had no apparent effect on this particular mechanical property. The Weibull analyses of defect free specimens indicated that the creep rupture life and percent reduction of area data each represented samplings from single failure populations. The percent elongation values, however, appeared to follow two different distribution curves, as indicated by the non-linearity of the Weibull plot for percent elongation. This suggested the possibility that some other undetected defect such as small cavitation porosity or interdendritic segregation may also have been present on the fracture surfaces of these creep rupture specimens.

The analysis of fracture surfaces indicated that microshrinkage defects were located on more than half the fractures. The detrimental effects of this casting defect on elevated temperature rupture life of equiaxed nickel-base superalloys has been well documented (19,20). Increasing microshrinkage has been characterized by property degradation regardless of test conditions, heat chemistry variations, specimen geometry or casting conditions. This behavior has been attributed to (1) the ability of microshrinkage to aid in the crack initiation process and (2) the decreased load carrying area of test specimens containing microshrinkage. In the present investigation microshrinkage defects were also found to be detrimental to the 1800°F (982°C) rupture life of D.S. specimens. It was significant, however, that degradation was not observed until the intermediate and severe defect conditions, where reductions in average life of approximately 30% were obtained compared to defect free material. The ductility properties, on the other hand, exhibited sensitivity to the microshrinkage defects at all severity levels. Reductions of approximately 20-25% were observed even at the mild condition and although the ductility properties appeared to increase slightly with severity level, all of the average values were still poor when compared to those of defect free material. A single instance of anomalous behavior was observed in the 1800°F (982°C) creep rupture tests in that a specimen containing mild microshrinkage failed through a defect free area and did not exhibit the usual reductions in ductility properties. In summary, the results suggested that while microshrinkage defects slightly in excess of the current 0.010" (.25 mm) allowable acceptability limit would not cause significant degradation in the 1800°F (982°C) rupture life, they would result in appreciable reductions in rupture ductility.

After microshrinkage, dross inclusions were the most common defects observed on the fracture surfaces of creep rupture test specimens. Unlike the microshrinkage defects, however, dross inclusions resulted in immediate reductions in average rupture lives even at the mild condition. For both the mild and the intermediate condition, reductions of approximately 20% in rupture lives were observed compared to defect free material. The ductility properties evidenced a similar sensitivity to dross inclusions which was characterized by reductions in both percent elongation and reduction of area of approximately 25% for both the mild and intermediate defect conditions. The non-linearity of the Weibull plot for percent elongation for the mild dross defects indicated that the data followed two distribution curves. This suggested that other defects such as the microshrinkage also located on some of the fracture

surfaces was exerting an important effect on the failure process in some complex manner. The mechanical property behavior of the single specimen containing the severe dross defect was difficult to rationalize particularly because it also contained severe microshrinkage on the fracture surface. This specimen exhibited rupture life and ductility values only slightly below those for the defect free material. In summary, the 1800°F (982°C) rupture life and ductility properties were quite sensitive to the presence of dross inclusions. Reductions were observed even for defects only slightly larger than the current acceptability limits.

Mold breakage inclusions were the third most common defect associated with creep rupture fracture surfaces. The mechanical properties were quite sensitive to these defects as evidenced by the progressive degradation in properties (rupture life as well as ductility) with increasing defect severity. Although only single valid specimens in each of the intermediate and severe defect conditions were found during the fracture analyses, both exhibited significantly large reductions in life and ductility compared to the defect free material. Significant reductions in the properties occurred even at the mild defect level. For example, a reduction of approximately 45% in the average percent elongation values compared to defect free material was observed for specimens containing the mild mold breakage inclusions. The results suggested little tolerance to the mold breakage inclusion defects even at sizes only slightly above the current acceptability levels.

In only one instance during the entire Task II testing program was a grain misorientation defect associated with a fracture surface. This occurred for an intermediate diverging adjacent grain specimen during 1800°F (982°C) creep rupture testing. The defect was associated with the fracture surface in that a portion of the growing crack deviated along one of the diverging adjacent grain boundaries for a short distance. This particular specimen is shown in Figure 25. The properties indicated a rupture life in excess of the average value for defect free material (73.3 versus 60.6 hours), but did exhibit inferior ductility (7.5% reduction of area versus 22.2% compared to defect free material). No other instances of this behavior were observed during the testing program nor were any occurrences fracture initiating at the surface intersections of emergent grains observed. For the majority of the test specimens other defects were usually found associated with the fracture surfaces In the previous study on the effect of off-axis grain growth on cylindrical cast bars of D.S. MAR-M247, 1800°F (982°C) stress rupture results indicated reductions of approximately 15% in ductility properties at off-axis angles of 30° (16). It was significant that no instances of failures associated with emergent grains were observed in the MAR-M247 study. In the present investigation of PWA 1422, no similar consistent trends could be established because of the presence of the other defects on the fracture surfaces. Certain specimens did exhibit poor ductility, but this was usually in the presence of microshrinkage or dross inclusions which were considered acceptable on the basis of NDI evaluation but which appeared more severe on the actual fracture surfaces. In other instances, however, the same type defects associated with the fracture surfaces did not result in property reductions.

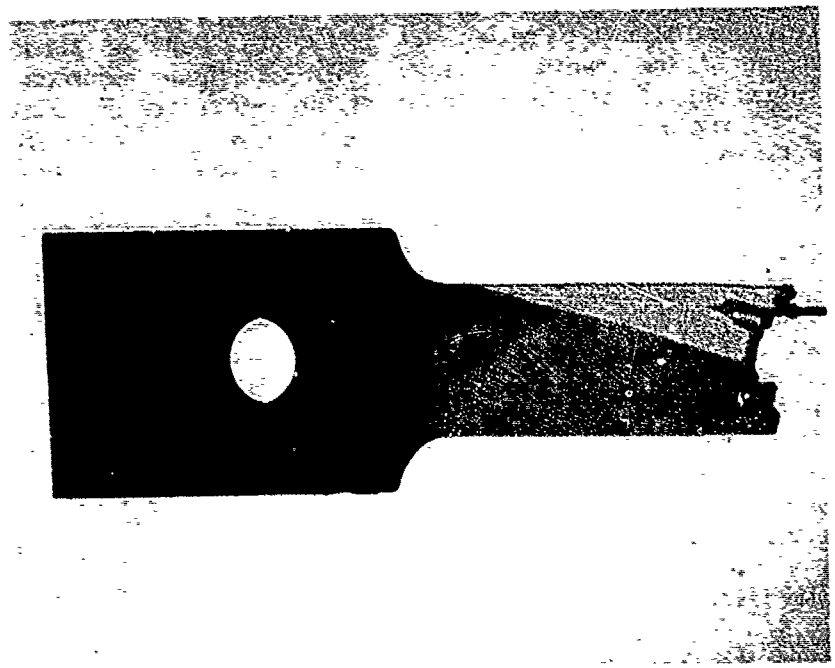

Figure 25. Photomacrograph of 1800°F (982°C) Stress Rupture Specimen Showing Location of a Crack Whose Path Deviated at a Diverging Adjacent Grain Condition.

In summary, the 1800°F (982°C) creep rupture results were similar to the other mechanical property results in that microshrinkage, dross inclusions and mold breakage inclusions were commonly associated with specimen fracture surfaces. Microshrinkage was observed in more than one half the fracture surfaces while dross inclusions were present in slightly less than 1/3 the fractures. With the exception of the grain misorientation defects, however, the specimens usually failed through the intended defects at the intended severity levels. Only one instance of failure associated with a grain misorientation defect was observed, involving a diverging adjacent grain defect. In general, the grain misorientation specimens usually contained other defects in the fracture surfaces. The general trends for the microshrinkage, dross and mold breakage defects were quite similar in that all properties exhibited extreme sensitivity to the defects, even at the mild severity levels. In particular, significant reductions in ductility properties were observed for all the defect types at all severity levels This suggested little tolerance for these casting defects.

4. 1800°F (982°C)/0-50 ksi (0-345 MPa) Low Cycle Fatigue Results

The low cycle fatigue testing included evaluations of both crack initiation and crack propagation. The crack initiation tests were conducted on the specimen geometry shown in Figure 2 while the crack propagation tests were conducted on edge notched specimens. The results are discussed separately in the following two sections.

a. Crack Initiation Results

The raw data from the low cycle fatigue tests are presented in Appendix L and the results of the statistical analysis of the data are presented in Appendix M. The Weibull analyses indicated that all the defect populations comprised single failure populations. Approximately 80% of the fatigue tests conducted in this portion of the study were valid. The majority of invalid failures occurred during initial testing with fracture commonly occurring in the fillet radii and usually being associated with microshrinkage in this region. Increasing the specimen fillet radius from 5/8" (15.9 mm) to 2" (50.8 mm) for the fatigue specimens significantly reduced the number of invalid failures. Of the valid tests, only approximately 36% failed through the intended defect region. These specimens contained microshrinkage, dross and mold breakage inclusions. The majority of specimens not failing through the intended defects included all of those spsecimens prepared to contain misorientation type defects. As such, then, no instances of fracture surfaces associated with misorientation defects were observed. The fatigue results were similar to the other mechanical property results in that microshrinkage and dross inclusions were commonly associated with fracture surfaces and at approximately the same number of occurrences. Microshrinkage was present on more than half the fractures and dross inclusions were present on slightly less than 1/3 the fractures.

The low cycle fatigue properties and the results of the statistical analyses of these properties are plotted in Figure 26 as a function of the defects and their severity levels as observed on the actual fracture surfaces. Included in the figures are the maximum values, minimum values, averages and -2σ values for the failure lives and the crack initiation lives plotted for the various defects. The defect free specimens exhibited an average failure life of 6137 cycles, with an average life to crack initiation of 5750 cycles. This indicated that approximately 90% of the fatigue life was involved in crack initiation as opposed to crack propagation. Once initiated the cracks followed a transgranular mode and propagated rapidly Similar behavior was observed for all the defect containing specimens.

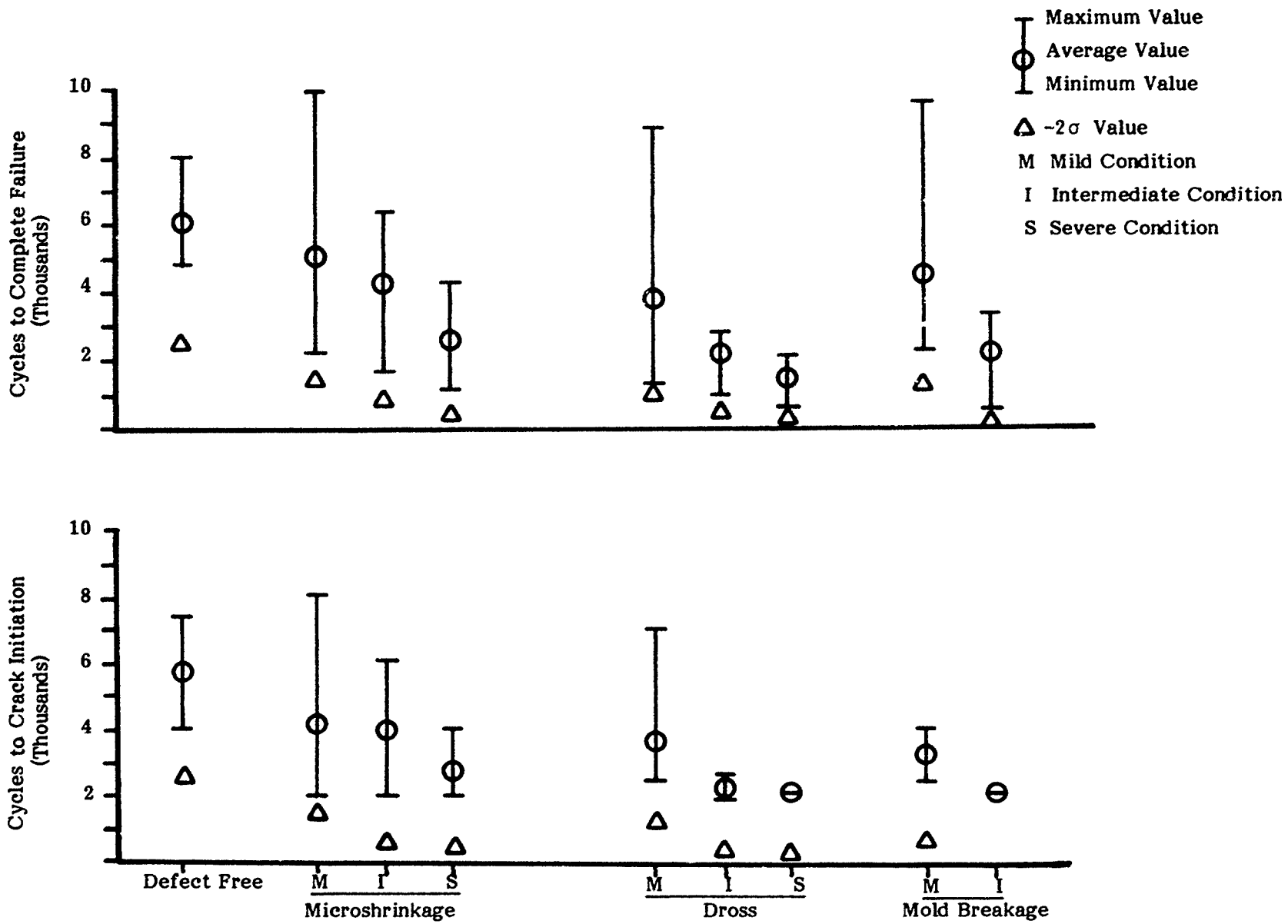

Figure 26. 1800°F (982°C) Low Cycle Fatigue Properties Versus Defect Type.

Microshrinkage was commonly observed on the fracture surfaces of fatigue specimens. Transgranular low cycle fatigue crack initiation at microshrinkage defects has been reported in D.S. specimens at both the free surfaces and within the interior of the specimens for a wide range of test temperatures (20). In addition to their role as fatigue crack initiation sites in D.S. specimens, microshrinkage defects also served as favorable paths for crack propagation. By thus assisting crack initiation and propagation, microshrinkage has resulted in low cycle fatigue property degradation in D.S. superalloy material (21,22). In the present investigation, microshrinkage defects resulted in significant reductions in low cycle fatigue properties at even the mild severity level (33% reduction in initiation life). The fatigue properties exhibited increased sensitivity to microshrinkage with increasing defect severity level and at the severe condition reductions of approximately 50% were observed in both fatigue life and crack initiation life. A single instance of anomalous behavior was observed in that a specimen containing mild microshrinkage failed through a defect free area. This particular specimen was invalid because failure occurred in the fillet radius in the transition between the gage section and the specimen grips. As such, the fatigue properties were not included in the analyses presented in Figure 26. In summary, the results indicated that low cycle fatigue properties were extremely sensitive to microshrinkage and suggested that defects only slightly in excess of the current 0.010" (.25 mm) acceptability limit would cause significant degradation in the fatigue properties.

Dross inclusions were the next most common defect found on the fracture surfaces of fatigue test specimens. While the results exhibited trends similar to those for the micoshrinkage defects, reductions in fatigue properties for the dross inclusions were much greater at comparable defect severity levels. At the mild condition, for example, a reduction in crack initiation life of approximately 40% was observed compared to defect free material. The results thus indicated little tolerance to the dross inclusion casting defects even at sizes only slightly above the current acceptability levels.

Mold breakage inclusions were the next most common defects located on fatigue specimen fracture surfaces. The trends were similar to both the microshrinkage and dross inclusion defects in that significant reductions in fatigue life and crack initiation life were observed even at the mild defect severity level. For example, reductions in crack initiation life of approximately 40% were obtained for defects at the mild severity level. The fatigue properties were thus quite sensitive to the presence of mold breakage inclusions.

None of the grain misorientation defect specimens exhibited fracture surfaces associated with these defects. In all instances, some other defect was observed on the fractures. In a similar study conducted on D.S. MAR-M246 cast to the same specimen geometry, similar results were obtained (23). For the MAR-M246 material, dross inclusions were primarily associated with fracture, while in the present investigation, microshrinkage and dross were usually present on the fracture surfaces. In the study of the effects of off-axis grains on D.S. MAR-M247, however, thermal fatigue evaluations indicated considerable reduction in thermal fatigue resistance with an increase in the off-axis angle (17). It was concluded though, that the angle between the airfoil longitudinal axis and growth axis was more effective in reducing thermal fatigue life than the presence of emergent surface grains. No instances of thermal fatigue cracks

initiating at emergent grains were found. It was observed that as the angle between the specimen longitudinal axis and growth axis increased, the modulus of elasticity increased and the thermal fatigue life decreased. It was thus suggested that if the D.S. grains are aligned in the low modulus of elasticity direction, a leading edge grain boundary intersection may not be detrimental. In the present investigation on PWA-1422 all tests were conducted under isothermal, stress controlled conditions and as such modulus of elasticity variations would not have affected the fatigue results. The significance of the MAR-M247 work, however, is related to any proposed relaxation of off-axis or emergent grain acceptance criteria. While emergent grain defects may not in themselves be detrimental to the airfoil performance, the resultant modulus variations and attendant thermal fatigue reductions associated with off-axis angles must be thoroughly evaluated.

In summary, the 1800°F (982°C) low cycle fatigue results indicated that microshrinkage, dross inclusions, and mold breakage inclusions were commonly associated with specimen fracture surfaces. Microshrinkage was observed in more than one half the fracture surfaces while dross inclusions were present in slightly less than 1/3 the fractures. Mold breakage inclusions were observed less frequently. No instances were observed of grain misorientation defects associated with fracture surfaces and, in general, the grain misorientation specimens usually contained other defects in the fracture surfaces. The general trends for the microshrinkage, dross and mold breakage defects wre identical in that all fatigue properties exhibited extreme sensitivity to the defects, even at the mild severity levels. This suggested little tolerance for these casting defects.

b. Crack Propagation Results

Fatigue crack propagation studies were conducted in order to determine the effect of pre-existing casting defects upon propagation and specimen life after the initiation of a fatigue crack The single edge notch specimen configuration used for this testing was oriented such that the fatigue crack was constrained to propagate perpendicular to the grain growth direction established during specimen solidification. The cracks that were propagated therefore represented chord-wise cracking, which is most commonly observed in actual gas turbine components (24).

The notch in the specimens used to initate the cracks was positioned so as to intersect the desired defect at a distance of approximately 0.062" (.16 cm). The stress used for the tests, based upon the cross section of the specimen was approximately 30 ksi (206.9 MPa). This stress resulted in the nucleation of a visible crack at the notch root in approximately 1000 cycles, and allowed several hundred cycles of growth to occur before specimen failure. In general, the range of stress intensities achieved was between 25 and 50 ksi $\sqrt{\text{in.}}$ (274.4 MPa$\sqrt{\text{cm}}$). The following equation was used to calculate K:

$$K_I = \sigma\sqrt{\pi a}\,(F(a/b)$$

where σ = section stress
a = crack length
b = specimen width

An empirical formula was used to determine the K correction factor, F(a/b) (25).

$$F(a/b) = 1.12 - 0.231\,(a/b) + 10.55\,(a/b)^2 - 21.72\,(a/b)^3 + 30.39\,(a/b)^4$$

The microshrinkage was of severe intensity, and the mold breakage and dross inclusions were of intermediate intensity.

The crack propagation data are preseted in Figure 27 and include a plot of da/dN versus ΔK for defect free specimens and for specimens containing microshrinkage, dross and mold breakage inclusions. All of the data points can be represented by a single line, indicating that the presence of the casting defects in the distribution evaluated in this study had little effect upon propagation behavior. Analysis of the crack length versus number of cycles (a versus N) data used to develop the da/dN versus ΔK plots indicated no discontinuities as the cracks propagated through the defects, confirming that the presence of the defects did not affect the crack propagation rate. Several possible explanations for this behavior are offered. The crack extension rate per cycle at the time of the intersection of the crack front with the defect was usually quite large, on the order of 5×10^{-3} in./cycle (12.7×10^{-3} cm/cycle). Very few cycles, therefore, would be required for the crack to grow through the defect, and resume the growth rate typical of defect free material. Therefore, under low cycle fatigue conditions, the effect of a defect on propagation rate could be masked. The presence of a defect may have a greater impact upon high cycle fatigue crack propagation, in which the crack front would remain in the defect for a comparatively larger number of cycles. A second possible explanation involves the interaction of the defect with the propagating crack front. At this intersection the crack front may accelerate its growth rate until the end of the defect had been reached. At this point the crack would have to re-initiate into the defect free material. The compensating effects of increased growth rate, followed by the necessity of a re-initiation step could result in an overall growth rate which was not significantly different than that for defect free material.

The number of cycles required to initiate visually detectable cracks in these specimens varied between approximately 450 and 1200 cycles. Once nucleated, however, the number of cycles to rupture only varied between 150 and 250 cycles. This relatively short cyclic life after initiation was consistent with the observations in low cycle fatigue testing, that the life of specimens after crack initiation was generally less than 1000 cycles (or less than 10% of the fatigue life). The data indicated that although defects did not increase the crack propagation rate, the presence of an initiated crack could not be tolerated by the test specimens. It is obvious, therefore, that the presence of cracks in blades should remain a cause for retirement.

5. Krypton Emission Technique (KET) Results

In conjunction with the present investigation, a limited study was conducted in order to establish the capability of the Krypton Emission Technique (KET) to detect casting defects in a D.S. nickel-base superalloy The KET effort was conducted under the sponsorship of the Naval Air Propulsion Test Center. Mechanical property test specimens generated in the present study were inspected by X-ray, grain etch, FPI and KET methods. Specimens were then metallographically examined to determine the nature of the defects located by KET. The relationship between the defects located by the various NDI methods and test specimen fracture surfaces was investigated through post-test fractography.

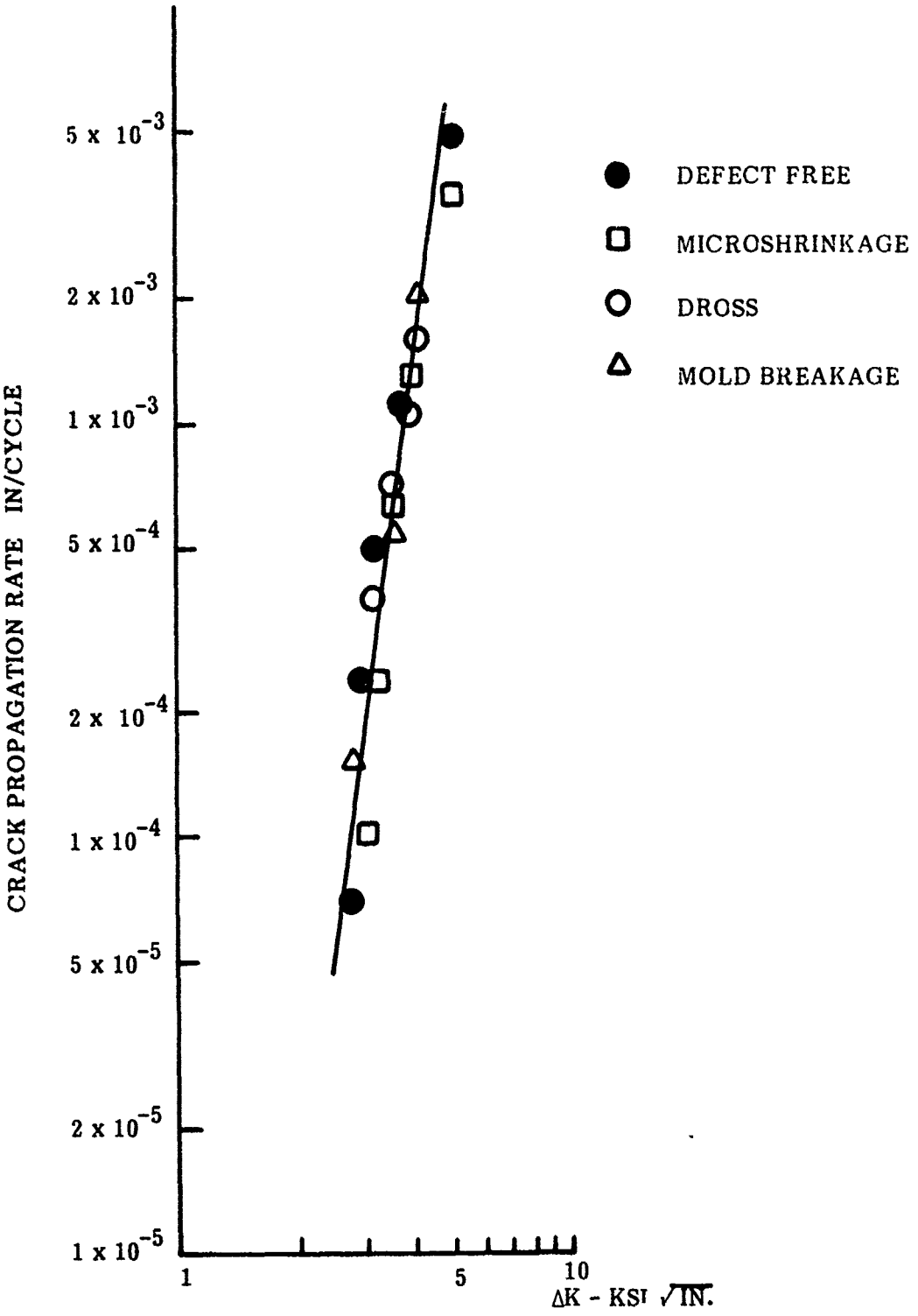

Figure 27. Transgranular Crack Propagation Rate Data for Defect Free and Defect Bearing PWA-1422.

The results of the KET investigation have been reported in detail elsewhere (14). Briefly, however, it was concluded that KET did not identify any defects which were not uncovered by current NDI methods. In general, the KET and FPI inspection operations yielded comparable results. In several instances, however, KET was effective in detecting an extensive network of surface connected defects which appeared only as small FPI pin point defects. An example of this is shown in Figure 28. This capability may be useful in determining whether components which contain surface connected defects should be repaired or not. Further work would be required to define the absolute correlation of KET indication size with actual defect size and hence the limits of resolution of the KET technique. The surface finish of the specimens was also found to be an important factor in determining the accuracy of KET inspection results. KET defect indications were found to arise from the presence of dirt and other surface contaminants. Stringent control of the surface finish and cleanliness of specimens should be maintained to assure accurate KET evaluation. Analysis of mechanical property test specimens indicated that KET did not have increased sensitivity for the location of fracture-causing defects. No test failures were observed in regions characterized as defective by KET alone. In two instances, failure did occur through KET indications, but these areas were also associated with FPI indications.

C. Summary

The Task II - Mechanical Property Testing effort was conducted to establish the effect of the various D.S. casting defects upon mechanical properties. The mechanical property evaluations included 1400°F (750°C) tensile and stress rupture and 1800°F (982°C) creep rupture and low cycle fatigue tests upon sets of sheet configuration specimens containing pre-existing casting defects. The defects included microshrinkage, dross and mold breakage inclusions and grain misorientation defects (emergent grains, diverging axis and diverging adjacent grains) each cast in one of three severity categories including mild, intermediate and severe. The specific ranges for the defects in these categories were established as a result of the defect characterization efforts in Task I. The NDI methods used to inspect the test specimens included standard production grain etch, X-ray and FPI inspections in addition to the Krypton Emission Technique (KET).

The mechanical property test results were interpreted not in terms of the intended defects, but rather in terms of those defects appearing on the actual fracture surfaces. This was done because in many instances failure did not occur through the intended defect, in other instances more than one defect was found on the fracture surfaces and in other cases defects on the fracture surfaces were more severe than indicated by NDI characterization. Evaluation of KET results indicated that this technique did not exhibit any advantage compared to standard FPI techniques for characterizing fracture-causing defects. In general, the tests results were quite similar in that microshrinkage, dross inclusions, and mold breakage inclusions were usually associated with the fracture surfaces. In only one instance was a grain misorientation defect observed to be associated with a fracture surface. In the majority of cases other defects were associated with the fracture surfaces. Microshrinkage appeared in approximately one half the fracture surfaces while dross inclusions were observed in approximately 1/3 the fractures. Mold breakage inclusions were observed less frequently.

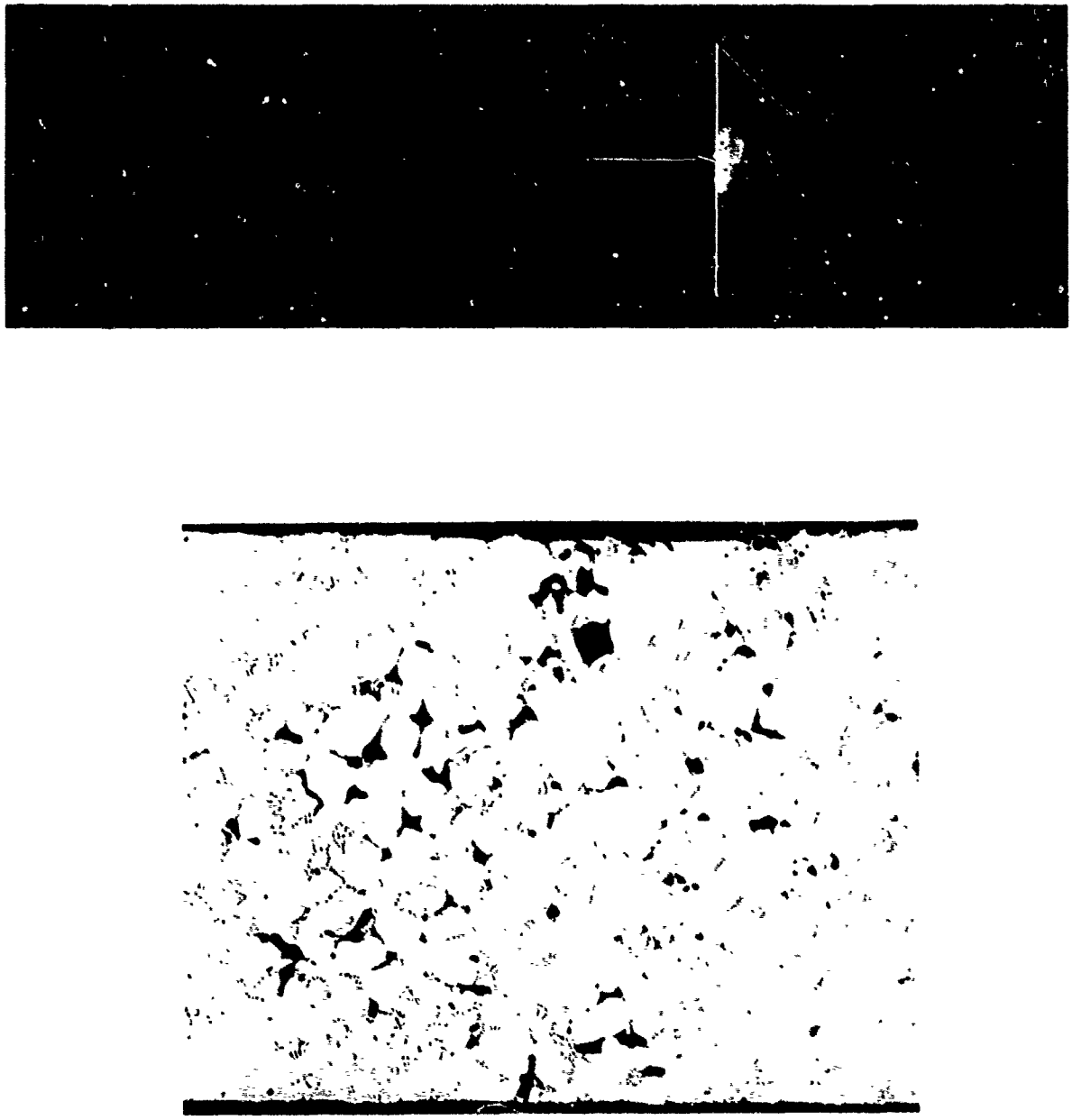

Figure 28. Metallographic Examination of KET Indication.

Top: Positive of KET Film

Bottom: Photomicrograph of Microshrinkage Associated wit h KET Indication at Section A-A. 50X

The general trends of the 1400°F (760°C) tensile results for the microshrinkage, dross and mold breakage defects were quite similar in that no significant degradation in either ultimate tensile or yield strength was observed as the result of the presence of these defects even at the most severe levels. An embrittling effect was observed, however, in the form of ductility reductions, but this was a function of the defect and the severity level. Microshrinkage and dross inclusion defects were not observed to be harmful at the mild severity level, but mold breakage inclusions were harmful at all three severity levels. Considerable scatter was observed during the 1400°F (760°C) stress rupture testing. Identifiable trends, however, indicated that defects at the mild severity level did not result in significant reductions in rupture life or ductility. These results thus indicated that defects in excess of the current 0.010" (.25 mm) limit could be tolerated as long as the linear grouping or clusters of defects in the castings were less than 0.30" (8 mm) in length or diameter.

The 1800°F (982°C) creep rupture and low cycle fatigue properties exhibited extreme sensitivity to the presence of microshrinkage, dross and mold breakage inclusions. In all cases significant reduction in either stress rupture life, ductility, low cycle fatigue life or cycles to crack initiation were observed even at the mild defect levels. The low cycle fatigue crack propagation rate at 1800°F (982°C), on the other hand, was relatively insensitive to the presence of the casting defects. This crack growth insensitivity, however, was of relatively minor importance to the overall fatigue life in view of the significant decrease in crack initiation life observed for the defect-containing specimens. These overall results suggested little tolerance to the microshrinkage, dross and mold breakage types of casting defects.

SECTION V

SUMMARY AND CONCLUSIONS

A program was conducted in order to determine the effects of various defects found in D.S. MAR-M200 + Hf (PWA-1422) superalloy castings upon mechanical properties. The work was directed toward providing a basis for the establishment of more realistic NDI acceptance criteria for production castings. The technical approach involved two tasks. In Task I - Defect Characterization, casting defects in F-100 1st and 2nd stage PWA-1422 turbine blades were defined in terms of the type, size and location of defects within production components. These defects included grain misorientation, porosity, macrosegregation, inclusions and surface cracking. It was determined in Task I that substantial decreases in the rejection rate at any nondestructive inspection step could be achieved with only minor relaxation of the acceptability criteria. For example, a decrease of up to 30% in rejection rate for diverging adjacent grains could be realized for an increase of 5° in diverging adjacent acceptance criterion. In addition, a survey of the cause for NDI rejection of D.S. blades over a two year period was conducted. Dross inclusions, detected by fluorescent penetrant inspection, were found to be the single most frequent cause for casting rejections. The survey also revealed that mold breakage inclusions and grain etch defects made substantial contributions to the overall rejection rate. Other defects, such as freckles and porosity had only a minimum effect upon the rejection rate. The size distribution of the observed defects suggested that minor relaxation of current reject criteria could result in significantly improved casting yield. The Task I results therefore identified specific defects and severity levels which would be most responsive to more tolerant NDI criteria in terms of increased casting yield.

In Task II - Mechanical Property Testing, efforts were directed toward establishing the effect of the defects upon mechanical properties. The mechanical property evaluations included $1400^{\circ}F$ ($760^{\circ}C$) tensile and stress rupture as well as $1800^{\circ}F$ ($982^{\circ}C$) creep rupture and low cycle fatigue tests conducted upon thin sheet type specimens containing pre-existing casting defects. The defects evaluated included microshrinkage dross, mold breakage inclusions and grain misorientation defects (emergent grains, diverging axis and diverging adjacent grains). Three severity levels of each defect type were tested. The severity levels were established as a result of the defect characterization efforts in Task I. The test specimens were inspected by production grain etch, fluorescent penetrant and X-ray techniques as well as by KET, a novel NDI inspection method. The results were interpreted in terms of the defects actually associated with specimen fracture, because in many instances failure was not associated with the intended defect or intended severity level, but with another defect/defect severity level in the specimen. KET inspection did not exhibit an improvement over standard NDI methods in detecting the defects associated with failure. Microshrinkage, dross and mold breakage inclusions were usually associated with fracture surfaces. In general, failures did not occur in association with grain misorientation defects, but were associated with other defects (i.e., microshrinkage) in the specimen. In only one instance (a diverging adjacent grain) was a grain misorientation defect associated with specimen failure.

The 1400°F (760°C) tensile test results indicated no strength degradation as a result of the presence of casting defects. Ductility reductions were observed, however, but the reductions were dependent upon defect type and severity level. Microshrinkage and dross adversely affected ductility, but only at the intermediate and severe levels, while mold breakage inclusions brought about significant ductility reductions at all severity levels. The 1400°F (760°C) stress rupture results showed that defects in the mild severity condition did not degrade life or ductility. Significant property reductions were observed, however, for defects at the intermediate and severe levels. These results indicated that defects in excess of the current .010" (.25 mm) acceptability limit could be tolerated as long as the linear groupings or clusters of defects in the casting were less than 0.30" (8 mm) in length or diameter.

With the exception of the grain misorientation defects, which could not be associated with any specimen, fracture, the 1800°F (982°C) creep and low cycle fatigue properties were extremely sensitive to the presence of casting defects. Significant reductions in rupture life and ductility, and in fatigue failure life and cycles to crack initiation were observed for defects even at the mild defect level. The low cycle fatigue crack propagation rates obtained at 1800°F (982°C) were insensitive to the presence of the casting defects. This insensitivity, however, was relatively minor in importance to the overall fatigue life in view of the significant decrease in crack initiation life observed for the defect-containing specimens. The results thus suggested little tolerance on the part of castings for microshrinkage, mold breakage and dross inclusion defects.

SECTION VI

RECOMMENDATIONS

The following discussion includes an appraisal of the effects of various D.S. casting defects upon mechanical properties in terms of the implication of these results on current production rejection criteria. The present investigation was conducted to provide a rationale or framework for establishing a reject criteria for D.S. superalloy materials. To accomplish this, work was directed towards developing an understanding of the effect of various casting defects and their severity levels on mechanical properties. The defects and the severity levels included in the study were selected after consideration of both minimum acceptance levels as included in current quality control specifications as well as the characterization studies conducted on reject production castings. In general, the mild level represented a defect condition somewhat similar to or a little worse than the current production minimum acceptance defect size or misorientation angle. More severe conditions represented greater deviations from this minimum condition. Specimens were allocated to the various defect categories on the basis of current standard NDI techniques such as grain etch, X-ray and FPI examination. The results indicated, however, that in many instances the fracture surfaces were not associated with the intended defects. Either other defects were found on the fracture or the actual defect severity levels were more severe than indicated by NDI examination. The most significant relationships, then, were developed not in terms of intended defects, but in terms of those defects actually appearing on the fracture surfaces.

The grain etch type defects included misorientation defects such as emergent grains, diverging adjacent and diverging axis grains. The most significant observation concerning these defects was that failure did not usually occur through the misoriented grains. In many instances other defect types were associated with fracture surfaces of specimens containing the misoriented grains. In only one instance during the entire test program (a diverging adjacent grain) was failure observed to be associated with a misorientation defect. Of particular importance was the fact that emergent grains, some oriented at greater than 60° to the turbine blade axis, were not the sites for fracture initiation. Although other defect types were found on the fracture surfaces of test specimens containing misoriented grains, the almost complete absence of failure through the defects did suggest that the rejection criteria associated with the defects be re-evaluated. The emergent grain defect category, in particular, represented an important candidate for re-evaluation because of the frequency of occurrence of these defects as causes for casting rejections. It is recognized, however, that any re-evaluation of the emergent grain acceptance criteria must also take into account the possible detrimental thermal fatigue effects associated with the high modulus of elasticity of off axis grains as observed with the MAR-M247 alloy (16). The most likely situation, then, for relaxation of emergent grain rejection criteria would include conditions in which grains are aligned in a low modulus of elasticity direction.

The present X-ray and FPI acceptance criteria are quite complicated (see Appendices III and IV) and include such defects as microshrinkage, dross inclusions and mold breakage inclusions. All three of these defects were observed with frequency on specimen fracture surfaces and had degrading effects upon the 1400°F (760°C) and 1800°F (982°C) mechanical properties. The extent of the degradation, however, was dependent upon the defect type and severity level. For both X-ray and FPI defects, current quality control criteria specify that indications .010" (.25 mm) or smaller in diameter which are clearly separated and not in linear alignment are acceptable. Linear indications and groupings or clusters of indications the lengths and diameters of which are much larger than the .010" (.25 mm) dimension are allowed depending upon their locations within the castings. Certain areas of the castings are considered critical (e.g., airfoil leading and trailing edges) and as such the tolerance levels for casting defects are quite stringent. Other areas of the castings are not considered quite so critical and as such the rejection criteria are much more tolerant to the presence of casting defects. The following discussion focuses on these rejection criteria not in overall general terms, but more specifically in terms of certain locations on the castings and their anticipated service temperature regimes.

In general, the root portions of turbine blade castings are exposed to temperatures in the 1000°F (538°C) - 1400°F (769°C) range. The results of the 1400°F (760°C) testing program indicated that the tensile and stress rupture properties were sensitive to microshrinkage, dross inclusion and mold breakage inclusion defects but usually only at the more severe levels. The tensile results indicated that microshrinkage and dross inclusion defects were detrimental to strength and ductility only when the clusters and/or linear groupings of indications were greater than 0.30" (8 mm) in diameter or length. Mold breakage inclusions, however, were found to be detrimental to tensile ductility even at levels close to the 0.10" (.25 mm) acceptability limit. The stress rupture properties at 1400°F (760°C) indicated little detrimental effect of the microshrinkage, dross inclusion, and mold breakage defects up to cluster/linear groupings as large as 0.50" (12.8 mm) in length or diameter. In terms of these particular mechanical properties, then, the results suggested that both FPI and X-ray reject criteria involving microshrinkage and dross inclusion defects in the root areas of castings be re-evaluated. For example, the reject criteria listed in Appendix III for FPI defects on casting root inlet and exhaust faces call for rejection when indications in groups 1/32" (0.8 mm) or larger are observed. The 1400°F (760°C) mechanical property results, however, suggested that defects in these size ranges would not be detrimental to D.S. castings. The results of the study indicated that because mold breakage inclusions significantly degraded tensile ductility at 1400°F (760°C) present rejection criteria for these defects should remain in effect.

An important consideration concerning the potential relaxation of X-ray and FPI rejection criteria for microshrinkage and dross inclusion defects in the root areas of turbine blade castings, however, involves the limits of their detectability by current NDI procedures. In the present investigation a number of specimens failed through non-detected casting defects or failed through defects more severe in nature than indicated by NDI examination. Effective relaxation of acceptance criteria for the microshrinkage and dross inclusion type defects can be accomplished only with the assurance that the severity of a particular defect be accurately determined by NDI techniques. In a number of instances during the present study sufficient accuracy in quantifying defect severity levels was not successfully demonstrated. This may limit the ability to successfully relax certain X-ray and FPI rejection criteria for the root areas of turbine blade castings.

The airfoil regions of turbine blade castings are exposed to a higher temperature regime than the root areas. In the present investigation, testing was conducted at 1800°F (982°C) to characterize airfoil performance and included creep rupture and low cycle fatigue testing. The mechanical property response indicated extreme sensitivity to the presence of all microshrinkage, dross inclusion and mold breakage inclusion defects even at the mild severity levels. Significant reductions were observed in rupture life, rupture ductility, fatigue life and cycles to first crack initiation in the presence of the casting defects. These results suggested that in stress rupture or low cycle fatigue limited areas such as turbine blade airfoils little justification existed for re-evaluation of current rejection criteria involving microshrinkage, dross inclusion or mold breakage inclusion type defects.

APPENDIX A

PRODUCTION D.S. BLADE INSPECTION PROCEDURES

Subsequent to the casting of D.S. components, stringent quality assurance requirements must be met before the parts can be used in a gas turbine engine. The following sequence of steps is followed after the PWA-1422 K parts are cast and broken out of the mold.

1. "Green" Visual Observation (VO) - This is a visual inspection step to ensure that the core material has been removed from the cooling passages.

2. "Green" X-ray. This X-ray step is also taken to ensure complete core removal prior to heat treatment. The parts are then heat treated in accordance with PWA-1422K:

   2200°F (1204°C)/2 hours in argon

   +1975°F (1080°C)/2 hours in air

   + 1600°F (871°C)/2 hours in air.

   The inspection sequence is then continued.

3. Grain Etch - Parts are anodically etched in a solution of approximately 67% H_3PO_4, and 33% water, to which has been added a small amount of 56% HCl. Parts are etched at 47 amp per piece for 4-1/2 minutes to reveal the macrostructure. Grain misorientation, freckles and cracks are revealed during this inspection step.

4. "Green" Visual - Obvious defects, such as handling damage, very large inclusions and other gross evidence of nonconformance are found at this inspection step. After "green" visual inspection, the parts undergo several manufacturing processes, such as belting and airfoil polishing. Inspection then continues.

5. Visual Inspection - This step is used to find any defects revealed or caused by the manufacturing operations. The parts undergo a thermal cycle of 1975°F (1080°C) for ten minutes in hydrogen followed by a controlled cooling rate prior to fluorescent penetrant insepction (FPI). The thermal cycle enlarges any cracks which may exist in the castings, causing them to be more easily observed during FPI.

6. Fluorescent Penetrant Inspection - This step is carried out to detect the presence of surface connected defects. The parts are cleaned ultrasonically using a detergent solution and dried at 250°F (121°C) for 10 minutes. They are then dipped in ZL-54 penetrant for at least 18 minutes. The parts are washed in 80°F (27°C) agitated water for 2 minutes and hot air dried at 190°F (88°C) for 1 minute and 45 seconds. They are dusted with ZP-4 powder and allowed to develop for 10 minutes prior to being read.

7. Dimensional Check - The parts are checked for overall dimensions using guillotine gages and the wall thickness is checked by ultrasonic techniques.

8. Final X-ray Inspection - The final X-ray inspection is performed at this point. In general, a sensitivity level of 1-1/2% is required and the orientations of the exposures are dependent upon part geometry. The following X-ray parameters are used for each view:

Film - Gaevert Fine Grain Industrial X-ray Film

Focal Spot - .16" (4 mm)

Amperage - 10 ma

X-ray Tube to Film Plate Distance - 48" (1219 mm)

View A - Trailing Edge

105 kv for 120 seconds

View B - Airfoil

160 kv for 120 seconds

View C - Thick Root Section

245 kv for 180 seconds

View D - Thin Root Section

220 kv for 130 seconds

View E - Tip

100 kv for 105 seconds

The entire casting is therefore examined by X-ray techniques which are designed to inspect for 1-1/2% indications in any location. Confidence is not placed in any single overall view.

9. Final Visual Observation - This is an inspection to ensure cleanliness of the cooling air passages, performed by visual observation. After these inspection operations are completed the part can be packed and shipped. During the packing operation, a final visual check of the components is performed.

APPENDIX B

GRAIN ETCH ACCEPTABILITY CRITERIA FOR CAST, DIRECTIONALLY SOLIDIFIED TURBINE BLADES

1. Acceptance Limits

A. Columnar grains shall be straight, parallel and without abrupt changes in size. Extending from the growth zone through the inner platform, airfoil and into the outer platform the following limits shall apply:

Defect Type	Maximum Deviation
a. Emergence	10^{o}
b. Divergence Between Adjacent Grains	20^{o}
c. Divergence From Airfoil Major Axis	15^{o}

B. Segregation is subject to the following limits:

Description	Maximum Quantity	Maximum Dimension
Segregation in Hollow Airfoils (Freckles)	3	1/32" (.8 mm) x 3/8" (9.5 mm) Not Exceeding a Total Length of 3/4" (19.1 mm)

APPENDIX C

FLUORESCENT PENETRANT ACCEPTANCE CRITERIA FOR CAST, DIRECTIONALLY SOLIDIFIED BLADES

1. Acceptance Limits

A. Indications .010" (.25 mm) diameter or less which are clearly separated and not in linear alignment are acceptable.

B. Indications of dross, shrinkage and porosity are acceptable in the areas specified and not exceeding the following limits:

Area	Maximum Quantity	Minimum Separation	Maximum Diameter
Leading and Trailing Edges	8 per part	1/8"(3.2 mm)	1/64" (0.4 mm)
Fillet	6 per side	1/8" (3.2 mm)	1/64" (0.4 mm)
		or	
	4 per side	1/4" (6.4 mm)	1/32" (0.8 mm)
Airfoil-Platform Radius	0		0.010 (.25 mm)
Airfoil	10 per side	1/8" (3.2 mm)	1/32" (0.8 mm)
Root Inlet and Exhaust Faces	4 per side	1/4" (6.4 mm)	1/32" (0.8 mm)
		or	
	1 per part linear alighment of 3 indication or cluster		1/64" (0.4 mm) each in a 3/16" (4.8 mm) diameter circle
Root Faces	4 per side	1/8" (3.2 mm)	1/32" (0.8 mm)
		or	
	1 per side linear alignment of 3 indications		1/64" (0.4 mm) each in a 3/16" (4.8 mm) diameter circle
Platform Root Side	5 per inch of area length	1/8" (3.2 mm)	1/32" (0.8 mm)
and		or	
Platform, Airfoil Side	1 linear alignment or cluster of no more than 3 indications	1/4" (6.4 mm)	1/64" (0.4 mm) each in a 3/16" (4.8 mm) diameter

Area	Maximum Quantity	Minimum Separation	Maximum Diameter
Platform, Airfoil Side Only	2 additional indications	1/4" (6.4 mm)	1/8" (3.2 mm)
	and		
	1 microshrink	1/4" (6.4 mm)	1/64" (0.4 mm) or less each indication contained in a 1/4" x 1/2" (6.4 mm) x 12.8 mm) area

C. Indications shall be no closer than .006" (0.15 mm) to fillet or edge radii excluding cooling hole edge radii.

APPENDIX D

X-RAY ACCEPTABILITY CRITERIA FOR CAST, DIRECTIONALLY SOLIDIFIED TURBINE BLADES

1. Acceptance Limits

A. Inclusion and Gas Holes - Imperfections in the areas specified and not exceeding the following limits:

Area	Maximum Quantity	Minimum Separation	Maximum Dimension
Leading and Trailing Edges, Platform Fillet and Airfoil Fillet, Root Attachment Airfoil	0		.010" (.25 mm)
	6 but limited to 2 in any 1" (25.4 mm) airfoil span length	.250" (6.4 mm)	.050" (1.3 mm)
Root (Except Fillet and Attachment Area)	3	.040" (1.0 mm)	.020" (.5 mm)
		or	
	2	.050" (1.3 mm)	.030" (.8 mm)

B. Shrinkage - Imperfections in the areas specified and not exceeding the following limits:

Area	Maximum Quantity	Minimum Separation	Maximum Dimension
Leading and Trailing Edges, Platform Fillet and Airfoil Fillets, Root Attachment Airfoil	0		.010" (.25 mm)
	15 of any size combination	.125" (3.2 mm)	.062" (1.6 mm)
		or	
		.250" (6.4 mm)	.125" (3.2 mm)
		or	
	1	.5" (12.8 mm)	.250" (6.4 mm)
Root (Except Fillet and Attachment Area)	3	.050" (1.3 mm)	.016" (.4 mm)
		or	
	2	.032" (.8 mm)	Cluster with a maximum diameter of .032" (.8 mm)

APPENDIX E

TYPICAL EXAMPLES OF EACH CASTING DEFECT AT EACH SEVERITY LEVEL

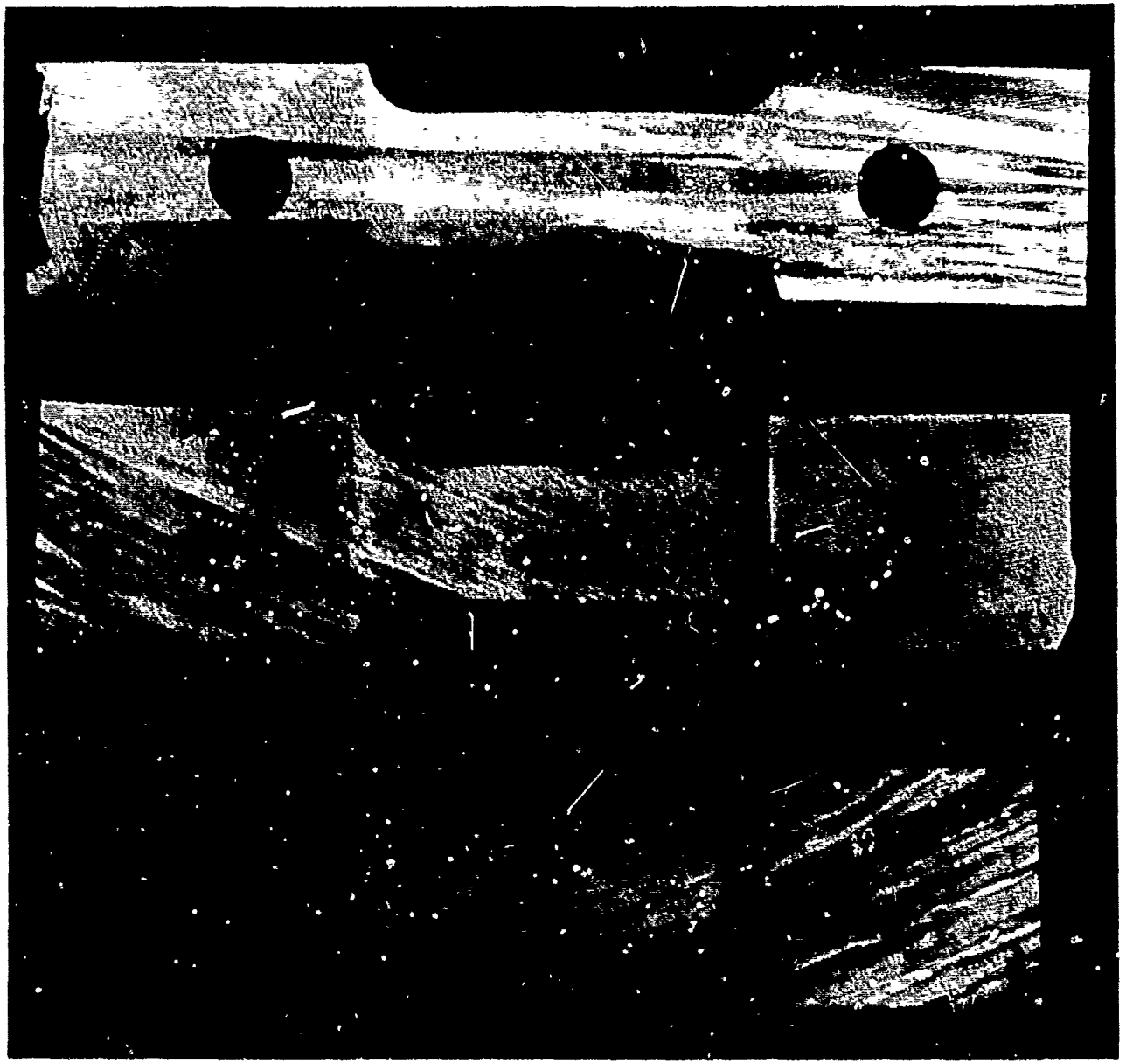

Examples of Emergent Gram Defects. Top - Mild, Center - Intermediate, Bottom - Severe. 1X Magnification.

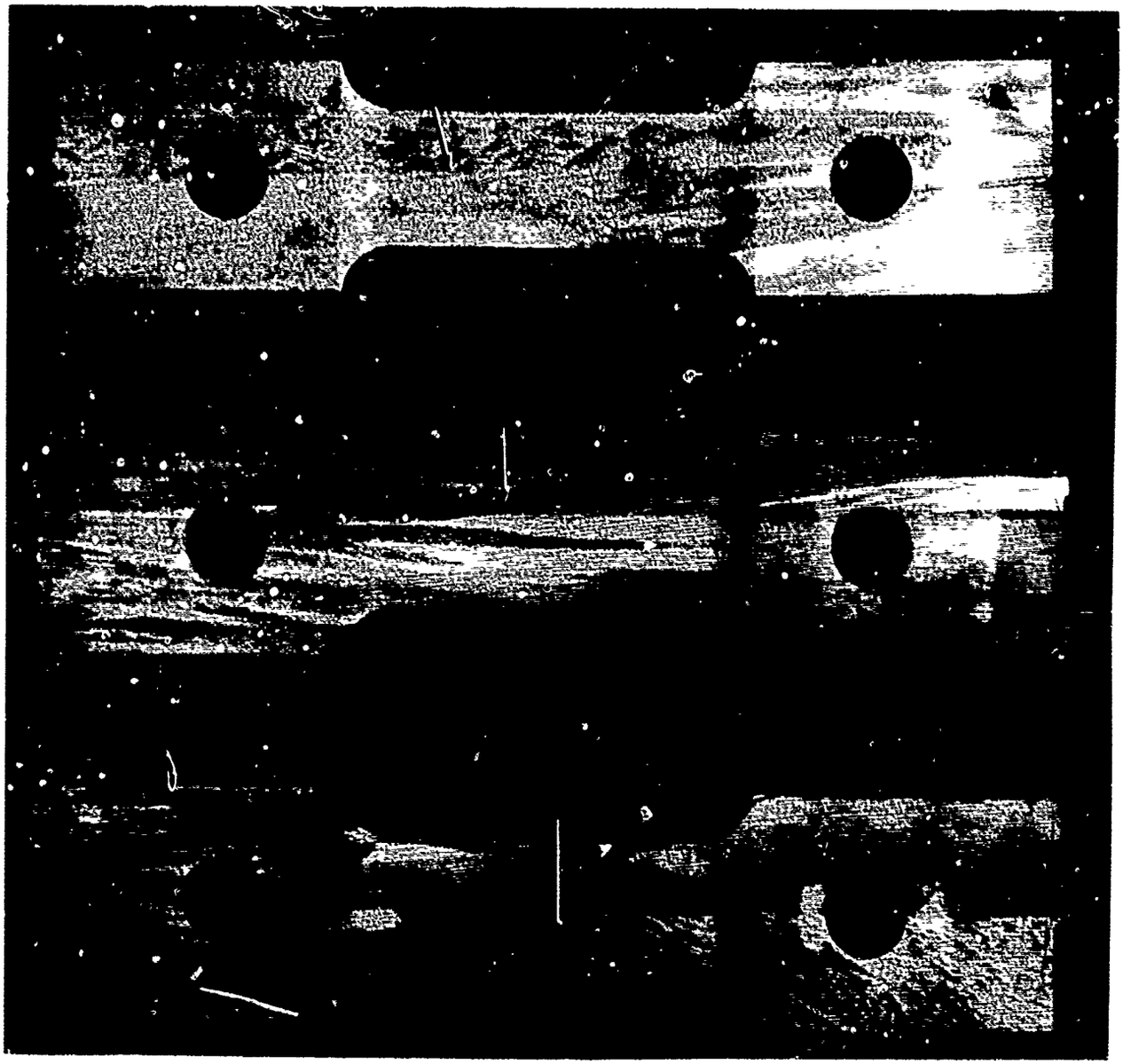

Examples of Diverging Axis Grain Defects. Top - Mild, Center - Intermediate, Bottom - Severe. 1X Magnification.

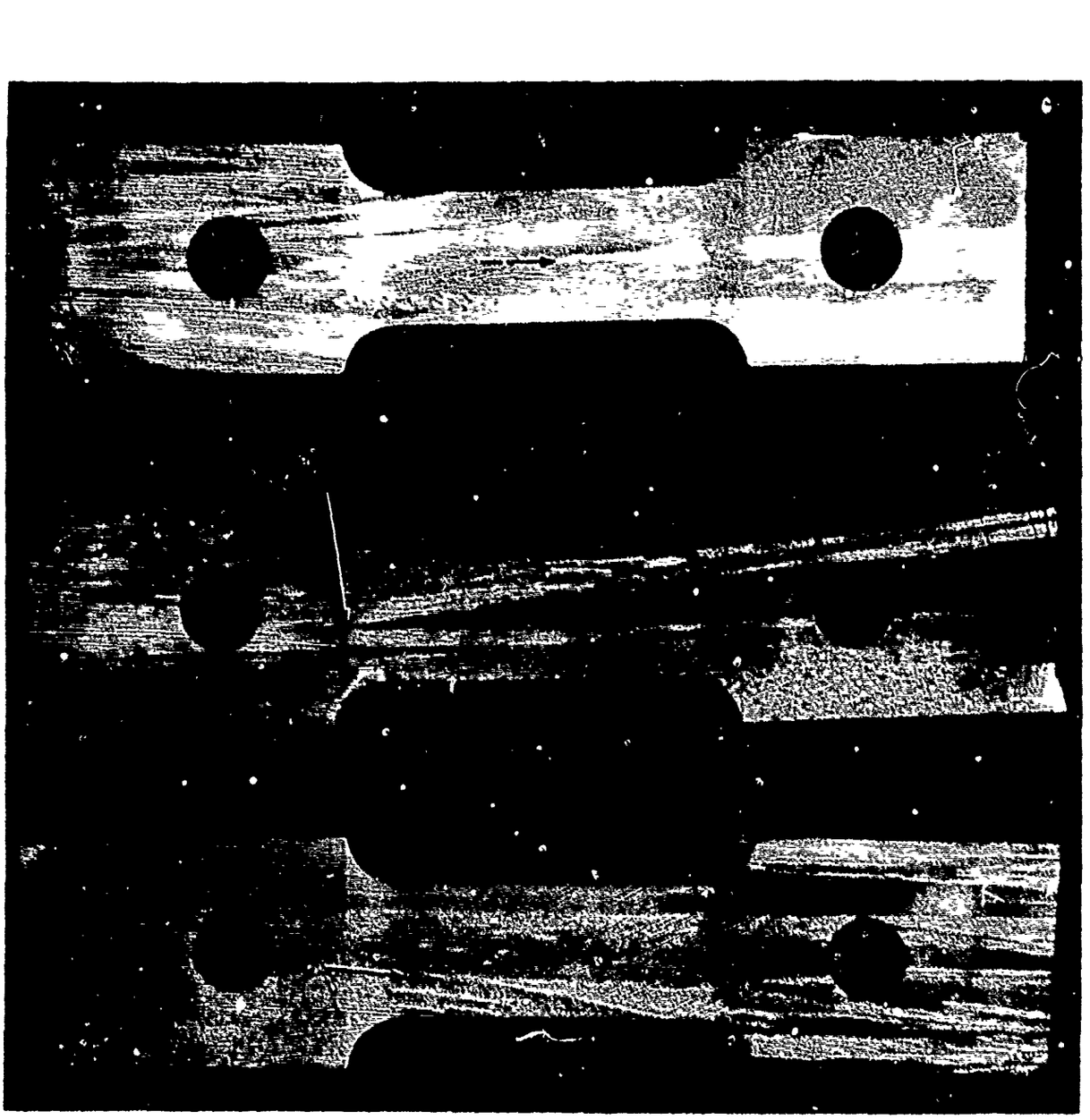

Examples of Diverging Adjacent Grain Defects. Top - Mild, Center - Intermediate, Bottom - Severe. 1X Magnification.

Examples of Positive X-Rays of Microshrinkage Defects. Top - Mild, Center - Intermediate, Bottom - Severe. 1X Magnification.

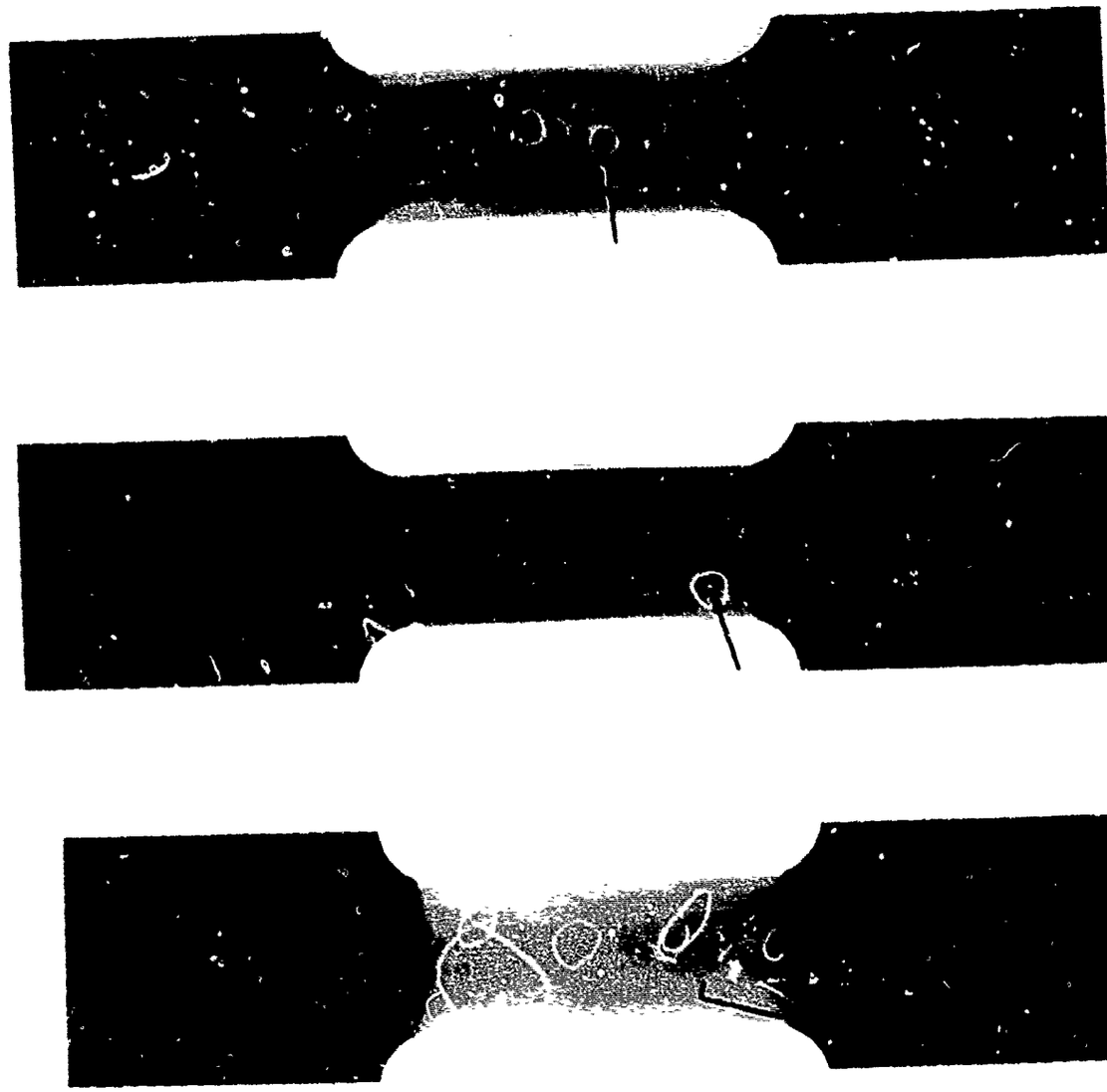

Examples of Positive X-Rays of Inclusion Type Defects. Top - Mild, Center - Intermediate, Bottom - Severe. 1X Magnification.

APPENDIX F

1400°F (760°C) TENSILE TEST RESULTS

APPENDIX F

1400°F (760°C) TENSILE TEST RESULTS

Defect Type	Valid	U.T.S. ksi	U.T.S. (MPa)	.2 Y.S. ksi	.2 Y.S. (MPa)	% El.	% R.A.	Failed Through: Intended Defect	Failed Through: Other NDI Defect	Failed Through: Undetected Defect	Defect Free
Defect Free	No	147.1	1014.2	131.1	903.9	2.5	6.2	X			X
		126.0	868.4	117.6	810.8	2.0	3.4	X			X
		103.3	712.2	90.3	622.6	3.0	18.0			X - Mild Shrink, Severe Dross	
		136.0	937.7	104.3	719.1	2.5	9.7		X - Mild Shrink		
		122.1	841.9	117.2	808.1	0.5	0.5		X - Mild Shrink		
		142.8	984.6	117.7	811.5	4.2	1.3				X
Mild Shrink	No	139.4	961.1	121.4	837.6	0.5	12.1	X			
		101.6	700.5	101.6	700.5	1.0	6.5				X
	No	150.4	1037.0	131.4	906.0	3.6	0.5		X - Intermediate Shrink in Shoulders		
	No	151.5	1044.6	*	*	2.3	1.6		X - Intermediate Shrink in Shoulders		
		107.8	743.3	96.2	661.3	0.5	8.9	X			
Intermediate Shrink		127.1	876.3	121.4	837.0	2.0	5.7	X			
		134.8	929.4	129.3	891.5	2.0	8.4	X			
		137.3	946.7	123.3	850.1	2.4	0.1	X			
		145.5	1003.2	129.3	891.5	3.0	0.6	X			
		145.9	1006.0	125.9	868.1	2.8	0.3	X			
		143.7	990.8	124.0	855.0	4.2	2.8	X		X - Mild Dross	
Severe Shrink		149.8	1032.8	129.7	894.3	3.0	12.1		X - Mild Shrink		
	No	122.1	841.9	117.7	811.5	0.5	0.5	X			
	No	141.3	974.2	125.8	867.4	2.9	5.5	X			
		133.1	917.7	-	-	1.7	5.9	X			
		133.1	917.7	130.1	897.0	1.6	3.3	X			
Mild Dross		141.5	975.6	124.6	859.1	2.0	7.2	X	X - Mild Dross		
		129.7	894.3	98.5	679.1	1.5	13.3		X - Intermediate Shrink	X - Mild Breakage	
		148.3	1022.5	129.5	892.9	3.5	2.7	X			
		138.3	953.5	126.5	872.2	2.0	6.1				X
		146.2	1008.0	122.5	844.6	2.9	5.1	X			
	No	135.1	931.5	122.8	846.7	3.5	5.1	X			

* Specimen failed before 0.2% Y.S.

APPENDIX F (CONTINUED)

Defect Free	Valid	U.T.S. ksi	U.T.S. (MPa)	.2 Y.S. ksi	.2 Y.S. (MPa)	% El.	% R.A.	Failed Through: Intended Defect	Failed Through: Other KDI Effect	Failed Through: Undected Defect	Defect Free
Intermediate Dross	No	134.6	928.0	121.8	939.8	2.0	8.3	X			
		142.9	985.3	125.0	861.8	3.5	11.4	X			
		138.3	953.5	135.2	932.2	1.7	1.9	X			
		117.2	808.1	-	-	1.9	4.5	X	X - Mild Shrink		
Severe Dross		136.0	937.7	102.3	705.3	1.5	5.0		X - Mild Shrink	X - Intermediate Mold Breakage	
		137.4	947.3	109.3	753.6	4.5	2.4	X			
		128.8	888.0	122.5	844.6	2.2	4.6	X	X - Intermediate Shrink		
Mild Mold Breakage		130.3	898.4	101.0	696.4	2.5	2.9	X	X - Mild Shrink		
		143.0	986.0	104.0	717.1	2.0	5.9			X - Intermediate Mold Breakage	
		148.6	1 24.6	133.2	918.4	3.9	7.5	X	X - Mild Shrink		
	No	136.9	943.9	122.1	841.9	3.8	5.5			X - Mild Shrink	
		133 1	917.7	124.0	855.0	3.0	4.8	X Secondary Crack	X - Mild Shrink		
		142.2	980.4	133.1	917.7	1.8	3.7			X - Severe Shrink	
Intermediate Mold Breakage	No	114.0	786.0	103.0	710.2	0.0	-			X - Intermediate Mold Breakage	
	No	125.1	862.5	103.1	710.9	0.0	-		X - Severe - Mis-interpreted Defect - Mold Breakage		
		139.6	962.5	126.6	872.9	3.6	5.1	X		X - Intermediate Shrink	
Severe Mold Breakage	No	105.0	724.0	-	-	0.0	1.7		X - Intermediate Shrink	X - Mild Dross	
		134.7	928.7	114.3	788.1	2.0	4.2	X Severe	X - Mild Shrink		
	No	125.8	867.4	97.9	675.0	1.5	9.2		X - Mild Shrink		
		129.1	890.1	100.2	690.9	0.5	7.7		X - Mild Shrink		
		153.5	1058.4	113.9	785.3	2.0	3.1	X	X - Intermediate Shrink		
Mild Emergence		110.5	761.9	91.0	627.4	6.5	14.6		X - Mild Shrinkage	X - Severe Dross	
		122.1	841.9	102.1	704.0	0.5	7.5		X - Mild Shrinkage		
		120.5	830.8	102.9	709.5	5.5	5.2				X
		118.6	817.7	102.4	706.0	9.7	11.8				X
		113.9	785.3	-	-	7.9	8.0				X
		121.2	835.6	109.1	752.2	10.0	11.8			X - Intermediate Dross	

APPENDIX F (CONTINUED)

Defect Type	Valid	U.T.S ksi	U.T.S (MPa)	.2 Y.S. ksi	.2 Y.S. (MPa)	% El.	% R.A.	Failed Through: Intended Defect	Failed Through: Other NDI Defect	Failed Through: Undetected Defect	Defect Free
Intermediate Emergence		113.4	781.9	93.3	643.3	14.0	22.4			Intermediate Dross	
		117.2	808.1	93.9	647.4	14.0	14.4		X - Mild Shrink + Dross		
	No	146.9	1012.8	106.0	730.8	1.5	2.0		X - Mild Shrink		
		132.9	916.3	99.2	684.0	2.0	9.3		X - Intermediate Shrink	X - Mild Breakage	
		115.8	798.4	110.9	764.6	3.4	8.8		X - Intermediate Shrink		
Severe Emergence		142.1	979.7	129.0	889.4	2.5	5.4		X - Mild Shrink		
	No	123.0	848.1	109.2	752.9	0.5	8.2		X - Mild Shrink		
		130.8	901.8	113.1	779.8	1.5	4.0		Acceptable X-ray Shrink		X
	No	130.1	897.0	115.6	797.0	3.4	0.1			X - Severe Dross in Shoulders	
		142.4	981.8	116.4	802.6	2.3	9.0				X
	No	131.7	908.0	-	-	2.0	0.6			X - Intermediate Shrink	
Mild Diverging Axis		138.4	954.2	119.5	823.9	1.0	3.5		X - Mild Shrink		
		133.7	921.8	123.4	850.8	2.5	3.2		X - Severe Mold Breakage Inclusion		
		126.0	868.4	126.0	868.7	1.0	5.4		X - Intermediate Mold Breakage		
		152.3	1050.1	136.9	943.9	2.9	4.0		X - Mild Shrink		
Intermediate Diverging Axis	No	108.9	750.8	108.9	750.8	1.5	0.5		X - Intermediate Dross		
		128.9	888.7	128.9	888.7	1.9	0.3		X - Severe Dross		
		143.9	992.2	-	-	3.2	4.0		X - Intermediate Dross		
		139.7	963.2	122.1	841.9	2.6	4.0			X - Severe Dross	
Severe Diverging Axis		135.0	930.8	118.0	813.6	3.3	4.6		X - Intermediate Shrink		
	No	138.6	955.6	125.9	868.1	3.1	2.1		X - Intermediate Shrink		
		125.8	867.4	103.3	712.2	1.5	2.6		X - Severe Mold Breakage		
Mild Diverging Adjacent		130.4	899.1	110.6	762.6	2.1	3.5		X - Mild Shrink		
		148.8	1025.9	-	-	1.8	3.7		X - Severe Dross - Mild Dross		
		150.1	1034.9	130.5	899.8	3.0	2.2		X - Mild Shrink		
Intermediate Diverging Adjacent		149.9	1033.5	130.3	898.4	2.8	6.7		X - Mild Dross		
		131.8	908.7	131.8	908.7	3.0	2.9		X - Intermediate Dross		
		145.7	1004.6	110.7	763.3	3.0	15.9		X - Intermediate Breakage	X - Mild Shrink	
Severe Diverging Adjacent		156.6	1079.7	135.7	935.6	3.3	3.5		X - Severe Dross		
		146.4	1010.1	127.8	881.2	3.3	5.4		X - Intermediate Dross - Mild Shrink		
		144.5	996.3	113.2	780.5	1.5	8.4		X - Mild Shrink		

APPENDIX G

ANALYSIS OF DATA
1400°F (760°C) TENSILE TEST RESULTS

APPENDIX G

ANALYSIS OF DATA

1400°F (760°C) TENSILE TSET RESULTS

Defect Type	Property	No. of Data Points	High Value	Low Value	Average Value	-2 σ Value
Defect Free	Ultimate Strength-ksi (MPa)	9	142.8 (984.8)	101.6 (700.7)	124.3 (857.2)	87.5 (603.4)
	.2% Yield Strength-ksi (MPa)	8	118.6 (917.9)	101.6 (700.7)	114.3 (788.3)	85.0 (586.2)
	Elongation (%)	9	9.7	1.0	4.1	0.35
	R.A. (%)	9	11.8	1.3	6.8	0.57
Mild Microshrinkage	Ultimate Strength-ksi (MPa)	20	152.3 (1050.3)	103.3 (712.4)	131.2 (904.8)	101.0 (696.6)
	.2% Yield Strength-ksi (MPa)	19	136.9 (944.1)	90.3 (622.8)	111.1 (766.2)	80.6 (551.7)
	Elongation (%)	20	14.0	0.5	3.6	0.23
	R.A. (%)	20	22.4	0.5	8.7	1.0
Intermediate Microshrinkage	Ultimate Strength-ksi (MPa)	12	153.5 (1058.6)	127.1 (876.6)	137.8 (950.3)	117.0 (906.9)
	.2% Yield Strength-ksi (MPa)	12	129.3 (891.7)	98.5 (679.3)	119.3 (822.8)	96.0 (662.1)
	Elongation (%)	12	4.2	1.6	2.6	1.15
	R.A. (%)	12	13.3	0.1	4.8	0.29

APPENDIX G (CONTINUED)

Defect Type	Property	No. of Data Points	High Value	Low Value	Average Value	-2 σ Value
Severe	Ultimate Strength-ksi (MPa)	4	145.0 (1000)	133.1 (917.9)	138.3 (953.8)	111.0 (765.5)
	.2% Yield Strength-ksi (MPa)	3	133.1 (917.9)	124.5 (858.6)	129.2 (891.0)	89.0 (613.8)
	Elongation (%)	4	2.1	1.6	1.8	1.1
	R.A. (%)	4	5.9	3.0	3.9	1.6
Mild Mold Breakage	Ultimate Strength-ksi (MPa)	5	148.6 (1024.8)	129.7 (894.5)	134.9 (930.3)	122.0 (841.4)
	.2% Yield Strength-ksi (MPa)	5	133.2 (918.6)	98.5 (679.3)	111.1 (766.2)	63.0 (434.5)
	Elongation (%)	5	3.9	1.5	2.6	0.55
	R.A. (%)	5	13.3	2.9	7.7	1.0
Intermediate Mold Breakage	Ultimate Strength-ksi (MPa)	5	145.7 (1004.6)	126.0 (869.0)	138.0 (951.7)	113.0 (779.3)
	.2% Yield Strength-ksi (MPa)	5	126.6 (735.2)	102.3 (705.5)	113.9 (785.5)	89.0 (613.8)
	Elongation (%)	5	3.6	1.0	2.2	0.36
	R.A. (%)	5	15.9	5.0	7.5	4.0
Severe Mold Breakage	Ultimate Strength-ksi (MPa)	2	153.5 (1058.6)	134.7 (929.0)	144.1 (993.8)	110.0 (758.6)
	.2% Yield Strength-ksi (MPa)	2	114.3 (788.3)	113.9 (785.5)	114.1 (786.9)	105.0 (724.1)
	Elongation (%)	2	2.0	2.0	2.0	2.0
	R.A. (%)	2	4.2	3.1	3.7	1.4

APPENDIX G (CONTINUED)

Defect Type	Property	No. of Data Points	High Value	Low Value	Average Value	-2 σ Value
Mild Dross	Ultimate Strength-ksi (MPa)	8	150.1 (1035.2)	117.2 (808.3)	139.5 (962.1)	111.0 (765.5)
	.2% Yield Strength-ksi (MPa)	3	130.5 (900.0)	93.9 (647.6)	121.2 (835.9)	100.0 (690)
	Elongation (%)	8	14.0	2.0	4.4	1.0
	R.A. (%)	8	14.4	2.2	6.0	0.83
Intermediate Dross	Ultimate Strength-ksi (MPa)	6	151.8 (1046.9)	117.2 (808.3)	138.7 (956.6)	105.0 (724.1)
	.2% Yield Strength-ksi (MPa)	4	135.2 (932.4)	121.8 (840.0)	129.2 (891.0)	98.0 (675.9)
	Elongation (%)	6	3.3	1.7	2.5	1.0
	R.A. (%)	6	8.3	1.9	4.5	0.82
Severe Dross	Ultimate Strength-ksi (MPa)	8	156.6 (1080.0)	103.3 (712.4)	131.8 (909.0)	88.0 (606.9)
	.2% Yield Strength-ksi (MPa)	7	135.7 (935.9)	90.3 (622.8)	114.2 (787.6)	70.0 (482.8)
	Elongation (%)	8	6.5	1.8	3.2	0.65
	R.A. (%)	8	18.9	0.3	5.6	0.13

APPENDIX H

1400°F (760°C)/90 KSI (620.7 MPa) STRESS RUPTURE TEST RESULTS

APPENDIX H

1400°F (760°C)/90 KSI (620.7 MPa) STRESS RUPTURE TEST RESULTS

Defect Free	Valid	Life	% El.	% R.A.	Failed Through: Intended Defect	Failed Through: Other NDI Defect	Failed Through: Undetected Defect	Failed Through: Defect Free
Defect Free		52.4	2.5	7.4	X			X
	No	215.6	2.0	6.9	X			X
		217.8	3.5	12.3	X			X
	No	199.5	3.5	5.6	X			X
		88.8	3.5	6.9			X - Severe Dross	
Mild Microshrinkage	No	357.6	2.1	3.5		X - Severe Microshrinkage		
		141.9	3.5	3.6	X			
		127.0	3.0	3.1	X			
		16.6	3.0	4.6			X - Severe Microshrinkage	
	No	.34	3.0	9.9			X - Severe Microshrinkage	
		186.6	3.8	4.5			X - Intermediate Microshrinkage	
Intermediate		8.2	2.0	7.4			X - Intermediate Dross and Microshrinkage	
		18.2	3.0	3.2	X			
		175.7	6.0	7.3	X		X - Mild Breakage	
		33.1	2.0	5.8	X		X - Mild Breakage	
		150.2	2.0	7.4	X			
Severe Microshrinkage		41.3	3.0	7.6				X
		46.1	3 5	6.4	X			
		16.2	3.0	3.8	X			
		254.2	3.6	10.2	X			
Mild Dross		165.3	4.0	9.5		X - Intermediate Microshrinkage		
		286.5	1.5	7.1		X - Severe Dross		
		670+	Overloaded				X - Mild Microshrinkage	
		320.1	Overloaded				X -Intermediate Breakage	

APPENDIX H (continued)

Defect Type	Valid	Life	% El.	% R.A.	Failed Through: Intended Defect	Failed Through: Other NDI Defect	Failed Through: Undetected Defect	Defect Free
Intermediate Dross		549.7	4.1	6.4	X			
		326.6+	Overloaded			X - Intermediate Microshrinkage		
	No	236.8	Overloaded		X			
		378.8	4.1	6.2	X			
Severe Dross		226+	Overloaded		X			
	No	436.4	2.1	3.6		X - Intermediate Microshrinkage		
Mild Mold Breakage		751.4	3.4	4.1			X - Severe Dross	
		502.1+	Overloaded				X - Mild Microshrinkage	
		1.7	1.9	8.5		X - Intermediate Microshrinkage		
		174.9	3.7	2.5	X			
		931.8	5.3	10.3		X - Mild Microshrinkage	X - Mild Dross	
	No	57.7	4.5	10.1	X		X - Mild Dross	
Intermediate Mold Breakage		27.2	2.0	2.7	X	X - Mild Microshrinkage		
	No	575.7	2.1	3.4	X			
Severe Mold Breakage	No	238.2			X			
	No	168.7+	Overloaded			X - Intermediate Microshrinkage		
Mild Emergence	No	223.8	7.5	13.7		X - Intermediate Microshrinkage		
		429.3	1.5	4.9		X - Intermediate Microshrinkage		
	No	33.7	1.5	7.9				
		103.1	2.0	6.8			X - Intermediate Dross	
		187.3	1.5	11.0			X - Intermediate Dross	
	No	107.8	1.4	3.2			X - Intermediate Dross	
Intermediate Emergence	No	8.5	1.2	3.2		X - Severe Microshrinkage		
		1166+	Overloaded				X - Mild Dross	

APPENDIX H (continued)

Defect Type	Valid	Life	% El.	% R.A.	Failed Through: Intended Defect	Failed Through: Other NDI Defect	Failed Through: Undetected Defect	Defect Free
Severe Emergence	No	346.2	4.7	5.6		X - Intermediate Dross		
		6.5	2.0	10.2		X - Intermediate Microshrinkage	X - Severe Mold Breakage	
		96.4	5.0	10.2			X - Mild Dross	
		185.0	6.0	8.1			X - Mild Microshrinkage	
	No	260.0	3.5	3.6		X - Intermediate Microshrinkage		
		131.5	4.5	9.7			X - Mild Microshrinkage	
Mild Diverging Axis		10.9	1.7	5.7		X - Intermediate Microshrinkage		
						X - Intermediate Dross		
		590.3	4.3	7.3		X - Intermediate Dross		
		77.3	2.4	4.5				X
Intermediate Diverging Axis	No	974.3	4.4	0.8			X - Mild Dross	X
		815.7	8.6	3.2				
		522.3	5.8	5.5		X - Intermediate Mold Breakage		
		713.2	3.4	4.9			X - Intermediate Dross	
Severe Diverging Axis		706.9	4.1	4.9		X - Mild Dross		
		847.8	4.3	5.2		X - Intermediate Dross		
						X - Mild Microshrinkage		
		401.7+	Overloaded				X - Intermediate Breakage	
							X - Intermediate Dross	
Mild Diverging Adjacent		678.4	6.4	4.4				
		21.2	3.1	9.5		X - Intermediate Microshrinkage		
		302.4	Overloaded			X - Intermediate Dross		
	No	24.4	Overloaded			X - Intermediate Microshrinkage		
								X
Intermediate Diverging Adjacent		170+	Overloaded				X - Mild Breakage	
		577+	Overloaded					
							X - Mild Microshrinkage	
Severe Diverging Adjacent		506+	Overloaded			X - Severe Microshrinkage		
		24	Overloaded					

APPENDIX I

ANALYSIS OF DATA
1400°F (760°C)/90 KSI (620.7 MPa) STRESS RUPTURE RESULTS

APPENDIX I

ANALYSIS OF DATA

1400°F (760°C)/90 KSI (620.7 MPa) STRESS RUPTURE RESULTS

Defect Type	Property	No. of Data Points	High Value	Low Value	Average Value	-2σ Value
Defect Free	Life (hours)	6	815.7	52.4	229.1	3.8
	El. (%)	5	5.6	2.4	3.4	1.2
	R.A. (%)	5	12.3	3.2	7.0	1.3
Mild Microshrinkage	Life (hours)	10	931.8	27.2	372.0	9.8
	El. (%)	7	6.0	2.0	4.1	1.2
	R.A. (%)	7	10.3	2.7	6.0	0.8
Intermediate Microshrinkage	Life (hours)	13	429.3	1.7	118.0	0.2
	El. (%)	12	6.0	1.5	2.8	1.1
	R.A. (%)	12	10.2	3.2	7.2	2.5
Severe Microshrinkage	Life (hours)	5	254.2	4.6	69.0	0.85
	El. (%)	5	3.6	1.0	1.9	0.5
	R.A. (%)	5	10.6	2.8	6.8	1.5
Mild Dross	Life (hours)	6	1166+	57.7	604.8	14.0
	El. (%)	4	5.3	4.1	4.7	3.7
	R.A. (%)	4	10.3	4.9	8.9	2.3
Intermediate Dross	Life (hours)	10	847.8	8.2	315.5	0.1
	El. (%)	10	6.4	1.5	3.2	0.92
	R.A. (%)	10	11.0	4.4	6.3	3.4
Severe Dross	Life (hours)	5	751.4	26+	338.1	17.5
	El. (%)	3	3.5	1.5	2.8	1.0
	R.A. (%)	3	7.1	4.1	6.0	2.1
Mild Breakage	Life (hours)	5	577+	33.1	203.7	1.0
	El. (%)	4	6.0	2.0	4.1	0.9
	R.A. (%)	4	10.1	2.5	6.4	.75
Intermediate Breakage	Life (hours)	4	522.3+	27.2	317.8	0.3
	El. (%)	2	5.5	2.0	3.8	0.4
	R.A. (%)	2	5.5	2.7	4.1	1.5

APPENDIX J

1800°F (982°C) CREEP RUPTURE TEST RESULTS

APPENDIX J

1300°F (982°C) CREEP RUPTURE TEST RESULTS

Defect Type	Valid	Life (Hrs.)	% El. (20 Hrs.)	% El.	% R.A.	Failed Through: Intended Defect	Failed Through: Other NDI Defect	Failed Through: Undetected Defect	Defect Free
Defect Free		58.7	0	7.0	9.5	X			X
		45.8	1.5	4.5	16.7	X			X
		59.9		15.5	26.5	X			X
		62.0		17.5	22.1	X			X
Mild Microshrinkage		57.2	1.0	7.0	8.4	X			
		50.7	1.5	12.0	28.6				X
		90.4	1.0	5.0	16.0	X		X - Mild Breakage	
		94.1	1.0	7.0	16.8	X			
	No	33.9	1.0	7.5	21.0	X	X - Mild Dross		
		59.6	1.5	19.0	38.2	X			
Intermediate Microshrinkage		46.6	.5	5.0	16.1	X			
		55.2	1.0	8.5	17.4	X			
		55.6	1.0	11.2	24.8	X			
	No	39.5	1.5	7.3	8.6	X			
		30.4	.5	7.9	15.8	X	X - Mild Breakage		
Severe Microshrinkage		46.0	1.0	7.0	19.0	X			
		67.8	0.5	9.5	26.8	X			
		32.2	5.0	9.0	16.9	X			
	No	73.9	1.5	9.3	16.7	X	X - Intermediate Mold Breakage		
		13.7	.5	5.0	9.7	X			
Mild Dross	No	61.8	1.0	12.5	24.7		X - Mild Microshrinkage		
		50.6	1.0	6.5	9.5		X - Mild Microshrinkage		
	No	46.1	1.0	10.8	20.6			X - Mild Breakage Int. Microshrinkage	
		50.1	.5	8.0	8.2	X		X - Mild Microshrinkage	
		48.6	.5	9.9	19.0	X		X - Mild Breakage	
		43.0	1.0	11.3	22.4	X	X - Intermediate Microshrinkage		

APPENDIX J (continued)

Defect Type	Valid	Life (Hrs.)	% El. (20 Hrs.)	% El.	% R.A.	Failed Through: Intended Defect	Failed Through: Other NDI Defect	Failed Through: Undetected Defect	Defect Free
Intermediate Dross		74.7	1.0	10.5	14.2	X	X - Mild Microshrinkage		
		57.1	1.0	10.5	14.5	X	X - Mild Microshrinkage		
		19.4	1.9	11.5	16.5	X			
Severe Dross		51.6	.5	13.2	20.1	X	X - Severe Microshrinkage		
	No	42.3	.5	14.6	18.7	X	X - Severe Microshrinkage		
Mild Breakage	No	33.4	1.5	6.0	18.5		X - Mild Microshrinkage		
	No	66.5	1.5	14.0	21.6			X - Mild Breakage	
		40.2	1.5	8.6	14.3	X		X - Mild Microshrinkage	
	No	44.3	.5	9.5	16.2	X			
	No	44.3	1.0	13.0	18.2	X	X - Mild Microshrinkage		
Intermediate Breakage	No	36.0	1.0	5.2	11.3	X	X - Intermediate Microshrinkage		
		31.4	1.5	3.9	10.6		X - Intermediate Microshrinkage		
Severe Breakage		38.0	.5	4.0	6.2	X			
	No	27.2	1.0	3.6	4.1	X			
Mild Emergence		70.7	1.0	15.0	14.7				X
		64.1	1.5	25.5	39.1				X
		50.8	1.0	15.8	19.4				X
	No	61.1	1.0	7.0	12.1		X - Mild Microshrinkage Mild Breakage		
Intermediate Emergence		51.9	1.5	10.5	18.3		X - Mild Microshrinkage		
		65.7	1.5	10.0	26.1			X - Mild Breakage	
		91.6	0.5	3.0	5.8		X - Mild Microshrinkage		

APPENDIX J (continued)

Defect Type	Valid	Life (Hrs.)	% El. (20 Hrs.)	% El.	% R.A.	Failed Through: Intended Defect	Failed Through: Other NDI Defect	Failed Through: Undetected Defect	Defect Free
Severe Emergence		65.4	1.0	12.0	18.8		X - Intermediate Microshrinkage Mild Dross		
		42.6	1.0	4.5	16.7		X - Mild Microshrinkage		
		35.7	2.0	6.5	11.0		X - Mild Dross Intermediate Microshrinkage		
		32.8	1.0	5.0	6.6		X - Intermediate Microshrinkage	X - Mild Dross	
Mild Diverging Adjacent		54.4	1.5	8.3	16.3		X - Intermediate Dross		
		43.7	1.5	8.5	11.2		X - Intermediate Breakage		
Intermediate Diverging Adjacent		73.3	0.5	7.5	7.5	X			
		82.8	0.5	16.2	23.5				X
		45.8	1.5	12.5	15.6		X - Mild Microshrinkage		
Severe Diverging Adjacent		46.3	0.5	11.2	20.7		X - Intermediate Microshrinkage		
		58.8	1.5	15.5	17.5		X - Mild Dross		
Mild Diverging Axis		42.0	.5	6.8	31.8		X - Intermediate Microshrinkage		
		48.7	2.0	5.6	23.8		X - Mild Microshrinkage		
Intermediate Diverging Axis		45.8	1.5	9.2	20.8		X - Mild Dross		
		56.0	1.0	9.2	13.3	X			
Severe Diverging Axis		49.6	1.0	6.0	18.5		X - Mild Microshrinkage		
		41.1	.5	7.5	19.7		X - Mild Dross		
		55.2	1.0	24.5	36.4		X - Mild Microshrinkage		

APPENDIX K

ANALYSIS OF DATA
1800°F (982°C)/30 KSI (207 MPa) STRESS RUPTURE TEST RESULTS

APPENDIX K

ANALYSIS OF DATA

1800°F (982°C)/30 KSI (207 MPa) STRESS RUPTURE TEST RESULTS

Defect Type	Property	No. of Data Points	High Value	Low Value	Average Value	-2 σ Value
Defect Free	Life (hours)	9	82.8	45.8	60.6	39
	El. (%)	9	25.5	4.5	14.3	9
	R.A. (%)	9	39.1	9.5	22.2	9.3
Mild Microshrinkage	Life (hours)	16	94.1	40.2	59.9	37
	El. (%)	16	24.5	3.0	9.3	2.4
	R.A. (%)	16	38.2	8.2	17.2	4.8
Intermediate Microshrinkage	Life (hours)	12	65.4	30.4	44.2	18
	El. (%)	12	12.0	3.9	8.3	2.9
	R.A. (%)	12	31.8	6.6	18.0	5.4
Severe Microshrinkage	Life (hours)	5	67.8	13.7	42.3	4.6
	El. (%)	5	13.2	5.0	10.6	2.9
	R.A. (%)	5	26.8	9.7	18.5	5.5
Mild Mold Breakage	Life (hours)	5	90.4	40.2	55.0	14.5
	El. (%)	5	10.0	5.0	8.3	3.0
	R.A. (%)	5	26.1	15.8	18.2	12.5
Intermediate Mold Breakage	Life (hours)	1	43.7	43.7	43.7	-
	El. (%)	1	8.5	8.5	8.5	-
	R.A. (%)	1	11.2	11.2	11.2	-
Severe Mold Breakage	Life (hours)	1	38.0	38.0	38.0	-
	El. (%)	1	4.0	4.0	4.0	-
	R.A. (%)	1	6.2	6.2	6.2	-
Mild Dross	Life (hours)	9	55.4	32.8	46.9	[illegible]
	El. (%)	9	15.5	5.0	9.4	3.9
	R.A. (%)	9	22.4	6.6	16.0	2.9

APPENDIX K (continued)

Defect Type	Property	No. of Data Points	High Value	Low Value	Average Value	-2σ Value
Intermediate Dross	Life (hours)	4	74.7	19.4	51.4	7.3
	El. (%)	4	11.5	8.3	10.2	6.6
	R.A. (%)	4	16.3	14.2	15.4	12.4
Severe Dross	Life (hours)	1	51.6	51.6	51.6	-
	El. (%)	1	13.2	13.2	13.2	-
	R.A. (%)	1	20.1	20.1	20.1	-
Intermediate Diverging Axis	Life (hours)	1	56.0	56.0	56.0	-
	El. (%)	1	9.2	9.2	9.2	-
	R.A. (%)	1	13.3	13.3	13.3	-

APPENDIX L

1800°F (982°C) LOW CYCLE FATIGUE DATA

APPENDIX L

1800°F (982°C) LOW CYCLE FATIGUE DATA

Defect Type	Valid	N_I	N_F	Intended Defect	Other NDI Defect	Undetected Defect	Defect Free
Defect Free	No	-	4199	X			
	No	2000	2987	X			
		7500	8006	X			
							X
							X
							X
Mild Microshrinkage	No	2000	3247				
	No	2000	3000	X			
		2000	3360	X			
		2000	2157	X			
		2000	2328				X
		2000	2411	X		X - Severe Dross	
						X - Severe Microshrinkage	
Intermediate Microshrinkage	No	3000	3649				
		2000	2752	X	X - Mild Microshrinkage		
		2500	3803				
		3000	3931	X		X - Mild Breakage	
		4500	5288	X	X - Mild Breakage		
Severe Microshrinkage	No	3000	3169				
		2000	2556	X	X - Mild Microshrinkage		
		-	1302	X			
Mild Dross	No	4000	4500			X - Mild Dross	
	No	4000	4556		X - Mild Microshrinkage		
		7000	8848	X		X - Mild Microshrinkage	
		3000	3457	X	X - Mild Microshrinkage		
		3000	3320	X	X - Mild Breakage		
		2500	3275	X		X - Mild Microshrinkage	
Intermediate Dross	No	-	15				
		-	988	X		X - Severe Dross	
Severe Dross		<684	684	X			
	No	2000	2400			X - Mild Microshrinkage	

APPENDIX L (continued)

Defect Type	Valid	N_I	N_F	Intended Defect	Other NDI Defect	Undetected Defect	Defect Free
Mild Mold Breakage		3000	3602			X - Mild Dross	
		4000	4814				X
		-	2155	X			
Intermediate Mold Breakage		2000	2499	X			
		-	647	X			
Severe Mold Breakage		4000	4505	X	X - Mild Microshrinkage		
	No	-	635			X - Crack (Misinterpreted)	
Mild Emergence		< 5047	5047		X - Intermediate Microshrinkage		
		< 9698	9698			X - Mild Breakage	
		< 3370	3370		X - Intermediate Mold Breakage		
		-	9933		X - Mild Microshrinkage		
		-	4445		X - Severe Mold Breakage		
		-	5593				X
Intermediate Emergence		-	1876		X - Intermediate Microshrinkage		
		4400	4900		X - Mild Microshrinkage		
		2500	2950		X - Mild Microshrinkage	X - Intermediate Dross	
		2000	2850		X - Intermediate Dross		
Severe Emergence		3000	3272		X - Mild Microshrinkage		
	No	-	1058				
		3000	3981		X - Mild Dross		
	No	4000	4208		X - Severe Microshinkage		
		3000	3837		X - Severe Microshrinkage		
		-	3029		X - Mild Microshrinkage		
	No	3000	3567		X - Severe Microshrinkage		
Mild Diverging Axis		4500	5133		X - Mild Microshrinkage		
		6000	6252		X - Intermediate Microshrinkage		

APPENDIX L (continued)

Defect Type	Valid	N_I	N_F	Intended Defect	Other NDI Defect	Undetected Defect	Defect Free
Intermediate Diverging Axis		8000	9540				
		5500	6268		X - Mild Microshrinkage		
	No	-	1617		X - Mild Microshrinkage		
						X - Severe Dross	
Severe Diverging Axis		4000	4371				
		4500	5079		X - Severe Microshrinkage		
					X - Intermediate Micro-shrinkage		
Intermediate Diverging Adjacent		4000	4367				
						X - Mild Breakage	
Severe Diverging Adjacent		2000	2583				
		3000	3469				
					X - Mild Microshrinkage	X - Intermediate Dross	

APPENDIX M

ANALYSIS OF DATA
ANALYSIS OF 1800°F (982°C) LOW CYCLE FATIGUE RESULTS

APPENDIX M

ANALYSIS OF 1800°F (982°C) LCF DATA

Defect Type	No. of Data Points	Property (Cycles)	High Value	Low Value	Average Value	-2σ Value
Defect Free	3	Failure Life	8006	4814	6137	2600
	2	Initiation Life	7500	4000	5750	2400
Mild Microshrinkage	14	Failure Life	9933	2157	5004	1400
	13	Initiation Life	8000	2000	3915	1300
Intermediate Microshrinkage	7	Failure Life	6252	1876	4317	950
	5	Initiation Life	6000	2000	4000	650
Severe Microshrinkage	5	Failure Life	4371	1302	2879	600
	4	Initiation Life	4000	2000	2750	510
Mild Dross	7	Failure Life	8848	1302	3970	1150
	6	Initiation Life	7000	2500	3580	1100
Intermediate Dross	4	Failure Life	2950	988	2342	450
	3	Initiation Life	2000	2500	2170	400
Severe Dross	3	Failure Life	2157	684	1500	175
	1	Initiation Life	2000	2000	2000	-
Mild Mold Breakage	6	Failure Life	9693	2155	4568	1100
	4	Initiation Life	4000	2500	3125	750
Intermediate Mold Breakage	3	Failure Life	3370	647	2172	85
	1	Initiation Life	2000	2000	2000	-

APPENDIX N

TYPICAL EXAMPLES OF FRACTURE SURFACES ASSOCIATED WITH EACH CASTING DEFECT AT EACH SEVERITY LEVEL

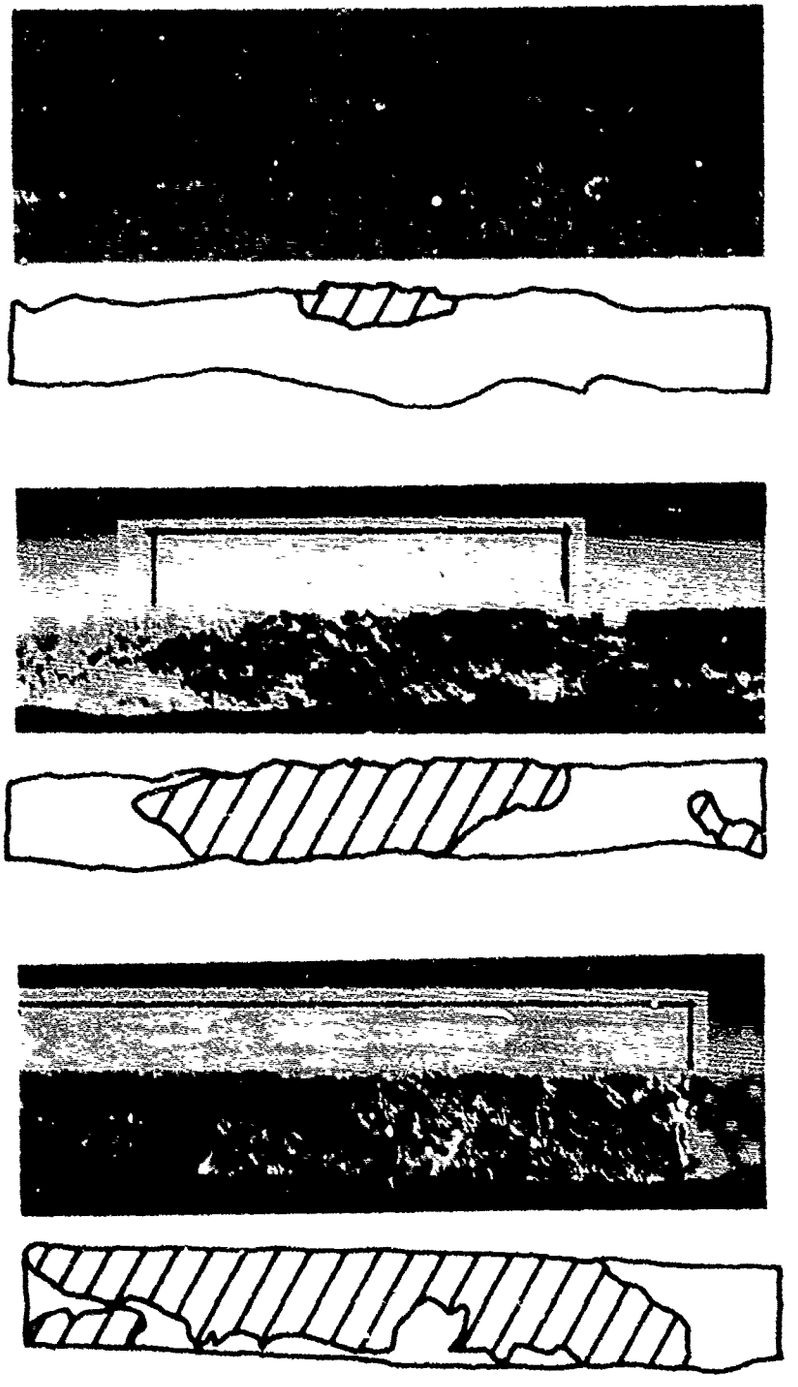

Fracture Surfaces Containing Microshrinkage Defects. Accompanying Sketches Indicate Extent of Defect as Cross Hatched Areas. Top - Mild. Center - Intermediate, Bottom - Severe. 10X Magnification.

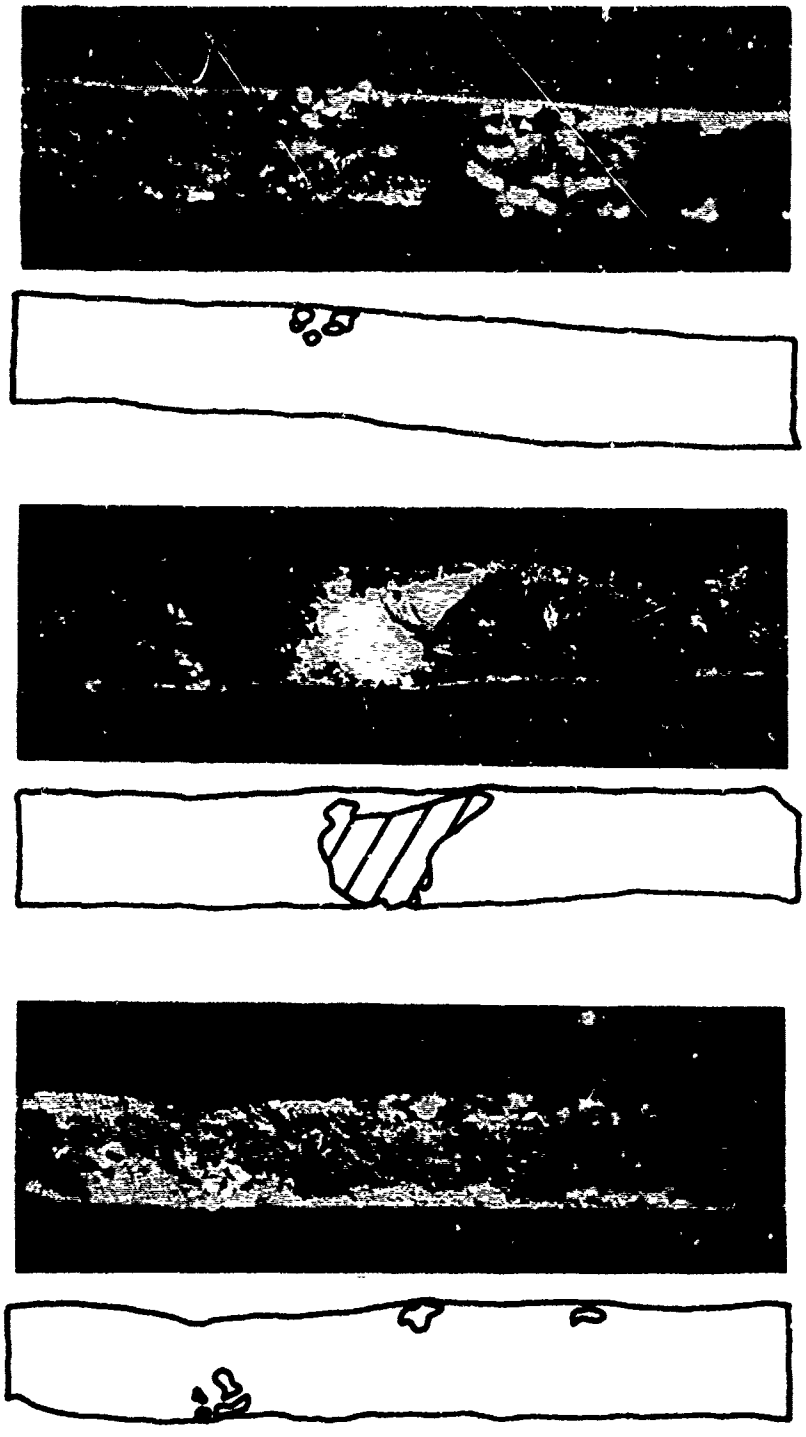

Fracture Surfaces Containing Mold Breakage Inclusion Defects. Accompanying Sketches Indicate Extent of Defect as Cross Hatched Areas. Top - Mild, Center - Intermediate, Bottom - Severe. 10X Magnification.

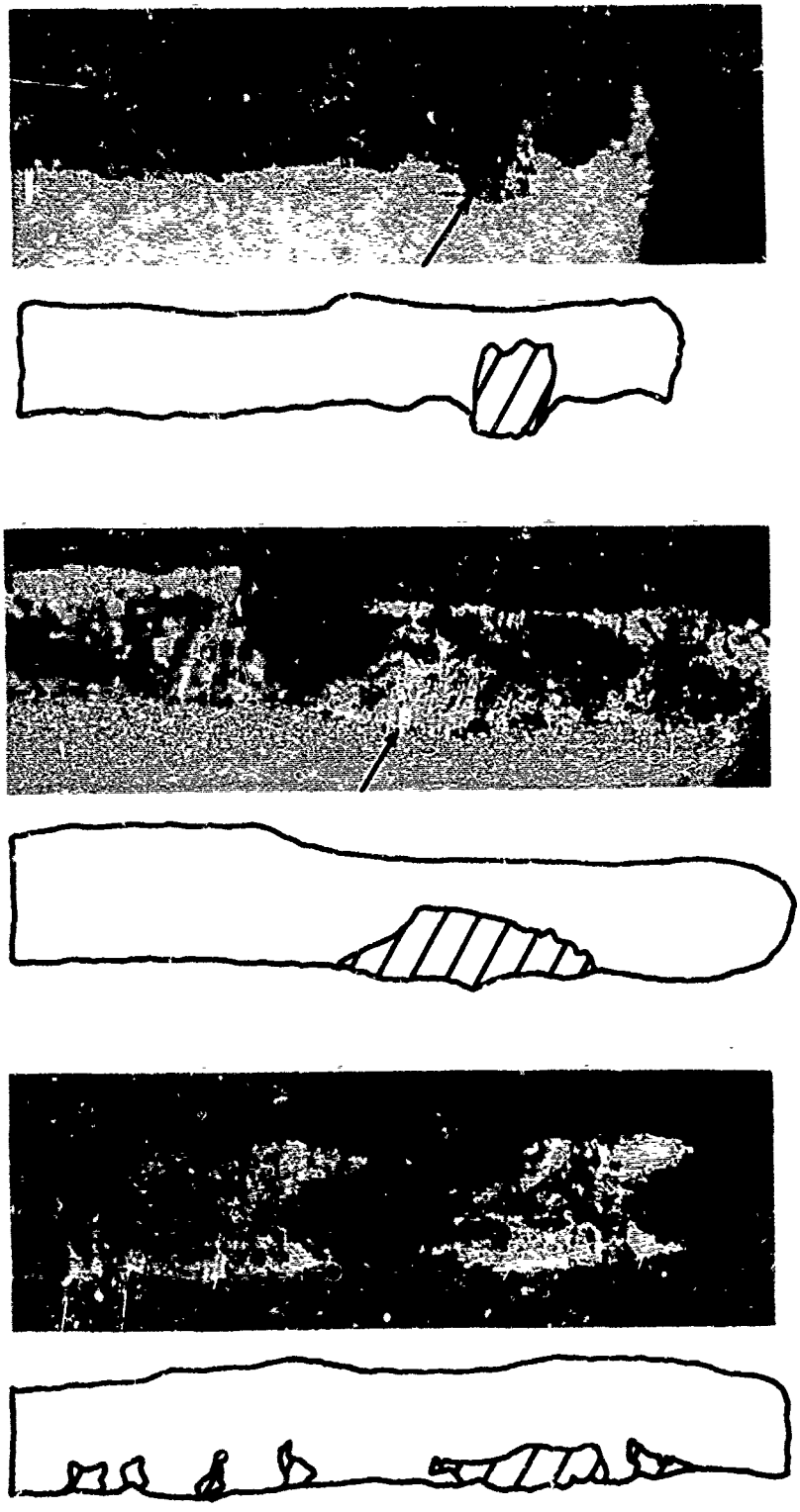

Fracture Surfaces Containing Dross Inclusion Defects. Accompanying Sketches Indicate Extent of Defect as Cross Hatched Areas. Top - Mild, Center - Intermediate, Bottom - Severe. 10X Magnification

REFERENCES

1. Committee on Implementation of Cost Saving Recommendations for Aerospace Construction, "Aerospace Cost Savings - Implications for NASA and the Industry," National Materials Advisory Board Report NMAB-326, (1975).

2. VerSnyder, F. L. and Shank, M. E. "Directional Solidification," Mat. Sci., and Tech., 7, (1970), p. S126.

3. Sullivan C. P. and Donachie, Jr., M. J., "Some Effects of Microstructure on the Mechanical Properties of Nickel-Base Superalloys," Metal Eng. Quarterly, (February 1967), p. 36.

4. Sims, C. T., "Nickel Alloys - The Heart of Gas Turbine Engines," Paper 70-GT-24 presented at the ASME Gas Turbine Conference and Products Show, Brussels, Belgium (May 24-28, 1970).

5. Gell, M., Leverant, G. R. and Wells, C. H., "The Fatigue Strength of Nickel-Base Superalloys," Achievement of High Fatigue Resistance of Metals and Alloys, ASTM STP 467, American Society for Testing and Materials (1970), pp. 113-153.

6. Decker, R. F., "Strengthening Mechanisms in Nickel-Base Superalloys," Steel-Strengthening Mechanisms, Climax Molybdenum Company, Greenwich, Connecticut, (May 1969), pp. 147-170.

7. Piearcey, B. J. and Terkelsen, B. E., "The Effect of Unidirectional Solidification on the Properties of Cast Nickel-Base Superalloys, Trans. AIME, 239, (August 1967), 1143.

8. Kear, B. H. and Piearcey, B. J., "Tensile and Creep Properties of Single Crystals of the Nickel-Base Superalloy MAR-M200," Trans. AIME, 239, (August 1967), 1209.

9. Piearcey, B. J., Kear, B. H. and Smashey, R. W. "Correlation of Structure with Properties in a Directionally Solidified Nickel-Base Superalloy," ASM Trans. Quarterly, 60, (December 1967), 634.

10. Floreen, S., "The Creep Fracture of Wrought Nickel-Base Alloys by a Fracture Mechanics Approach," Met. Trans. A, Vol. 6A, (September 1975).

11. McLean, M. and Schobert, F. "Mechanical Properties of Directionally Solidified Superalloys and Eutectics, "Conference Proceedings, High Temperature Alloys for Gas Turbines, Liege, Belgium, (25-27, September 1978).

12. Collins, H. E. and Piwonka, T. S. "Characterization of Cracking in PWA 1422 Castings," TRW Report TM 4723, (February 1973).

13. KET - An Advanced NDT Option - Qual-X Corporation, Hilliard, Ohio (1974), (Brochure).

14. Marder, J. M. "A Metallographic Evaluation of Krypton Emission Indications in a D.S. Superalloy," TRW Report ER-8000 prepared under Contract N00140-76-C-1142, (June 1978).

15. Weibull, W. "A Statistical Distribution Function of Wide Applicability," J. Appl. Mech., 18, pp. 293-7 (1951).

16. Personal communication with L. D. Graham, Manager Quality Control, Metals Plant of TRW Turbine Components Division (June 1978).

17. Bizon, P. T. Calfo, F. D., Dreshfield, R. L., "Effect of Grain Orientation on the Thermal Fatigue Resistance of a Directionally Solidified Nickel-Base Superalloy," (MAR-M247) NASA-Lewis Research Center, Cleveland, Ohio 44135. Paper presented at 1978 TMS-AIME Annual Meeting, New Orleans, Louisiana, (February 18-22, 1979).

18. Lupinc, V., "Factors Influencing the Creep Behavior of Ni-Cr-Base Alloys," Proceedings: High Temperature Alloys for Gas Turbines, Liege, Belgium, Applied Science Publishers Limited, London, (1978).

19. Lloyd, R. D., "The Effect of Casting Variables and Section Size on the Stress-Rupture Life of a High Temperature Nickel-Base Alloy," Society of Automotive Engineers, Report No. 700538, (July 1970).

20. Bachelet, E. and Lesoult, G., "Quality of Castings of Superalloys," Proceedings: High Temperature Alloys for Gas Turbines, Liege, Belgium, Applied Science Publishers Limited, London, (1978).

21. Leverant, G. R. and Gell. M., "The Elevated Temperature Fatigue of a Nickel-Base Superalloy, MAR-M200,in Conventionally-Cast and Directionally-Solidified Forms," Transactions of the Metallurgical Society of AIME, Vol. 245, (June 1969).

22. Tien, J. K. and Gamble, R. P., "The Suppression of Dendritic Growth in Nickel-Base Superalloys During Unidirectional Solidification," Pratt & Whitney Aircraft, Materials Engineering and Research Laboratory, Middletown, Conn., Materials Science and Engineering, (September 1971).

23. Marder, J. M., "The Effect of Grain Misorientation Defects on the Mechanical Properties of Directionally Solidified MAR-M246 + Hf," TRW Report ER-8013, prepared under Contract No. R8JSK-147171, (May 1978).

24. Gemma, A. E., Langer, B. S. and Leverant, G. R., "Thermal Mechanical Fatigue Crack Propagation in an Anisotropic (Directionally Solidified) Nickel-Base Superalloy," Thermal Fatigue of Materials and Components, ASTM STP 612, (1976).

25. Tada, H., Paris, P. C. and Irwin, G. R., The Stress Analysis of Cracks Handbook. Del Research Corp., Hellertown, Pennsylvania, p. 2-11, (1973).

*U.S.Government Printing Office: 1979 — 657-002/181